Microstructural deformation of tendon

Tyler M Grant
Christ Church

Supervisor: Dr Mark S Thompson

Department of Engineering Science
University of Oxford

A thesis submitted for the degree
Doctor of Philosophy

Trinity Term 2014

Abstract

Tendon disorders are painful, disabling, and a major healthcare problem, with millions of people affected by tendon injuries each year. Current treatment strategies are inadequate and knowledge of the underlying mechanobiological mechanisms is required to develop novel therapies. Although the tissue–level properties of tendon are well–documented there remains a lack of understanding of the deformation mechanisms of this complex tissue. Therefore, the aim of this thesis is to characterize the microstructural deformation of tendon through biological imaging, mechanical testing, and computational modeling. Emphasis is placed on the structure and function of elastic fibers in tendon, whose role is poorly understood.

First, histology, immunohistochemistry, and multiphoton microscopy are used to characterize the organization of elastic fibers in healthy and damaged tendon providing detailed microstructural information on their morphology and location for the first time. Elastic fibers are found to have a sparse distribution in the extracellular matrix, but are highly concentrated in the endotenon sheath and pericellular matrix. Moreover, damaged specimens are found to have a severely disrupted elastic fiber network. Elastic fibers likely contribute to fascicular deformation mechanisms and the micromechanical environment of tenocytes, which are expected to be disrupted in damaged tendon.

Second, mechanical testing and enzyme treatments are used to analyze the mechanical contribution of elastic fibers to tendon. Elastase is found to significantly affect the mechanical properties of the tissue and remove the elastin component of both tendon and a control collagen–elastin biomaterial. However, elastase is also found to degrade non–elastin structural molecules that may contribute to tendon mechanics. The mechanical changes associated with the elastase treatment suggest that elastic fibers do not contribute to the elastic recoil of tendon as previously hypothesized.

Third, multiphoton microscopy in combination with a novel microtensile testing machine is used to observe the deformation of collagen fibrils and tenocytes in tissue exposed to load. Tissue displacement is consistent with a helical arrangement of fibrils and nuclei experience significant elongation under physiological conditions. These results suggest that a helical arrangement of fibrils is responsible for the nonlinear stress–strain response of tendon and that nuclei are prime candidates for sensing mechanical forces in tendon.

Finally, computation modeling and structural imaging are used to generate a microstructural finite element model of tendon. A helical model with embedded pericellular matrix is able to reproduce the stress–strain response and cell–level deformation of the tissue. The pericellular matrix is found to amplify mechanical forces exposed to cells, which is required to initiate mechanobiological stimulation of tenocytes under physiological conditions. Therefore, the structure and composition of the PCM during health and disease is expected to significantly affect mechanobiological mechanisms of tendon.

The work presented in this thesis has used new experimental methods to provide novel insight into the structure, function, and deformation mechanisms of tendon. The techniques and concepts developed are widely applicable to the study of collagenous tissues in health and disease. In particular, observations regarding the pericellular matrix may lead to the development of new tissue–engineered and pharmacological strategies for the treatment of tendon disorders.

"If I have seen further it is by standing on the shoulders of giants."

-Isaac Newton

Acknowledgements

I am grateful for the generous help that I received during my doctoral studies from numerous individuals and organizations. This research project would not have been possible without their assistance.

First and foremost, I would like to express my deepest gratitude to my supervisor, Dr Mark Thompson, for his continued support of my development as a researcher. His enthusiasm for biomedical engineering and guidance has greatly helped me throughout my doctoral studies.

I would like to thank the many individuals at Oxford for providing valuable and insightful assistance over the past three years. In particular, I would like to thank the Urban group (Dr Jill Urban and Dr Jing Yu), the Thompson group (Dr Russ Tucker, Dr Nasim Zargar Baboldashti, and Dr Isaiah Adekanmbi), the Carr Group (Prof Andy Carr, Dr Osnat Hakimi, and Dr Richard Murphey), the IBME Workshop (James Fisk and David Salisbury), and others at Oxford (Dr Clarence Yapp, Dr Qi Zang, and Dr David Ferguson).

I am grateful for the financial support of my funding bodies including the Rhodes Trust, Natural Sciences and Engineering Research Council of Canada (NSERC), Imperial Order Daughters of the Empire of Canada (IODE), and Rosetrees Trust.

Last but not least, I would like to thank my family and friends for their continued support and encouragement.

Publications and Contributions

The following peer–reviewed papers and abstracts were written during my DPhil and are based upon the contents of this thesis:

Journal Articles

- Grant, T.M., Thompson, M.S., Urban, J., and Yu, J. (2013) Elastic fibres are broadly distributed in tendon and highly localized around tenocytes. Journal of Anatomy 222(6), 573-579.

Conference Abstracts

- Grant, T.M. and Thompson, M.S. (2014) A microstructural finite element model of tendon. World Congress of Biomechanics.
- Grant, T. M., Urban, J., Yu, J., Murphy, R. J., Carr, A. J., and Thompson, M. S. (2013) Elastic fibres contribute to the pericellular matrix of tendon. Orthopaedic Research Society.
- Grant, T.M. and Thompson, M.S. (2012) Structure and function of elastic fibres in tendon. European Society of Biomechanics.
- Grant, T. M., Thompson, M. S., Urban, J., and Yu, J. (2012) The distribution of elastic fibres in bovine flexor tendon. British Society for Matrix Biology.

Table of Contents

Table of Contents v

List of Figures x

List of Tables xii

Nomenclature xiv

1 Introduction 1

1.1 Motivation and Scope 1

1.2 Thesis Outline 2

2 Background 8

2.1 Tendon Structure 8

2.1.1 Molecular Composition of the Extracellular Matrix 8

2.1.2 Hierarchical Organization of Tendon 10

2.1.3 Distribution of Tenocytes 12

2.1.4 Vasculature of Tendon 14

2.1.5 Gross Tendon Anatomy 15

2.2 Mechanical Properties of Tendon 16

2.2.1 Mechanical Function of Tendon 16

2.2.2 Quasi–Static Mechanical Properties 18

2.2.3 Viscoelastic Mechanical Properties 20

2.2.4 Deformation Mechanisms of Tendon 21

2.3 Mechanobiology 22

2.3.1 Mechanotransduction 22

2.4 Tendon Injury and Disease 24
2.4.1 Tendinopathy 24

3 Organization of Elastic Fibers in Tendon 27
3.1 Introduction 27
3.1.1 Ultrastructure of Elastic Fibers 27
3.1.2 Mechanical Properties of Elastic Fibers 28
3.1.3 Distribution of Elastic Fibers in Tendon 29
3.1.4 Analysis of Elastic Fibers with Multiphoton Microscopy . . . 30
3.1.5 Aims and Objectives 31
3.2 Materials and Methods 32
3.2.1 Sample Collection and Preparation 32
3.2.2 Histological Staining and Immunostaining of Elastic Fibers . 33
3.2.3 Light, Confocal, and Multiphoton Microscopy 35
3.2.4 Image Analysis of Healthy and Damaged Tendon 36
3.3 Results 37
3.3.1 Overall Organization of Elastic Fibers in Tendon 37
3.3.2 Specific Localization of Elastic Fibers in Tendon 40
3.3.3 Distribution of Elastic Fibers in Damaged Tissue 41
3.4 Discussion 41
3.4.1 Overall Organization of Elastic Fibers 41
3.4.2 Elastic Fibers Distributed in the Pericellular Matrix 45
3.4.3 Mechanical Contribution of Elastic Fibers 46
3.4.4 Multiphoton Microscopy of Tendon 47
3.5 Conclusion 47

4 Effect of Elastase on the Structure and Function of Tendon 48
4.1 Introduction 48
4.1.1 Use of Enzyme Treatments to Analyze Tissue Mechanics . . 48
4.1.2 Elastase Treatment of Tendon 49
4.1.3 Aims and Objectives 50
4.2 Materials and Methods 51
4.2.1 Tissue Collection and Preparation 51

4.2.2 Enzyme Treatment for Elastin Digestion 51
4.2.3 Collagen–Elastin Scaffold Preparation 52
4.2.4 Mechanical Testing of Tendon Specimens 52
4.2.5 Structural Analysis of Tendon Specimens 55
4.2.6 Biochemical Assays of Tendon Specimens 57
4.3 Results 58
4.3.1 Degradation of Scaffold with Elastase 58
4.3.2 Mechanical Properties of Elastase–Treated Tendon 59
4.3.3 Structural Organization of Elastase–Treated Tendon 59
4.3.4 Molecular Compositions of Elastase–Treated Tendon 61
4.4 Discussion 64
4.4.1 Mechanical Role of Elastic Fibers in Tendon 64
4.4.2 Nonspecific Degradation and Tissue Swelling of Tendon . . . 67
4.5 Conclusion 68

5 Deformation of Collagen Fibrils and Tenocytes 69
5.1 Introduction 69
5.1.1 Microscopy in Combination with Mechanical Testing 69
5.1.2 Previous Microtensile Testing Machine Designs 71
5.1.3 Aims and Objectives 71
5.2 Materials and Methods 72
5.2.1 Design Specifications of Microtensile Testing Machine 72
5.2.2 Mechanical Testing in Combination with Imaging Protocol . 73
5.2.3 Automated Characterization of Cell Displacement 76
5.2.4 Modeling Deformation of Collagen Fibril Waveforms 78
5.3 Results 82
5.3.1 Microtensile Testing Machine Design 82
5.3.2 Effectiveness of Microtensile Testing Machine 84
5.3.3 Stress–Relaxation Response of Tendon During Imaging . . . 85
5.3.4 Cell–Level Displacement of Tenocytes in the Toe Region . . 86
5.3.5 Cell–Level Displacement of Tenocytes at Large Strains . . . 87
5.4 Discussion 89
5.4.1 Microtensile Testing Machine and Imaging Protocol 89

5.4.2 Microstructural Organization of Tendon 91
5.4.3 Displacement and Deformation of Tendon Nuclei 92
5.5 Conclusion 94

6 Microstructural Finite Element Model of Tendon 95
6.1 Introduction 95
6.1.1 Computational Tendon Models 95
6.1.2 Aims and Objectives 97
6.2 Materials and Methods 98
6.2.1 Geometric Characterization of Tendon Microstructure 98
6.2.2 Finite Element Model Definition 100
6.2.3 Sensitivity Analysis of Elastic Modulus 104
6.3 Results 105
6.3.1 Geometry and Assembly of Finite Element Model 105
6.3.2 Overall Stress–Strain Response of Tendon Model 105
6.3.3 Cell-Level Deformation of Tendon Model 108
6.4 Discussion 109
6.4.1 Geometry and Mechanical Response of Tendon Model 109
6.4.2 Role of the Pericellular Matrix in Cell–Level Deformation . . 112
6.4.3 Nuclear Deformation of Tendon Cells 114
6.5 Conclusion 115

7 Discussion 116
7.1 Summary and Future Directions 116
7.1.1 Overall Summary of Thesis 116
7.1.2 Organization of Elastic Fibers in Tendon 117
7.1.3 Effect of Elastase on the Structure and Function of Tendon . 118
7.1.4 Deformation of Collagen Fibrils and Tenocytes 120
7.1.5 Microstructural Finite Element Model of Tendon 121
7.1.6 Future Research Projects 123
7.1.7 Use of Mechanobiology for Treatment of Tendon Disorders . 124

Appendix A 126

Appendix B **131**

Appendix C **138**

Appendix D **141**

References **142**

List of Figures

1.1 Overview of Chapters 3 and 4 4
1.2 Overview of Chapters 5 and 6 6

2.1 Molecular composition of tendon 9
2.2 Hierarchical organization of tendon 11
2.3 Structure of collagen fibrils 11
2.4 Transverse electron micrograph of rat tail tendon 13
2.5 Organization of blood vessels in tendon 15
2.6 Structural variation of tendon 17
2.7 Quasi–static and viscoelastic response of tendon 19
2.8 Mechanotransduction mechanisms 23
2.9 Commonly injured tendons in the human body 26

3.1 Elastic fiber ultrastructure 28
3.2 Multiphoton microscopy 30
3.3 Location of bovine flexor tendon dissections 33
3.4 Location of supraspinatus tendon biopsy 34
3.5 Analysis of human supraspinatus tendon 37
3.6 Overall distribution of elastin, fibrillin–1 and fibrillin–2 in tendon . 38
3.7 Histology of bovine and human tendon 39
3.8 Multiphoton microscopy analysis of tendon 40
3.9 Specific organization of elastic fibers in tendon 42
3.10 3D reconstruction of elastic fibers and cell nuclei 43
3.11 Healthy and damaged human supraspinatus tendon 44

4.1 Tensile testing machine . . . 53
4.2 Loading profile of tendon . . . 54
4.3 Quasi–static tensile test mechanical properties . . . 55
4.4 Hysteresis test mechanical properties . . . 56
4.5 Crimp angle and wavelength . . . 57
4.6 Collagen–elastin scaffold degradation . . . 58
4.7 Mechanical properties of controls and elastase–treated tendon . . . 60
4.8 Multiphoton images of controls and elastase–treated tendon . . . 61
4.9 Structural organization of controls and elastase–treated tendon . . . 62
4.10 Molecular composition of controls and elastase–treated tendon . . . 63
4.11 Mechanical role of elastic fibers in tendon . . . 65

5.1 Microscope environment for microtensile testing machine . . . 74
5.2 Load profile for microscopic analysis . . . 75
5.3 Alignment of microscopic images . . . 76
5.4 Characterization of cell nuclei . . . 77
5.5 Simulation of sinusoidal and triangular crimp waveforms . . . 79
5.6 Microtensile testing machine design . . . 83
5.7 Microtensile testing machine assembly . . . 85
5.8 Representative stress–relaxation response . . . 86
5.9 Automated characterization of nuclei . . . 87
5.10 Change in alignment of nuclei . . . 88
5.11 Representative displacement profile of nuclei . . . 89
5.12 Nuclear elongation of tenocytes . . . 90

6.1 Categorization of mechanical tendon models . . . 96
6.2 Characterization of collagen fibrils and tenocytes . . . 99
6.3 Cross–sectional schematic of finite element model . . . 104
6.4 Assembly of finite element model . . . 106
6.5 Influence of fibril stiffness on the stress–strain response . . . 107
6.6 Influence of ground substance on the stress–strain response . . . 107
6.7 Influence of PCM stiffness on cell–level strain . . . 108
6.8 Elongation of nuclei with the application of tissue strain . . . 109
6.9 Representative mesh sensitivity curve for collagen fibrils . . . 110

List of Tables

2.1 Mechanical Properties of Select Human Tendons 20

3.1 Primary and Secondary Antibodies Used for Immunohistochemistry 35

6.1 Geometry and Material Properties of Finite Element Model Parts . 101

Nomenclature

ϵ: Strain

λ: Wavelength

σ: Stress

A: Area

2D: Two Dimensions

3D: Three Dimensions

ANOVA: Analysis of Variance

DAPI: 4',6–diamidino–2–phenylindole

DAQ: Data Acquisition Unit

DMEM: Dulbecco's Modified Eagle Medium

DMMB: Dimethyl Methylene Blue

E: Elastic Modulus

ECM: Extracellular Matrix

FCS: Fetal Calf Serum

GAG: Glycosaminoglycan

H&E: Hematoxylin and Eosin

IBME: Institute of Biomedical Engineering

IHC: Immunohistochemistry

LVDT: Linear Variable Differential Transformer

MCL: Medial Collateral Ligament

MMP: Metalloproteinase

MPM: Multiphoton Microscopy

MTJ: Myotendinous Junction

MTM: Microtensile Testing Machine

OCT: Optical Cutting Temperature

OTJ: Osteotendinous Junction

PBS: Phosphate Buffered Saline

PCM: Pericellular Matrix

qPCR: Quantitative Polymerase Chain Reaction

RTTF: Rat Tail Tendon Fascicle

SHG: Second Harmonic Generation

SLRP: Small Leucine Rich Proteoglycan

T_M: Melting Temperature

TEM: Transmission Electron Microscopy

TGF–β: Transforming Growth Factor Beta

TIMP: Tissue Inhibitor of Metalloproteinase

TPF: Two Photon Fluorescence

UTS: Ultimate Tensile Strength

XRD: X–Ray Diffraction

Chapter 1

Introduction

1.1 Motivation and Scope

Millions of people are affected by tendon disorders every year and are plagued with debilitating pain and loss of mobility. Tendon injuries are particularly common amongst athletes and have been estimated to account for 30–50% of all sports–related injuries (Järvinen et al., 2004). Moreover, 23% of people over the age of 50 experience severe shoulder tendon pain due to rotator cuff disease (Tempelhof et al., 1999). As a result of increasing performance demands amongst athletes and rising life expectancies, tendon disorders will continue to burden health care systems, which currently costs the USA $30 billion per year (Chen et al., 2009). Although much work has been done to improve repair strategies, there is a high rate of failure associated with current treatments (Leesa et al., 2004). Further knowledge of the underlying mechanisms responsible for tendon disorders is required to develop more effective treatments.

The use of tissue–engineered constructs to treat tendon disorders has received

much interest over the past decade. Through the inclusion of cells and biologics, constructs promote healing of tendon while providing temporary mechanical stability to tissue. A key factor in designing effective constructs is to ensure that the mechanical properties of the material complement the deformation mechanisms of the tissue. Additionally, the micro–architecture of the construct should promote integration of cells into the matrix. The significance of mechanobiology, i.e., how forces influence cell function, is becoming increasingly clear and making use of mechanobiological mechanisms may enhance treatment strategies. Therefore, the major aim of this thesis is to elucidate the microstructural deformation mechanisms of tendon and to better understand the role of mechanobiology in health and disease. These relationships can then be used to improve the design of tissue–engineered constructs intended for the enhancement of tendon regeneration.

1.2 Thesis Outline

This thesis consists of six chapters including a background, four experimental chapters, and a summary. Each experimental chapter has an independent aim that has been derived from findings presented in the previous chapters. A summary of the aims, methods, and findings of the experimental chapters (Chapters 3–6) is illustrated in Figures 1.1 and 1.2 and provides a broad overview of this thesis.

First, the background chapter introduces the composition, structure, and mechanical function of tendon as currently understood. The hierarchical structure of tendon is described as well as the viscoelastic response of the tissue. This chapter is concluded with a discussion regarding the changes associated with tendon disorders and how they are currently managed.

The first experimental chapter aims to describe the organization of elastic fibers in tendon to better understand their function. Elastic fibers contribute to approximately 2% of the dry weight of tendon (Mithieux and Weiss, 2005), but their role is poorly understood. Histology and immunohistochemistry (IHC) are used to highlight the organization of elastic fibers in healthy and diseased tissue. Elastic fibers are found to be highly localized around groups of cells and between tendon fascicles. From this organization I suggest that elastic fibers contribute to the mechanical properties of the pericellular matrix (PCM) and endotenon sheath, but not likely the macroscopic mechanical response of the tissue. Moreover, observations in damaged tissue indicate that elastic fiber organization is significantly disrupted, which may influence the mechanical environment of cells and the endotenon sheath.

Given the sparse elastic fiber organization described in Chapter 3, an enzyme treatment in combination with mechanical testing is used to better understand the contribution of elastic fibers to tendon mechanics in the fourth chapter. Elastase is used to degrade elastic fibers in tendon and the elastic and viscous mechanical properties are characterized. Structural imaging and biochemical assays are used to better understand the degradation of elastase on the structure and composition of tendon. It is shown that a standard elastase treatment influences the mechanical response of tendon, but also causes nonspecific degradation of the extracellular matrix (ECM). Therefore, I conclude that the mechanical changes associated with the elastase treatment are the result of degradation of the ECM and elastic fibers rather than only elastic fibers. These findings increase the uncertainty of elastic fiber function in tendon and additional experiments are required to better understand their role.

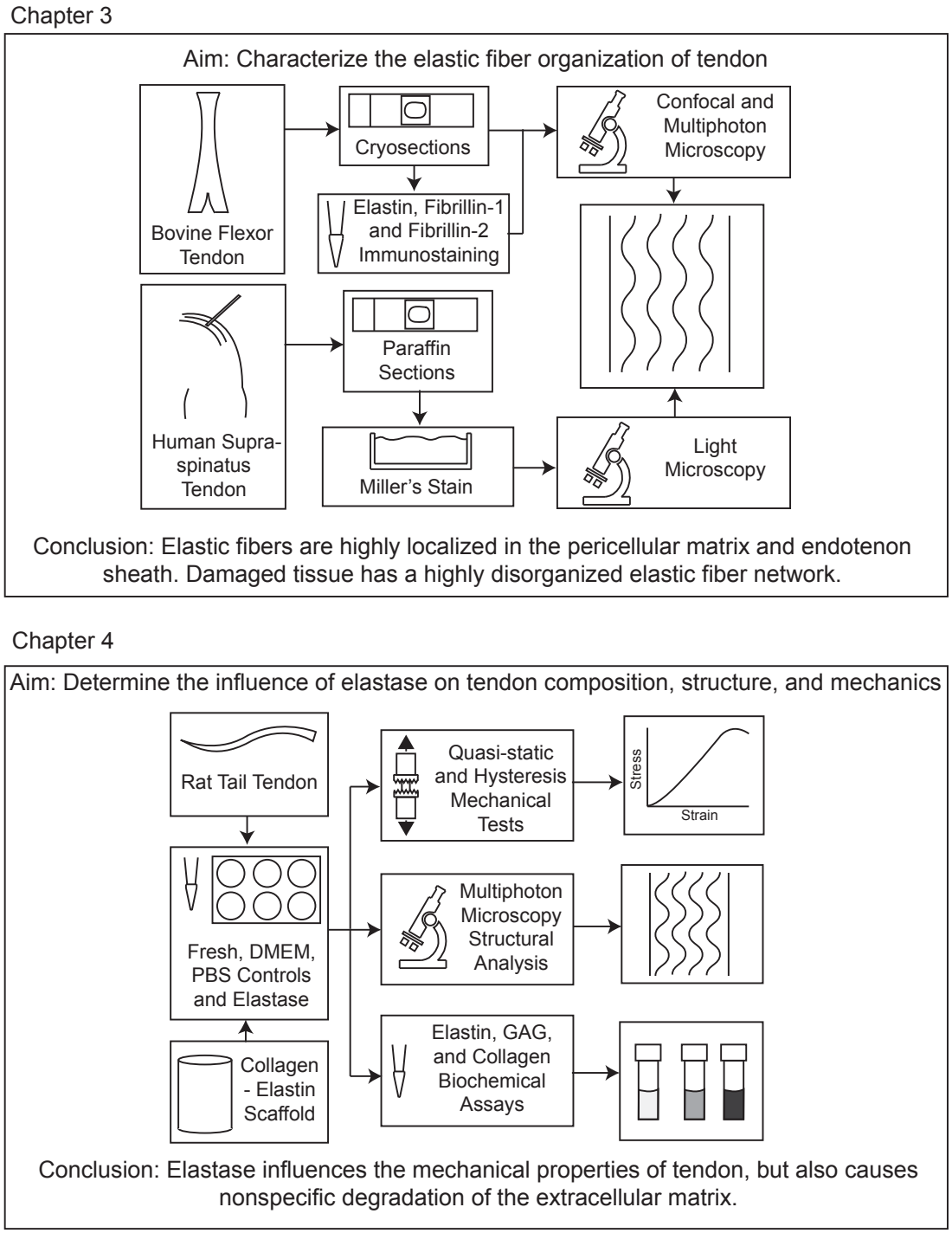

Figure 1.1: Overview of Chapter 3 (Organization of Elastic Fibers in Tendon) and Chapter 4 (Effect of Elastase on the Structure and Function of Tendon) highlighting major aims, methods, and conclusions from experiments.

The dense organization of elastic fibers surrounding arrays of cells as described in Chapter 3 suggests that elastic fibers contribute to the PCM of tendon. To better understand the influence of the micromechanical environment on tendon function, the displacement of the ECM and cells is observed by combining mechanical testing and microscopy in the fifth chapter. First, a microtensile testing machine (MTM) is designed and manufactured for use with a confocal/multiphoton microscope. This novel design provides detailed force and displacement measurements while allowing for collection of high–resolution images. Through tracking cell nuclei and collagen fibrils new insight into the microstructural deformation of tendon is achieved. It is shown that nuclei displacement is indicative of a helical organization and that nuclear deformation occurs under physiological conditions. These results suggest that tendon has a helical organization and that nuclei may act as mechanosensors in tendon.

The final experimental chapter makes use of previous findings to develop a novel microstructural finite element model of tendon. The model consists of helically oriented collagen fibrils that are bound to cells by means of the PCM. A parametric analysis is conducted to determine the influence of material properties of parts on the microstructural deformation of tendon. It is shown that a helical collagen fibril organization reproduces the mechanical response of tendon and that the PCM amplifies mechanical forces. Therefore, elastic fibers, which are predicted to contribute to the mechanical properties of the PCM, may play a key role in transmitting mechanobiological signals. This is particularly relevant given the disruption of elastic fibers observed in damaged specimens.

The final chapter summarizes the results from experimental chapters and provides insight into future directions of this research. Potential experiments are

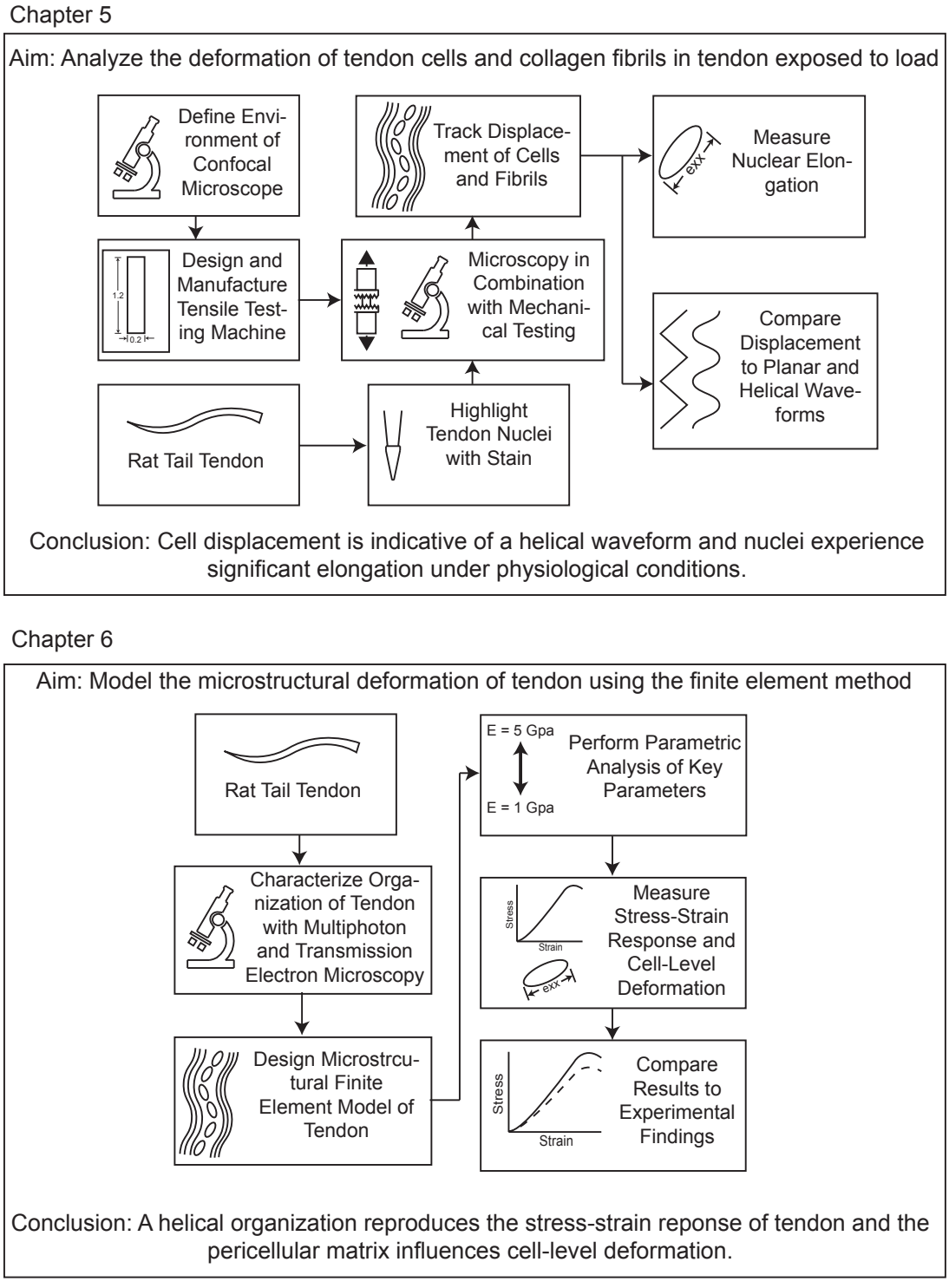

Figure 1.2: Overview of Chapter 5 (Deformation of Collagen Fibrils and Tenocytes) and Chapter 6 (Microstructural Finite Element Model of Tendon) highlighting major aims, methods, and conclusions from experiments.

proposed for each experimental chapter that will expand our understanding of tendon structure and function. The chapter is concluded with a brief discussion on the application of the current findings that may improve tendon treatment strategies.

Chapter 2

Background

2.1 Tendon Structure

2.1.1 Molecular Composition of the Extracellular Matrix

Tendon is composed of collagen, glycosaminoglycans , elastic fibers and other structural molecules (Figure 2.1) that are uniquely combined together to form a dense connective tissue. Type I collagen is the main structural molecule and accounts for 60–85% of the dry weight of tendon (Riley, 2005). Although non–collagenous molecules are present in small numbers, they may play important roles in mediating the production and maintenance of the ECM.

Type I collagen forms a supramolecular structure and is part of the fibrillar sub–family. Tropocollagen is the most basic molecule and forms collagen fibrils, which are the major load bearing elements of tendon. Other varieties of collagen are present in tendon including type III and type VI, which are localized in the endotenon sheath (Duance et al., 1977) and around arrays of tenocytes (Ritty et al.,

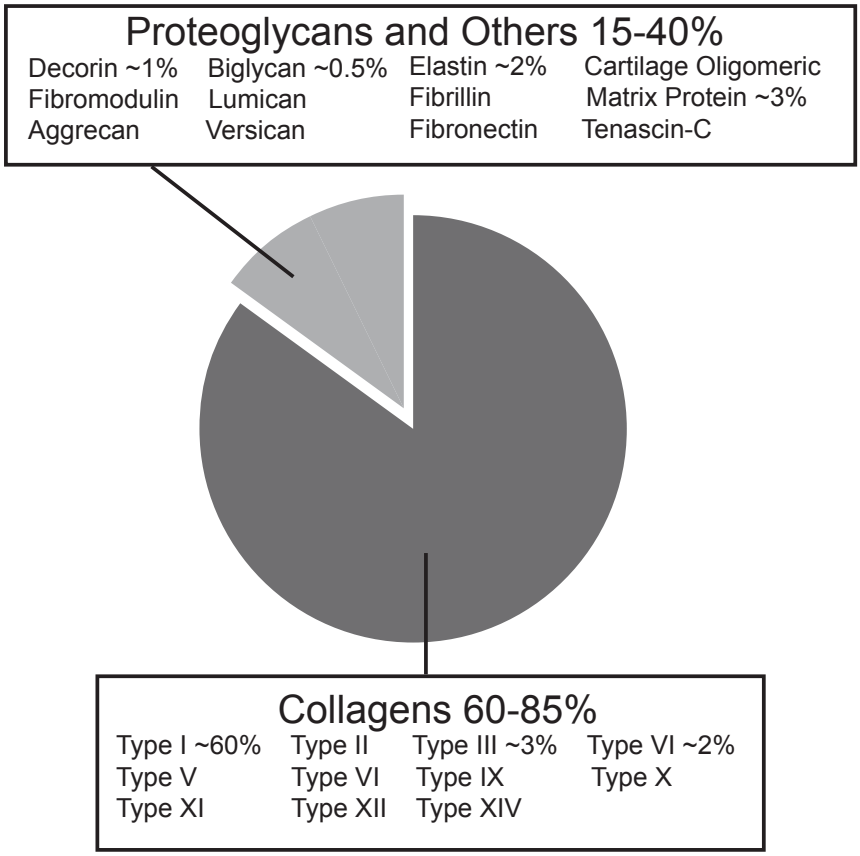

Figure 2.1: Molecular composition of tendon. All percentages represent contribution to total dry weight of tendon. Type I collagen is the most prevalent ECM structural molecule and accounts for approximately 60% of the total dry weight (Kadler et al., 1996; Riley, 2005).

2003), respectively. The role of these and other collagens is poorly understood, but has been suggested to support the structure and function of type I collagen fibrils (Myllyharju and Kivirikko, 2004).

Included in tendon ECM are small leucine rich proteoglycans (SLRPs) which have domains for binding GAG side chains. These structural molecules are found throughout tendon and have been shown to stabilize type I collagen fibrils and may contribute to fibrillogenesis (Ameye and Young, 2002). In addition to SLRPs,

there exist large modular proteoglycans, including aggrecan, which are generally found in the fibrocartilage region of tendon (Yoon et al., 2005). Proteoglycans in cartilage contribute to the compressive strength of the tissue (Evans et al., 1990) and therefore, aggrecan may play a similar role in the fibrocartilage region of tendon. GAGs are highly hydrophilic and have a high water binding capacity, which contributes to tendon mechanics and diffusion of water–soluble molecules into the tissue.

Elastin accounts for approximately 2% of tendon (dry weight) and has been suggested to contribute to elastic recovery following the removal of load (Mithieux and Weiss, 2005). Elastin and microfibrils form elastic fibers, which are able to withstand large deformations.

2.1.2 Hierarchical Organization of Tendon

Tendon has a complex hierarchical structure that is primarily composed of collagen fibrils oriented parallel to the long axis of tendon (Figure 2.2). Tropocollagen has a triple–helix structure that is approximately 300 nm in length and 1.5 nm in diameter (Tang et al., 2010). Collagen fibrils are composed of tropocollagen arranged in quarter–staggered arrays with each subsequent collagen molecule offset by 67 nm giving rise to the banding pattern commonly documented in transmission electron microscopy (TEM) studies (Figure 2.3). The assembly of fibrils is driven by an entropic process similar to the self–assembly of proteins, which is stabilized by covalent cross–linking and intermolecular adhesion (Kadler et al., 1996).

At early stages of development, collagen fibrils have a small diameter and a unimodal size distribution, but with age, fibrils increase in diameter and form a

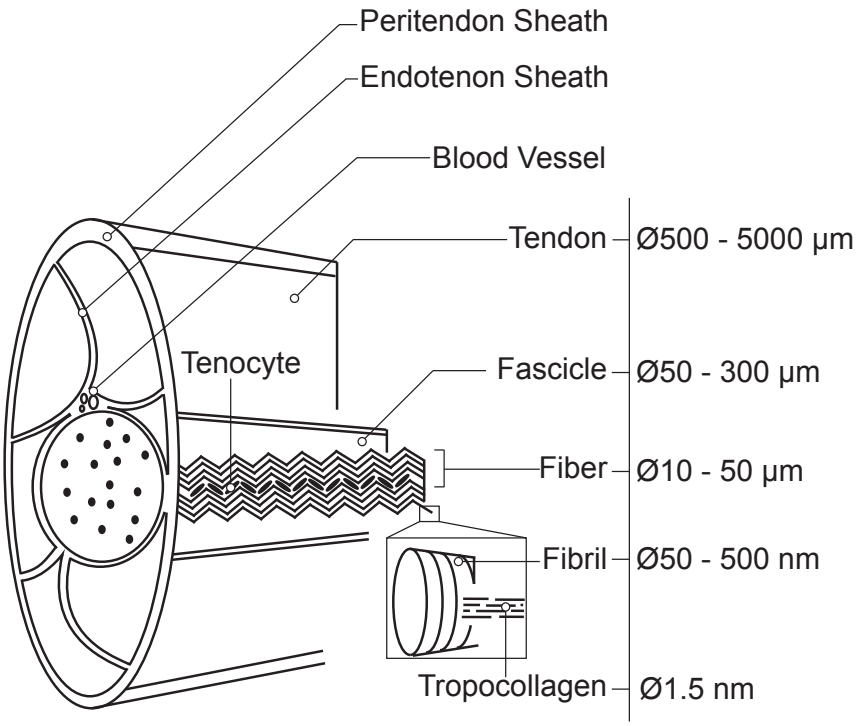

Figure 2.2: Hierarchical organization of tendon. Tenocytes are distributed in longitudinal arrays and are surrounded by collagen fibrils. The endotenon sheath separates fibrils into fascicles and the peritendon sheath envelopes tendon and enhances sliding between adjacent structures. Modified from Grant et al. (2013).

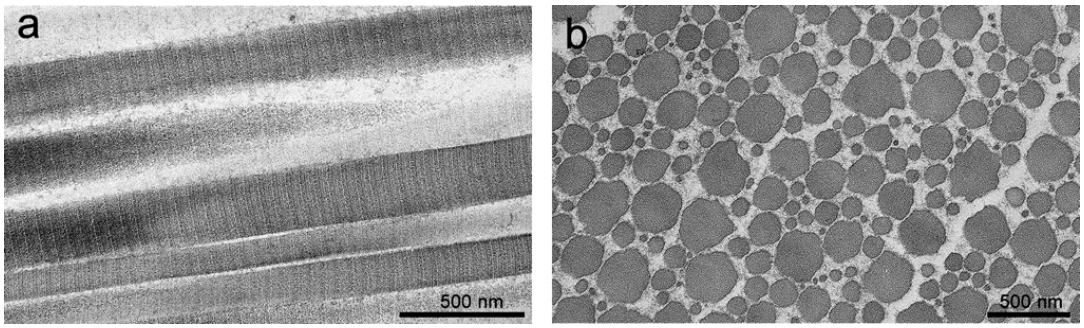

Figure 2.3: Structure of collagen fibrils as observed with TEM. (a) Longitudinal organization of collagen fibrils with distinct banding pattern from overlapping tropocollagen molecules. (b) Transverse organization of collagen fibrils depicting bimodal size distribution (Section 6.2.1).

bimodal distribution (Parry et al., 1978). Small fibrils fill spaces between large fibrils and therefore increase the density of load bearing elements in the tissue. In addition to temporal effects, the size of collagen fibrils vary throughout tendon (Williams et al., 2008). Fibrils have a crimped morphology, which improves tissue compliance (O'Brien, 1997). However, the origin of fibril crimp is a highly debated topic and researchers have yet to reach a consensus as to whether fibrils form a helical or planar organization.

Groups of collagen fibrils form tendon fascicles, which are enveloped by an endotenon sheath. The endotenon sheath is a thin layer of connective tissue that binds together fibrils and allows fascicles to glide next to each other. In addition, blood vessels, lymphatic vessels and nerves travel along groups of fascicles through the endotenon sheath (Hess, 1989). The endotenon originates from the epitenon sheath, which wraps around the outer tendon surface. The epitenon is contiguous with the inner surface of the paratenon sheath, which promotes gliding between the tendon and surrounding tissue. Because the epitenon and paratenon form part of a complimentary unit they are occasionally referred to as the peritendon. Tendon sheaths have been shown to have a different structural organization and composition to the tendon proper, including increased levels of type III collagen and elastic fibers (Kannus, 2000).

2.1.3 Distribution of Tenocytes

Tenocytes are specialized fibroblast that are found in tendon and serve many important roles including secretion of ECM structural molecules (Figure 2.4). Immature tenocytes are called tenoblasts, which have a high metabolic rate. As

tenoblasts mature they elongate, become less numerous and develop long finger–like processes that extend into the ECM (Benjamin et al., 2008). These processes are necessary for maintaining intercellular communication within an expanding matrix. It has been shown that cells maintain contact through desmosomial junctions, tight junctions, and gap junctions and relay signals in response to biological cues (Kannus et al., 1998).

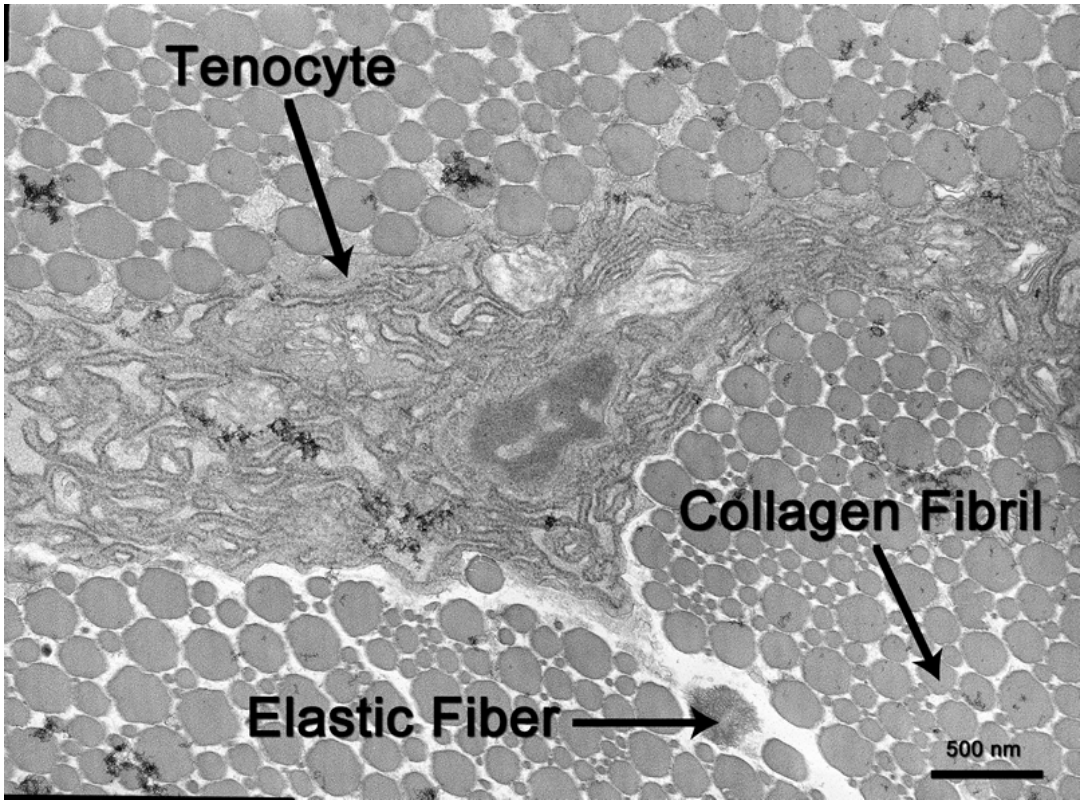

Figure 2.4: Transverse electron micrograph of rat tail tendon. Image depicts tenocyte embedded in collagen fibril matrix and an elastic fiber in close vicinity to the tendon cell. (Section 6.2.1).

Tendon has a low cell mass fraction and metabolic rate compared to other tissues in the human body. For example, the cell mass fraction of tendon is 1% to 3%, whereas liver is 95% (Kannus, 1997). Consequently, tendon is associated with

long healing times following tissue damage (Williams et al., 2008).

2.1.4 Vasculature of Tendon

Tendon is a relatively avascular tissue, which has been suggested to be partially responsible for the poor healing properties of the tissue. Blood vessels travel through the endotenon sheath and longitudinally surround fascicles (Petersen et al., 1999; Smith, 1965) (Figure 2.5). The blood vessels are arteriolar in size, but do not penetrate into collagen bundles (Edwards, 1946). By means of diffusion, oxygen and nutrients travel through the ECM to cells. There are several major arteries that supply blood to tendons including six in the rotator cuff, two in the Achilles tendon, and four in the digital flexor tendon (Fenwick et al., 2002). These blood vessels originate from the paratenon sheath, muscular branches, or vessels at the bone insertion site (Smith, 1965).

The vasculature of tendon appears to be an important factor in maintaining healthy tissue because areas of low blood supply are more susceptible to damage (Pufe et al., 2005). For example, the mid–point of the Achilles tendon is the most likely location to sustain a rupture and has been associated with a low blood supply (Theobald et al., 2005). When tendon is damaged there is a significant increase in vasculature (Fenwick et al., 2002), which is associated with ECM degradation to support infiltration of blood vessels (Pufe et al., 2005). Consequently, it has been suggested that neoangiogenesis predisposes tendon to microdamage. Interestingly, a study that destroyed neovessels in tendon through sclerosing therapy showed that patients experienced significant pain reduction (Öhberg et al., 2001).

2.1.5 Gross Tendon Anatomy

There are hundreds of tendons in the human body. Healthy tendons have a brilliant white color and vary in shape and size. Tendons can be flat, cylindrical, fan, or ribbon shaped depending on their anatomical location and function (Józsa and Kannus, 1997). In general, short broad tendons are associated with muscles that generate large forces and long thin tendons are associated with muscles that generate small forces (Józsa and Kannus, 1997).

When there is a large amount of friction associated with a joint the corresponding tendon may be surrounded by an additional sheath. This sheath consists of an outer fibrotic layer and an inner synovial layer creating a thin film of synovial fluid within a cavity (Marieb and Hoehn, 2007). The two–layer structure is common in

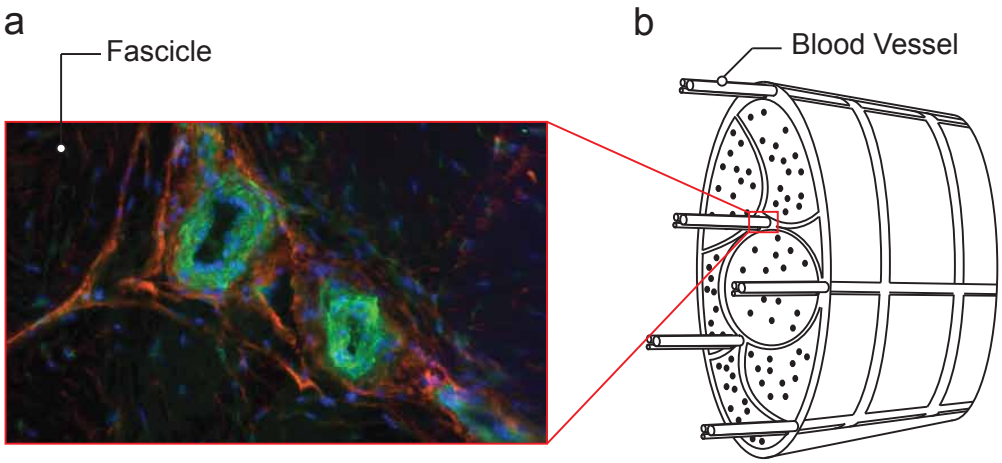

Figure 2.5: Organization of blood vessels in tendon. (a) Transverse elastin (green) and fibrillin–1 (red) dual immunostain highlighting two blood vessels traveling through the endotenon sheath (Section 3.2.2). (b) Cartoon diagram of blood vessel organization in tendon showing longitudinal organization in the endotenon sheath. Modified from Smith (1965).

tendons present in the hands and feet, but a single paratenon sheath surrounds most tendons in the human body.

The majority of tendon consists of longitudinal arrays of tenocytes deposited in a crimped fibril matrix known as the tendon proper. However, as tendon approaches junctions its structure changes to accommodate binding with muscle or bone (Figure 2.6). At the myotendinous junction (MTJ), i.e., muscle–tendon junction, collagen fascicles penetrate deep into muscle processes. The tendon fuses to the basement membrane of the muscle forming a firm connection (Watanabe et al., 2012). At the osteotendinous junction (OTJ), tendon fascicles merge into bone by adjusting their phenotype from the tendon proper to fibrocartilage, mineralized fibrocartilage and finally bone.

2.2 Mechanical Properties of Tendon

2.2.1 Mechanical Function of Tendon

The role of tendon is to enable joint locomotion by transferring forces from muscles to bones. Tendon is a stiff tissue and transfers large forces while minimizing energy dispersion. The unique ability of tendon to withstand large forces makes it an important part of the muscle–tendon unit. Tendon can withstand the large stresses that are generated when crossing over bony projections. Moreover, tendon enables the muscle belly to be conveniently positioned away from the joint, improving range of motion.

Tendon is capable of storing and dissipating energy as a consequence of its viscoelastic behavior. In broad terms, tendon can be categorized as two major

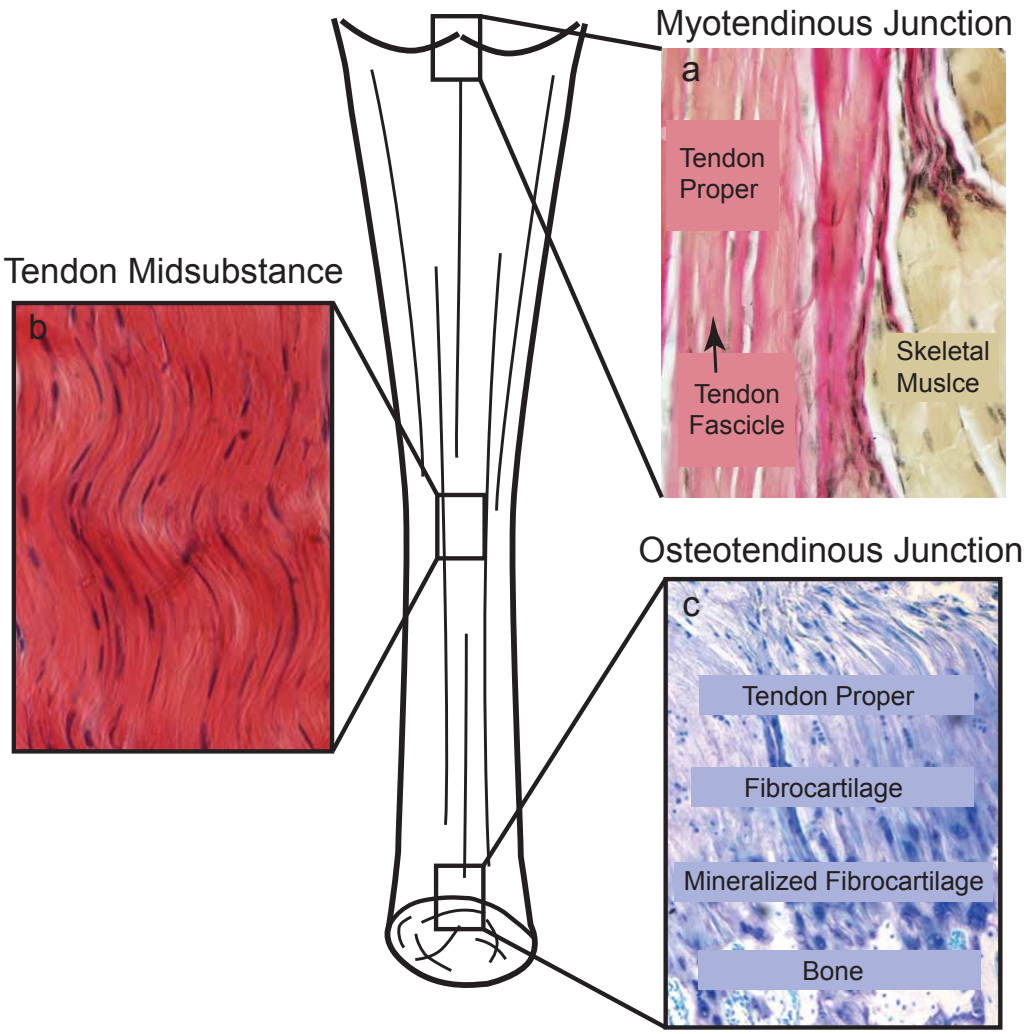

Figure 2.6: Structure of the MTJ, midsubstance and OTJ of tendon. (a) MTJ depicting collagen fibrils merging with muscle fibers (Slomianka, 2014). (b) Tendon midsubstance illustrating arrays of tenocytes present in a crimped structure (Section 3.2.2). (c) OTJ transitioning from the tendon proper to fibrocartilage, mineralized fibrocartilage and finally bone (Schwartz and Thomopoulos, 2013).

types: positional and energy storage tendons. Energy storage tendons are generally found in the legs and feet and are exposed to large forces. These tendons are capable of storing potential energy during locomotion saving substantial muscular

energy (Alexander, 1984). Positional tendons found in the arms and hands are exposed to much smaller forces and perform precise movements. Previous work has shown that the mechanical properties of the two types of tendon vary significantly (Shadwick, 1990).

2.2.2 Quasi–Static Mechanical Properties

The quasi-static stress–strain curve of tendon has been widely studied and has been shown to have a J–shape (Figure 2.7). At low strains, the response is nonlinear and corresponds to the straightening of crimped collagen fibrils (Diamant et al., 1972). As strain is increased, the response becomes linear until the tendon begins to rupture. The nonlinear region of the curve transitions into the linear region at approximately 4% strain, but depends on the type of tendon. The stress–strain response within the nonlinear region is of particular interest because physiological strains that occur during everyday use are generally restricted to this region (Cook and McDonagh, 1996).

A number of mechanical properties can be extrapolated from quasi–static stress–strain curves including the linear modulus, ultimate tensile strength (UTS), and failure strain. The values of these measurements can vary significantly depending on the anatomical site, loading history and species of tendon under investigation (Table 2.1).

A healthy human Achilles tendon would normally operate at an approximate cyclic stress of 5 MPa and have a UTS of approximately 70 MPa (Bennett et al., 1986). This corresponds to a safety factor (Material Strength / Design Load) of approximately 14, which is comparable to the design recommendation for wire

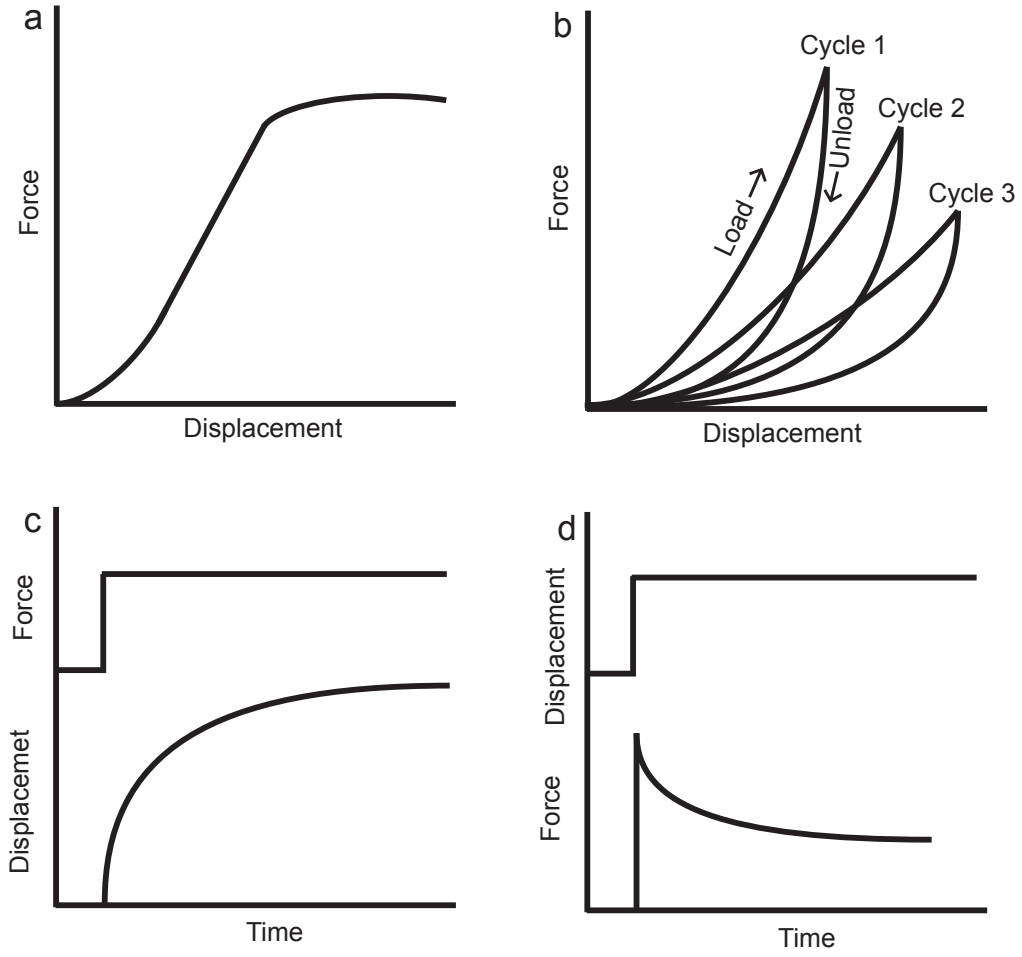

Figure 2.7: Quasi–static, hysteresis, creep and stress–relaxation curves of tendon. (a) Quasi–static force–displacement relationship of tendon. The low force–displacement response has a nonlinear relationship, which becomes linear and then plateaus at failure. (b) Hysteresis force–displacement relationship of tendon. The area between the loading and unloading curves represents the dissipated energy during one loading cycle. The curve changes slope with loading cycles and stabilizes after approximately 10 repetitions, which is a process called preconditioning. (c) Creep curve indicating an increase in displacement with time as tendon is exposed to a constant force. (d) Stress–relaxation curve representing reduction in stress when displacement is held at a constant value.

Table 2.1: Mechanical Properties of Select Human Tendons

Tendon	Linear Modulus (MPa)	Ultimate Tensile Strength (MPa)	Failure Strain (mm/mm)
Achilles[1]	816 ± 218	71 ±17	0.13 ± 0.017
Patellar[2]	643 ± 53.0	69 ± 6.0	0.14 ± 0.0070
Quadriceps[3]	463 ± 68.5	38 ± 5.0	0.11 ± 0.022
Biceps[4]	421 ± 212	33 ± 5.3	0.101 ± 0.027

1. (Wren et al., 2001); 2. (Butler et al., 1986); 3. (Stäubli et al., 1999); 4. (McGough et al., 1996)

ropes (Shigley et al., 1989). This safety factor protects tendons from extreme loads, such as one–legged hopping, which can generate tissue strains up to 10% (Birch, 2007). The area under a stress–strain curve represents the energy required to deform a tendon and rupture occurs when sufficient energy is supplied to the tissue to reach the failure strain.

2.2.3 Viscoelastic Mechanical Properties

The viscoelastic response of tendon is observed when performing hysteresis, creep, or stress relaxation tests (Figure 2.7). Like many soft tissues, tendon is sensitive to strain rate and the history of loading affects the stress–strain response. It has been shown that tendon becomes less deformable at high strain rates (Danto and Woo, 1993). Cyclic loading has been shown to lower the yield point of excised tendon and following the application of multiple loading cycles, the response be-

comes repeatable due to changes in the internal tissue structure. This process is known as preconditioning and is commonly used during mechanical testing of biological tissues to obtain repeatable measures between specimens. The mechanisms responsible for preconditioning are unknown, but have been suggested to involve sliding of fibrils, which change in the resting length of tissue specimens (Goulam Houssen et al., 2011).

Although the viscoelastic behavior of tendon is well documented, the microstructural origin for tendon viscoelasticity is not fully understood. Tendon viscoelasticity has been suggested to be the result of interactions between collagen fibrils and noncollagenous matrix components and fluid flow through a porous matrix (Lujan et al., 2009). Of significant importance are GAGs, which have a high affinity for binding water. Tendon is a highly hydrated tissue consisting of approximately 70% water per volume (Gupta et al., 2010).

2.2.4 Deformation Mechanisms of Tendon

The mechanical response of extensible connective tissues, such as tendon, is determined by the unique composition and organization of structural molecules in the ECM. In general, connective tissues (e.g., skin, tendon, cartilage, blood vessels) are composed of a fibrous network bound together by an amorphous ground substance. It is the interaction of these two structures that generate the overall mechanical response of the connective tissue.

Tendon extension is determined by the combination of simultaneous deformation mechanisms occurring at various length scales. A decrease in hierarchical organization (e.g., fascicles to fibrils) corresponds to an increased stiffness (Sasaki

and Odajima, 1996), which is indicative of sliding mechanisms occurring between adjacent structural components at higher hierarchical levels. Sliding has been documented at the molecular (Mosler et al., 1985), fibril (Fratzl et al., 1998), fiber (Cheng and Screen, 2007) and fascicle (Snedeker et al., 2009) levels of organization. Therefore, cross–links between structural units likely play a significant role in tendon deformation.

2.3 Mechanobiology

2.3.1 Mechanotransduction

Mechanobiology is the field of study that describes how cells respond to biophysical cues. Mechanical forces are translated into biochemical activity through a process called mechanotransduction. There are a number of mechanosensors capable of sensing forces by undergoing force–induced conformational changes. Through mechanotransduction, forces can modify protein synthesis, proliferation and other cellular mechanisms involved in tissue health and disease (Ingber, 2006). Although mechanotransduction was previously thought to influence only specialized cells, numerous cell types have been shown to respond to mechanical force, including tenocytes.

There are several components that contribute to mechanotransduction including the ECM, cytoskeleton, integrins, stretch–activated ion channels and surface processes (Ingber, 2006; Kjaer, 2004; Wang, 2006) (Figure 2.8). Of these components, integrins have been highlighted as a key structure that form focal adhesion complexes on the cellular membrane. The actin cytoskeleton binds to focal

adhesions and the cell nucleus, linking the two cellular structures. It has been suggested that forces are transmitted from the ECM to the nucleus through the focal adhesion–actin cytoskeleton pathway (Schwartz, 2010) causing deformation of the nucleus and consequently a biochemical response.

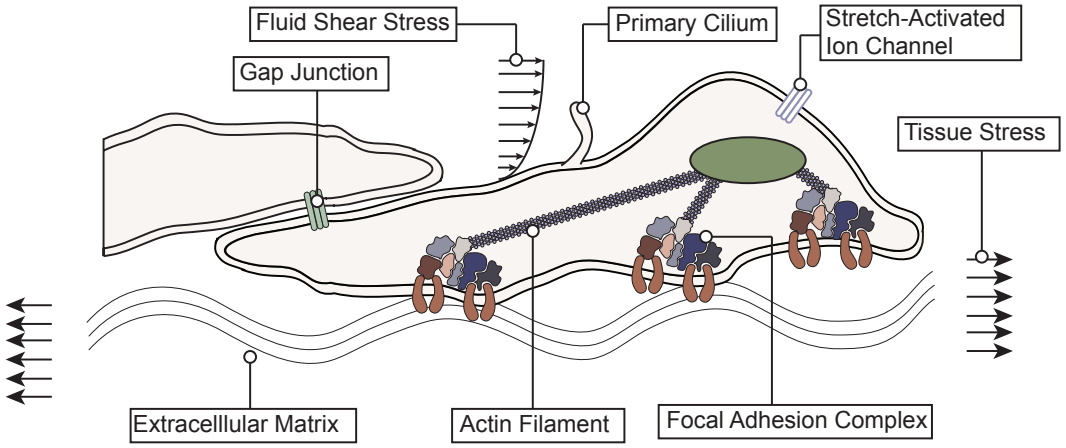

Figure 2.8: Mechanotransduction mechanisms. Potential mechanosensors in tendon including the primary cilium, stretch–activated ion channels and the focal adhesion complex. Fluid shear stress and tissue stress are two examples of mechanical stimulus that have been shown to induce a biological response in cells.

The mechanical environment of mechanosensors is dependent on the architecture of the surrounding tissue. Hierarchical structures have been suggested to focus forces onto mechanosensitive components by transmitting load along specific pathways (Ingber, 2006). Modification of these pathways (e.g., tissue degradation) could lead to disruption of tissue homeostasis.

2.4 Tendon Injury and Disease

2.4.1 Tendinopathy

Tendinopathy is a general term that describes the pathology of tendon including tendinitis and tendinosis. Tendinitis involves an inflammatory repair response and tendinosis arises from an imbalance between the synthesis and degradation of the ECM (Selvanetti et al., 1997). Although the term tendinitis is commonly used to described tendinopathy, many injuries do not involve an inflammatory response and the term tendinopathy should be used prior to diagnosis of the specific pathological condition.

Tendon disorders can be broadly categorized as being acute or chronic. Acute injuries typically occur when a limb is forcefully moved against a strong muscle contraction. High stress is placed on the tendon leading to a strain injury or complete rupture. Eccentric contractions impose high stresses on the muscle–tendon unit (Curwin and Stanish, 1984) and occur when a muscle contracts as the muscle–tendon unit lengthens, e.g., during uphill running or slipping off a step. Age, gender, anatomical location and tendon microstructure are a few factors that are associated with tendon failure. The etiology of spontaneous tendon rupture is not well understood, but has been attributed to intrinsic abnormalities present prior to rupture (Ker, 2007). It has been found that cumulative microdamage can occur from stresses that fall within the physiological range if the tissue is not given sufficient time to heal (Selvanetti et al., 1997). Therefore, spontaneous tendon rupture may occur unexpectedly as a result of cumulative microdamage reducing the mechanical integrity of the tissue. It has been estimated that two–

thirds of Achilles tendon ruptures involve prior mechanical damage to the tissue (Kvist, 1994).

Chronic overuse injuries involve a failed healing response that leads to abnormal production of ECM structural molecules. Overuse injuries can occur at the MTJ, the OTJ, or the midsubstance, i.e., middle of tendon, of tendon. The most commonly injured tendons are the Achilles tendon, Patellar tendon, Extensor Carpi Radialis Brevis tendon and Rotator Cuff (Khan et al., 1999) (Figure 2.9). There are a numerous changes that occur during overuse injuries including an increased ratio of type III to type I collagen, change in collagen fibril structure, alteration of cell shape and infiltration of blood vessels (Åström and Rausing, 1995; Maffulli, 1998). The origin of pain in chronic injuries is not well understood, but may occur from mechanical disruption of the tissue. Tissue degeneration is often associated with patients that have suffered from midsubstance injuries (Kannus and Jozsa, 1991) and therefore, acute disorders may have significant long–term consequences that involve a poor healing response.

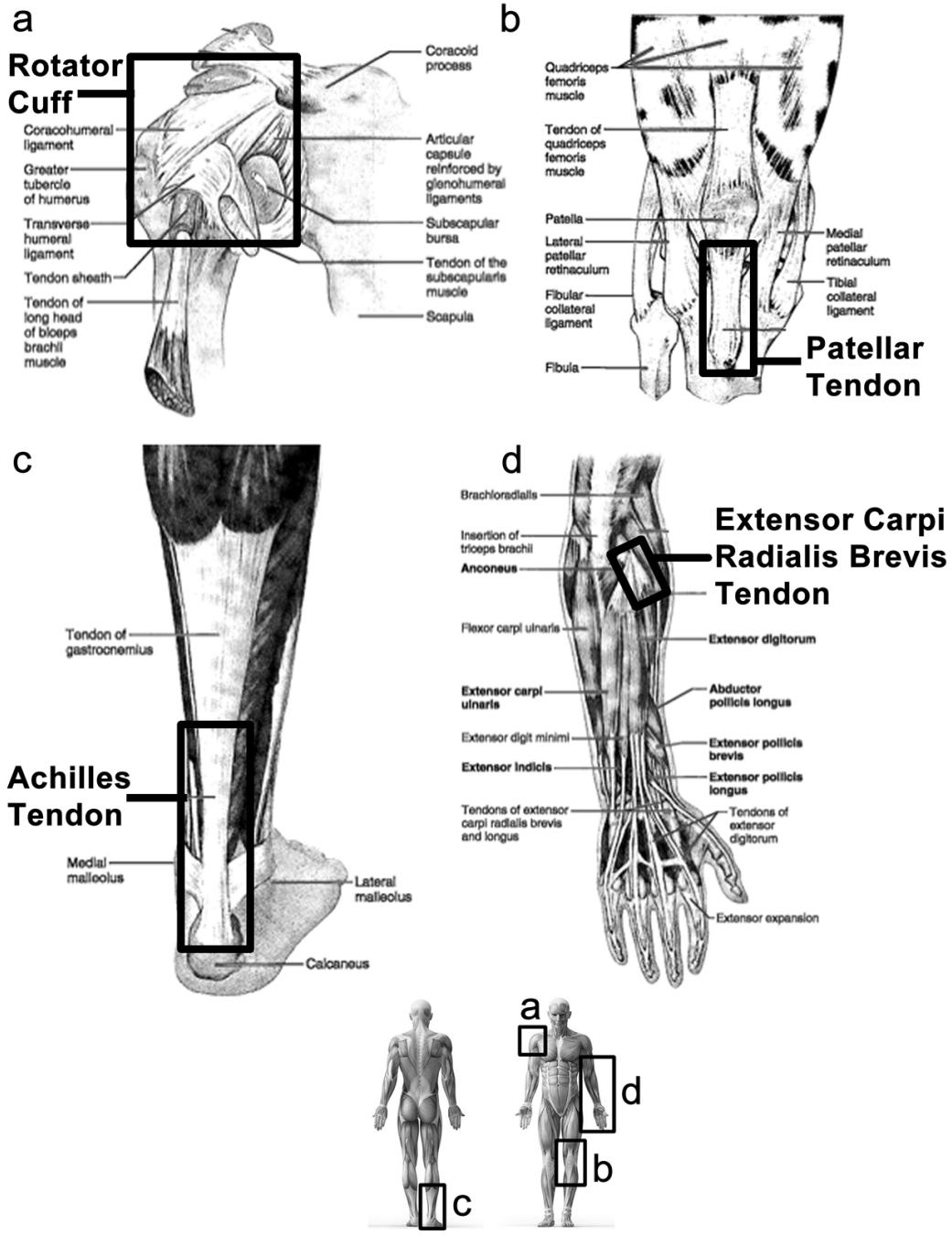

Figure 2.9: Commonly injured tendons in the human body. (a) Rotator cuff composed of multiple tendons and ligaments. (b) Patellar tendon positioned below the patella. (c) Achilles tendon that is responsible for transmitting large forces during locomotion. (d) Extensor carpi radialis brevis tendon commonly injured in racquet sports. Diagrams modified from Marieb and Hoehn (2007).

Chapter 3

Organization of Elastic Fibers in Tendon

3.1 Introduction

3.1.1 Ultrastructure of Elastic Fibers

As introduced in Section 2.1.1, tendon is primarily composed of collagen fibrils, but also consists of other structural molecules whose organization and function are yet to be defined. For example, tendon consists of 2% elastin (dry weight), but its organization and role are not well understood. To better understand the function of elastic fibers in tendon I examine the detailed organization of elastin and microfibrils in this chapter.

Elastic fibers are composed of an elastin core and are surrounded by a sheath of microfibrils (Mithieux and Weiss, 2005), which are largely composed of fibrillin–1 and fibrillin–2 (Ritty et al., 2002; Smith and Fazzalari, 2009) (Figure 3.1). The role

of the microfibril sheath is unknown, but has been suggested to act as a scaffold for tropoelastin deposition during elastogenesis (Kielty, 2006). The terms elastin fiber and elastic fiber are commonly interchanged in the literature, but refer to distinct structures. Elastic fibers contain variable concentrations of elastin and have been categorized accordingly: elastin fibers contain approximately 90% elastin, elaunin fibers contain small levels of elastin and oxytalan fibers are entirely composed of microfibrils (Montes, 1996).

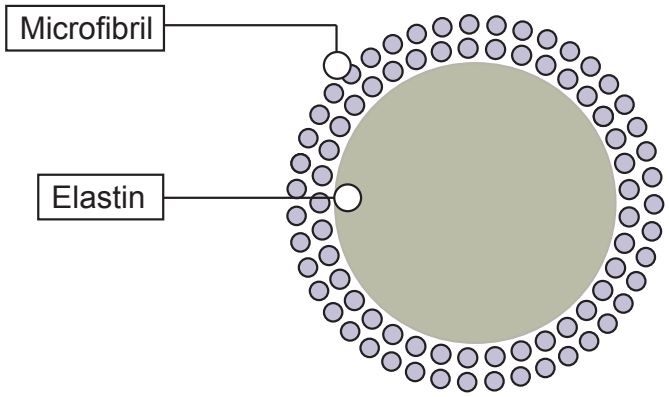

Figure 3.1: Elastic fiber ultrastructure. Elastic fibers consist of an elastin core that is surrounded by a microfibril sheath primarily composed of fibrillin–1 and fibrillin–2.

3.1.2 Mechanical Properties of Elastic Fibers

Elastic fibers are found in a range of dynamic tissues and have been suggested to contribute to the elastic recoil and low stress–strain response of tissue. The elastic modulus of elastin is approximately 300–400 kPa (Fung, 1993) and microfibrils are 7–96 MPa (Sherratt et al., 2003). The modulus of an elastic fiber is dependent on the ratio of elastin to microfibrils and has been found to vary between 300–600 kPa

(Mithieux and Weiss, 2005). The diameters of elastic fibers are generally larger than those of collagen fibrils and has been shown to be approximately 200–800 nm (Lorber, 1989).

Elastin is best known for its unique ability to sustain large deformations of up to 100–220% of its initial length (Fung, 1993). Consequently, tissues that are exposed to large deformations, such as blood vessels, typically contain significant quantities of elastin. The ability of elastic fibers to elongate is thought to be the result of an entropic process, where stretching fibers decreases the total entropy of the system (Aaron and Gosline, 1981). Moreover, elastic fibers have been shown to sustain water loss when stretched suggesting that there is a viscoelastic effect (Green et al., 2014).

A further understanding of elastic fiber function can be achieved by analyzing genetic disorders that involve elastic fiber components. Marfan Syndrome is a fibrillin–1 genetic disorder and leads to joint hypermobility while Beals Syndrome is a fibrillin–2 disorder and causes joint contractures (Gupta et al., 2002; Urbán and Boyd, 2000).

3.1.3 Distribution of Elastic Fibers in Tendon

Much of what is known about the organization of elastic fibers in tendon has been derived from TEM studies. However, gauging the overall distribution using this technique is difficult due to the high magnifications involved. Ritty et al. (2002) performed the first in–depth immunohistological study of elastic fibers in tendon. They found that elastic fibers run parallel to collagen fibrils and areas of tissue exposed to large strains have increased levels of elastic fibers. More recently, Smith

et al. (2011) found that elastic fibers are distributed parallel to collagen fibrils and between fascicles in ligaments.

3.1.4 Analysis of Elastic Fibers with Multiphoton Microscopy

Multiphoton microscopy (MPM) is a nonlinear imaging technique involving the simultaneous absorption of two photons that can be used to generate structural images of biological tissue (Figure 3.2). This microscopic technique is particularly valuable due to its ability to simultaneously characterize the elastin organization through the two photon fluorescence (TPF) signal and the collagen organization through the second harmonic generation (SHG) signal without the use of stains.

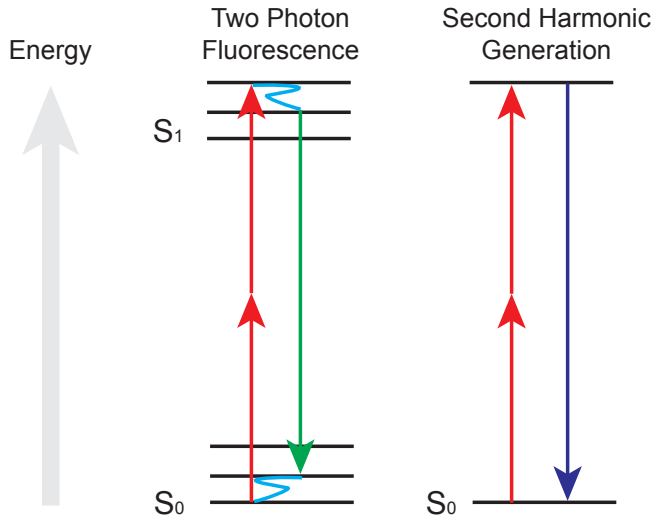

Figure 3.2: Multiphoton microscopy imaging modalities. Two photon fluorescence requires the coincidence of two photons of the same energy to stimulate the emission of a single photon of higher energy. Second harmonic generation requires two photons, typically infra–red frequency, to stimulate the emission of a single visible photon of exactly twice the energy of the coincident.

Elastin has been shown to autofluoresce at approximately 500 nm (Zoumi et al.,

2004), due to pyridinoline aggregates in the structure (Monici, 2005). When elastin absorbs two photons at a suitable excitation wavelength it becomes excited and releases fluorescence, i.e., the TPF signal, upon relaxation. This property has been used in numerous studies to analyze the organization of elastin. The SHG signal does not involve the absorption and release of a photon, but rather the instantaneous conversion of two photons into a single photon of half the wavelength due to interaction with highly organized structures such as noncentrosymmetric crystals (Theodossiou et al., 2006). The structure of fibrillar collagens, such as types I, II, III, satisfy this geometric requirement and act as SHG sources.

3.1.5 Aims and Objectives

The aim of this chapter was to characterize the detailed organization of elastic fibers in healthy and damaged tendon to better understand the contribution of elastic fibers to tendon mechanics. The first objective involved immunostaining tendon specimens with elastin, fibrillin–1 and fibrillin–2 antibodies and analyzing the distribution with confocal microscopy. These images were compared to traditional histological staining techniques to determine if they yielded a similar organization without the use of stains. Moreover, a MPM analysis was conducted on fresh tendon to establish if the technique could be used to efficiently characterize the elastic fiber organization. The second objective was to analyze the organization of elastic fibers in damaged specimens to identify any changes in tendon structure. Biopsies were gathered from human supraspinatus tendon (n=81) and elastic fibers were highlighted using traditional staining techniques.

3.2 Materials and Methods

3.2.1 Sample Collection and Preparation

Deep digital flexor tendons were excised from 10 young adult steers (18–24 months). Samples of approximately 25 mm^3 were dissected from the midpoint of tendon as depicted in Figure 3.3. In addition to bovine specimens, the organization of elastic fibers in human supraspinatus tendon was analyzed. With the help of Dr. Richard Murphy (Botnar Research Institute), 71 tendon biopsies were gathered from patients with normal (n=16) and damaged (n=55) tissue under ultrasound guidance (Figure 3.4). The study was approved by the local Research Ethics Committee.

Bovine and human tendon specimens intended for histological staining were fixed in 10% formalin for 24 h, dehydrated in increasing concentrations of ethanol and then incubated in xylene. Following dehydration, samples were embedded in paraffin wax, allowed to harden for 24 h and then cut into 5 μm serial sections using a microtome. The orientation of specimens was maintained between slides to allow for comparison between serial sections. Slides were heated at 65°C for 24 h to adhere specimens to the surface and then stored at room temperature prior to staining.

Bovine tissue specimens intended for IHC were snap frozen in liquid nitrogen and immediately embedded in optical cutting temperature (OCT) compound (Sakura Finetek, USA). Transverse and longitudinal sections were acquired by slicing specimens at 20 μm increments using a cryostat at -20°C. The sections were adhered to slides (VWR International Ltd, UK) and then stored at -80°C prior to immunostaining.

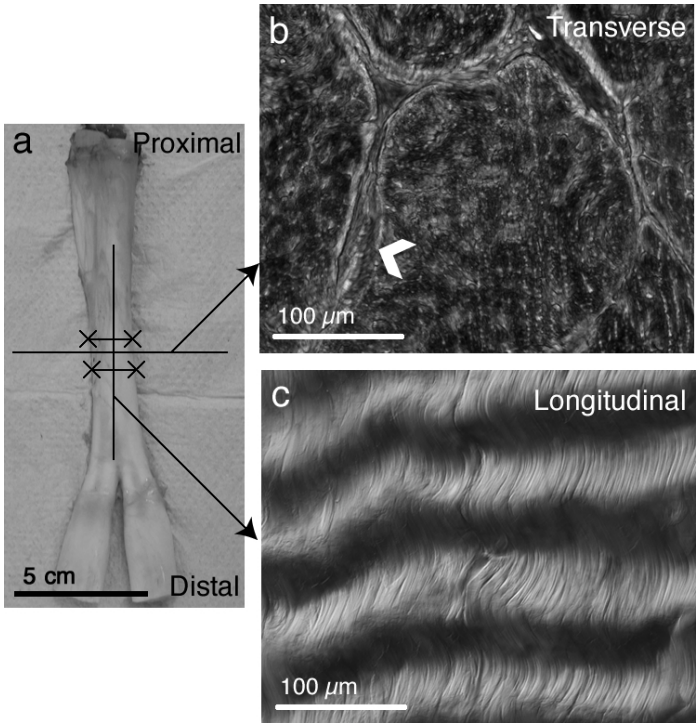

Figure 3.3: Location of bovine flexor tendon dissections for transverse and longitudinal sections. (a) Bovine flexor tendon with excision area indicated by solid lines (X—X). Vertical and horizontal lines (+) represent longitudinal and transverse cutting planes, respectively (b) Transverse section depicting endotenon sheath (arrowhead) enclosing tendon fascicles. (c) Longitudinal section highlighting crimped organization. (Grant et al., 2013) with permission from John Wiley and Sons.

3.2.2 Histological Staining and Immunostaining of Elastic Fibers

Bovine and human histological sections were rehydrated in decreasing concentrations of ethanol and finally phosphate buffered saline (PBS) . Serial sections were stained using hematoxylin and eosin (H&E) for general structure and Miller's stain for elastic fibers. The H&E stain indicated the location of cells and the overall organization of fibril crimp and the Miller's stain highlighted elastic fibers black

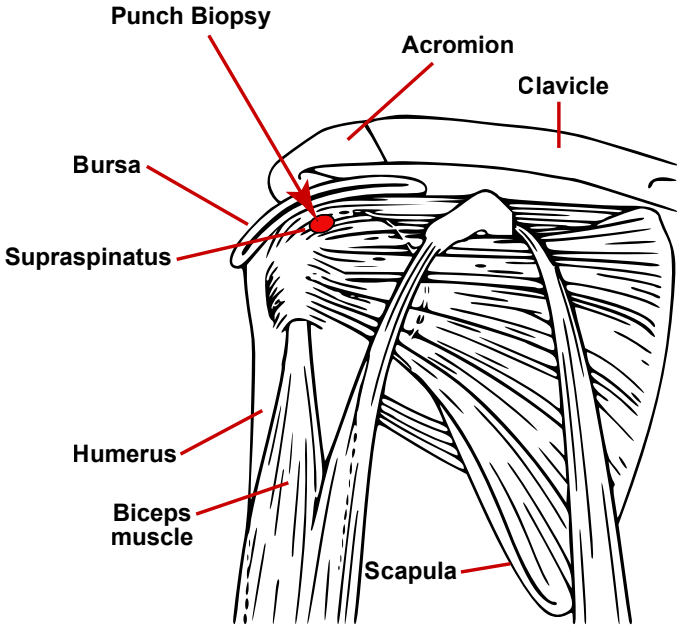

Figure 3.4: Location of supraspinatus tendon biopsy. Circle represents the area where tissue is removed under ultrasound guidance. Modified from the National Institute of Arthritis and Musculoskeletal Diseases.

and collagen in red.

Frozen bovine sections intended for IHC were rinsed for three minutes in PBS and then blocked using 10% normal donkey serum (Stratech Scientific, UK). Excess blocking reagent was removed from the specimen after 30 min, which was then incubated with the fibrillin–1 antibody (Table 3.1) for 24 h at 4°C. Specimens were then rinsed three times with PBS and incubated for 40 min in the secondary antibody. An identical protocol was used for the second primary antibody (elastin or fibrillin–2) on the same tissue specimen. Following immunostaining, cell nuclei were highlighted by applying 4',6–diamidino–2–phenylindole (DAPI) mounting media (Vector Laboratories, UK) to tissue specimens.

Table 3.1: Primary and Secondary Antibodies Used for Immunohistochemistry

	Primary Antibody	Secondary Antibody
Elastin	Anti-human alpha elastin raised in rabbit, 1:50 (AbD Serotec, UK; Cat. No. 4060-1054, Batch No. 20092751)	Dylight-488 conjugated donkey anti-rabbit IgG, 1:100 (Stratech Scientific, UK; Cat. No. 712-485-153)
Fibrillin-1	Anti-bovine fibrillin-1 raised in mouse, 1:50 (Abcam, UK; Cat. No. ab3090)	Cy3-conjugated donkey anti-mouse IgG, 1:100 (Stratech Scientific, UK; Cat. No. 715-165-151)
Fibrillin-2	Anti-human fibrillin-2 raised in rabbit, 1:50 (Elastin Products, USA; Cat. No. PR225)	Dylight-488 conjugated donkey anti-rabbit IgG, 1:100 (Stratech Scientific, UK; Cat. No. 712-485-153)

(Grant et al., 2013) with permission from John Wiley and Sons.

To test for nonspecific staining, negative controls were analyzed by omitting the primary antibody from the immunostaining protocol. Moreover, primary and secondary antibodies were used to immunostain bovine artery specimens as a positive control.

3.2.3 Light, Confocal, and Multiphoton Microscopy

Histological sections were analyzed using an upright light microscope (Zeiss, USA) at 100x magnification and images were captured using a color camera and AxioVision software (Zeiss, UK).

Immunohistological sections were analyzed using an LSM 710 inverted confocal laser–scanning microscope (Zeiss, UK). Red, green and blue channels were defined

using digital filters corresponding to the emission spectrum of the secondary fluorophores. Both 40x and 63x objective lenses were used to analyze the elastic fiber organization. The detailed 3D tissue structure was extracted by performing z–stack imaging at 0.9 μm intervals. Images were captured using Zen 2010 (Zeiss, UK) and then analyzed in Image J (NIH, USA).

Cryosections were stained with DAPI (Invitrogen, UK) and analyzed with MPM using an LSM 710 confocal microscope fitted with a tunable pulsed femtosecond titanium–sapphire Chameleon laser (Coherent, UK) operating at 860 nm. Both 40x and 63x oil immersion objective lenses were used to analyze the organization in channel and nondescanned modes. The SHG signal was collected at 430 nm and the TPF signal at 520 nm in channel mode and band pass filters (430/50 and 520/40 nm) were used to collect images in nondescanned mode. SHG and TPF signals were collected in the forward direction and the average power at the sample was 15 mW and the spectra acquisition time was eight seconds.

3.2.4 Image Analysis of Healthy and Damaged Tendon

A magnification of 100x was required to observe elastic fibers in Miller's stained specimens (n=81). As a result, only a very small portion of the tissue was visible in each image. To better represent the overall distribution a 10x10 grid was assigned to each specimen and 5 random cells chosen for analysis (Figure 3.5). The position of the objective lens was used to orientate the specimen to the location of interest. The origin of the specimen (healthy or damaged) was not identified prior to imaging to allow for qualitative analysis of the tissue under blind experimental conditions.

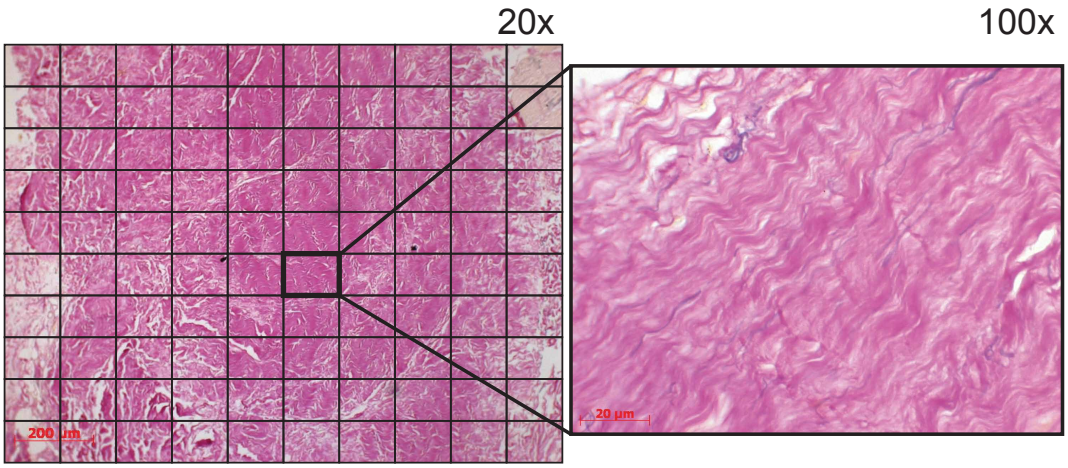

Figure 3.5: Analysis of human supraspinatus tendon. Tendon specimens are divided into a 10x10 grid and five random elements are analyzed at 100x objective lens magnification to observe elastic fibers.

3.3 Results

3.3.1 Overall Organization of Elastic Fibers in Tendon

Elastic fibers were distributed parallel to tendon and had a wavy configuration as indicated by histology and IHC (Figure 3.6 and Figure 3.7). Multiple elastic fibers surrounded arrays of tenocytes and were distributed between collagen fascicles. Fibrillin–1 and fibrillin–2 strongly colocalized, but fibrillin–1 was occasionally observed independent of elastin. Elastin immunostaining appeared weaker than fibrillin–1 and fibrillin–2 and results were consistent between all specimens. Positive controls indicated that elastin, fibrillin–1 and fibrillin–2 highlighted elastic fibers in bovine artery and negative controls indicated that results were not significantly affected by nonspecific staining (data not shown).

Histological staining of elastic fibers depicted a much sparser distribution than

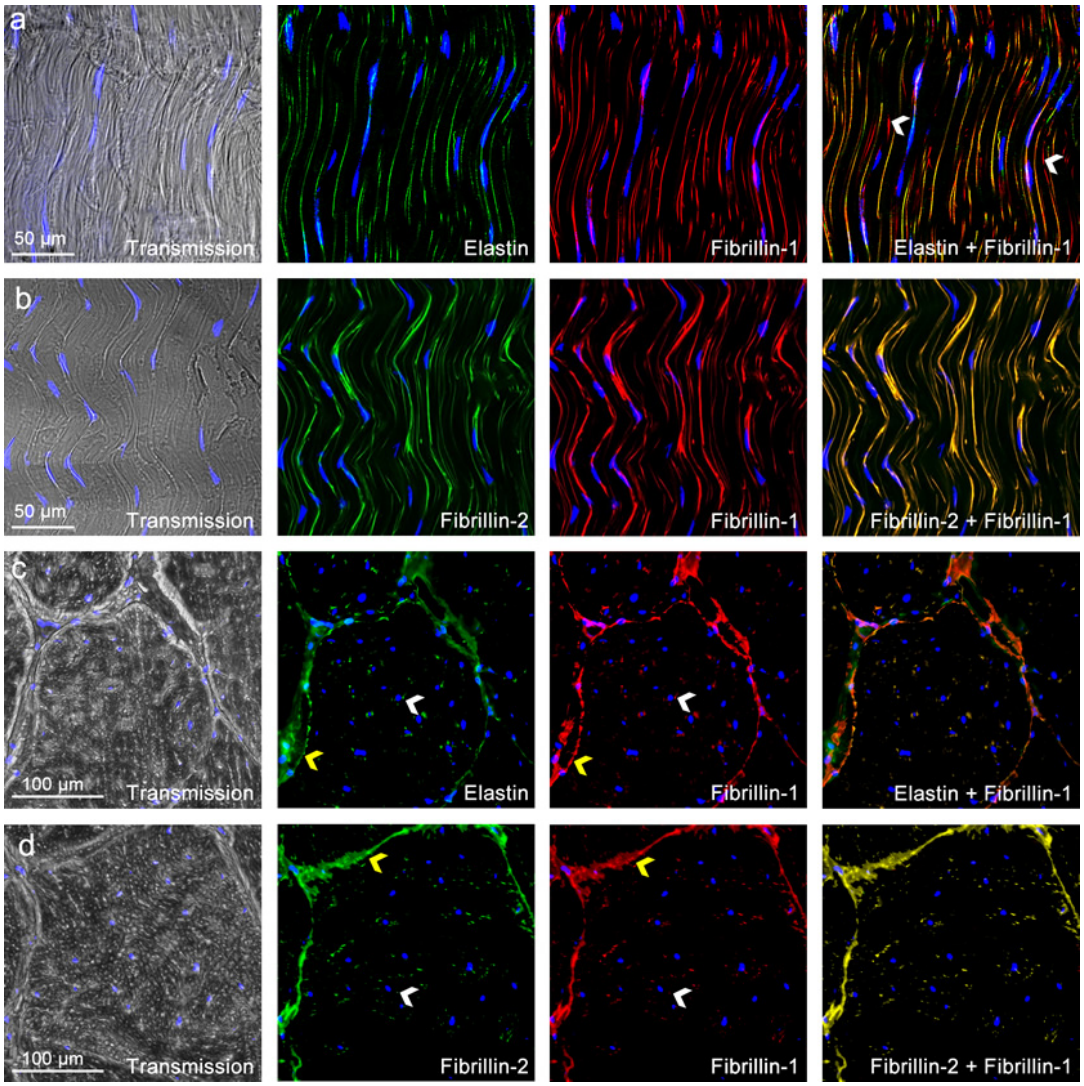

Figure 3.6: Overall distribution of elastin, fibrillin–1 and fibrillin–2 in tendon. (a) Longitudinal section: Both elastin and fibrillin–1 appear to have a wavy organization and travel parallel to tendon. Fibrillin–1 is occasionally found independent of elastin (arrowhead). (b) Longitudinal section: Fibrillin–1 and fibrillin–2 travel parallel to tendon and always colocalize. (c) Transverse section: Elastin and fibrillin–1 appear as points within tendon (white arrowhead) and are heavily distributed between fascicles (yellow arrowhead). (d) Transverse section: Fibrillin–1 and fibrillin–2 are deposited around cells (white arrowhead) and between fascicles (yellow arrowhead) and are highly colocalized. (Grant et al., 2013) with permission from John Wiley and Sons.

IHC (Figure 3.7). However, elastic fibers were observed to be longitudinally oriented and had a wavy structure. Through alignment of Miller's and H&E serial sections it was found that elastic fibers were distributed in the vicinity of arrays of tenocytes. Elastic fiber organization in bovine and human specimens was very similar.

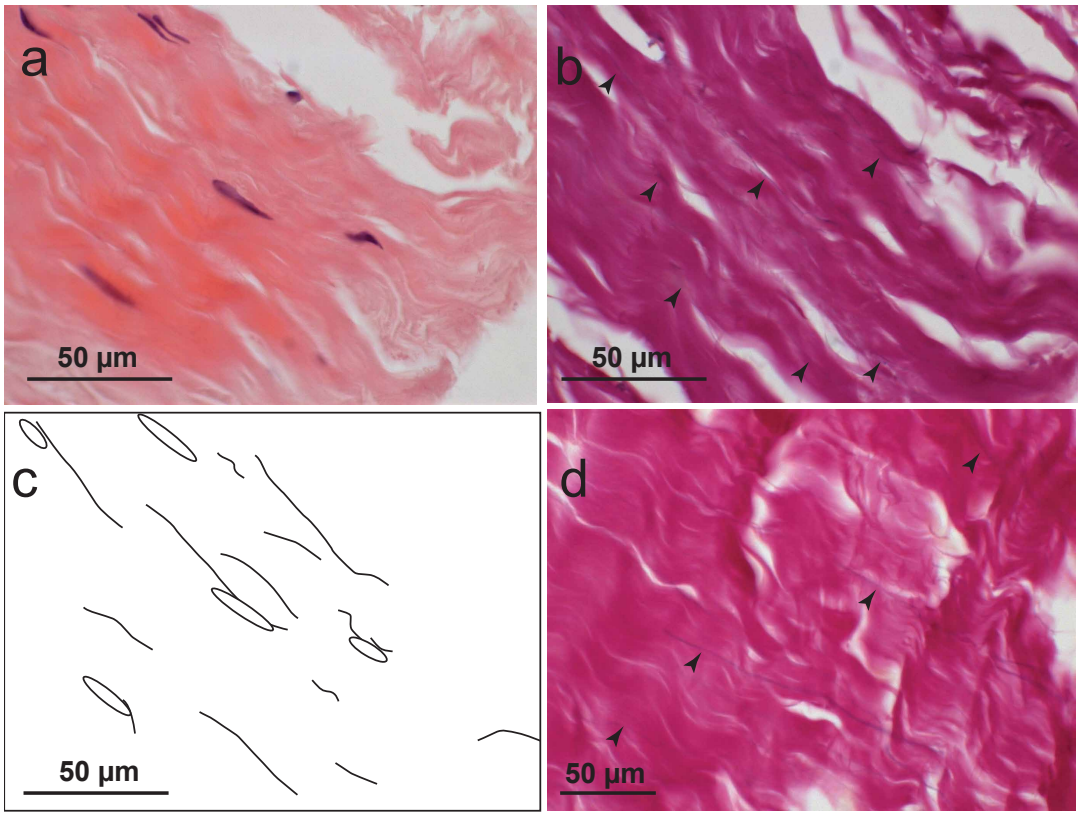

Figure 3.7: Histology of bovine and human tendon. (a) H&E stained human specimen highlighting the general structure of tendon with longitudinally aligned tenocytes (b) Miller's stained human serial section depicting sparse elastic fiber distribution (arrowheads). (c) Outline of tenocytes and elastic fibers as generated from H&E and Miller's stained specimens with elastic fibers distributed around cells. (d) Miller's stained bovine tendon specimen indicating similar elastic fiber distribution (arrowheads) to human tendon.

The MPM analysis provided similar results to histological and immunohisto-

logical staining (Figure 3.8). As indicated by the TPF signal, elastic fibers ran parallel to collagen fibrils and were distributed in the vicinity of cells. Elastic fibers in MPM images appeared to be thinner and sparser than immunohistological results. When increasing the laser power more elastic fibers were visible, but the specimen became quickly damaged. Collagen fibrils as indicated by the SHG signal had a crimped organization and had a relatively constant wavelength and crimp angle.

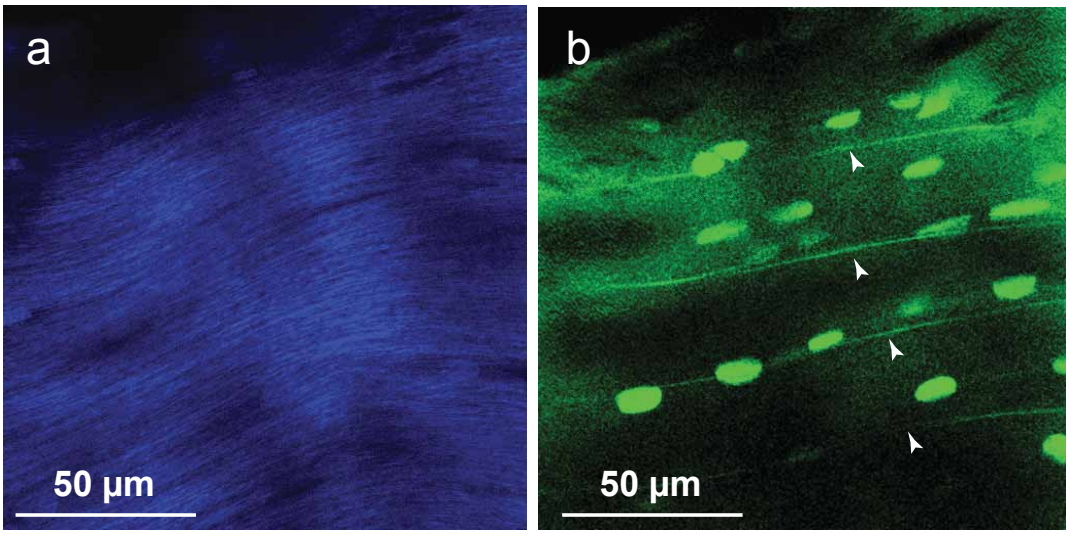

Figure 3.8: MPM analysis of tendon. (a) SHG signal showing collagen fibril structure. (b) TPF signal depicting elastic fibers (arrowheads) running parallel to arrays of DAPI stained cell nuclei.

3.3.2 Specific Localization of Elastic Fibers in Tendon

In transverse images elastic fibers were observed as points as they intersected the cutting plane (Figure 3.9). Within tendon fascicles, the elastic fiber density was greatest around arrays of tenocytes (Figure 3.10). Elastic fibers distributed around

cells almost always contained elastin whereas fibers present between arrays of cells occasionally contained only fibrillin–1.

A mesh–like distribution of elastic fibers was observed between fascicles. Blood vessels and lymphatics were also immunostained by the protocol and were deposited in the interfascicle space (Figure 2.5). There was more fibrillin–1 and fibrillin–2 present between fascicles than elastin.

3.3.3 Distribution of Elastic Fibers in Damaged Tissue

Following a qualitative analysis of elastic fiber organization in human tendon biopsies significant differences were observed between control (n=16, 80 images) and damaged specimens (n=55, 275 images) (Figure 3.11). Control tendons contained a sparse distribution of elastic fibers within a dense matrix. However, with increasing severity of injury, the visibility of elastic fibers increased and the organization of elastic fibers became more disordered.

3.4 Discussion

3.4.1 Overall Organization of Elastic Fibers

Results of the present chapter indicated that elastic fibers were mainly distributed around arrays of tenocytes and between tendon fascicles. Elastic fibers surrounding arrays of cells were oriented parallel to tendon in contrast to fibers present between fascicles that had an oblique orientation. There was strong colocalization between elastin, fibrillin–1 and fibrillin–2, however, fibrillin–1 was occasionally observed independent of elastin.

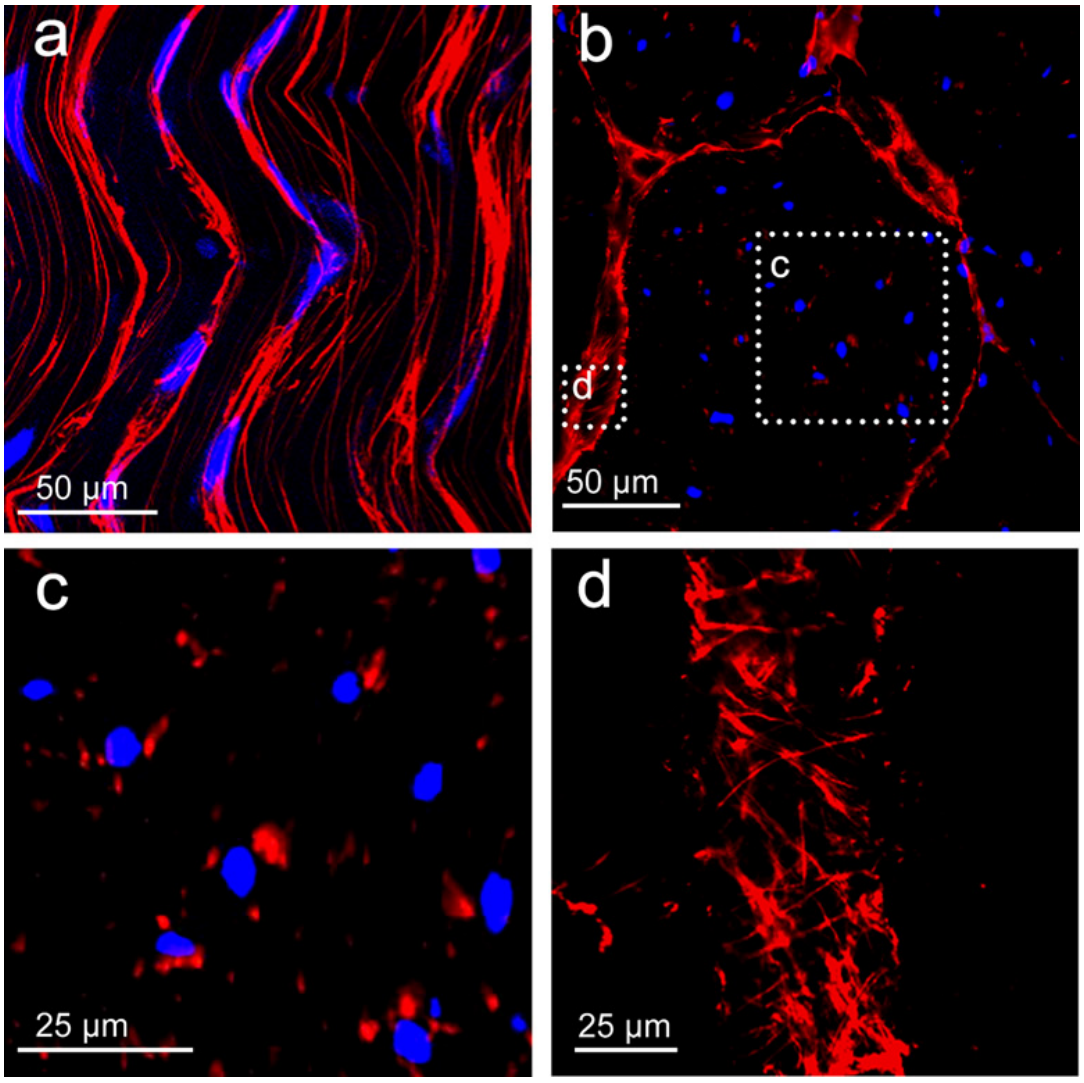

Figure 3.9: Specific organization of elastic fibers in tendon as observed with fibrillin–1 IHC (red) and DAPI (blue). (a) Merged z–stack (total depth 10 μm) longitudinal image depicting multiple elastic fibers surrounding arrays of tenocytes. (b) Transverse image highlighting two regions of tendon that contain high concentrations of elastic fibers. (c) Multiple elastic fibers surrounding cell nuclei in transverse section. (d) Obliquely oriented elastic fibers in the interfascicle space of tendon as observed in transverse section. (Grant et al., 2013) with permission from John Wiley and Sons.

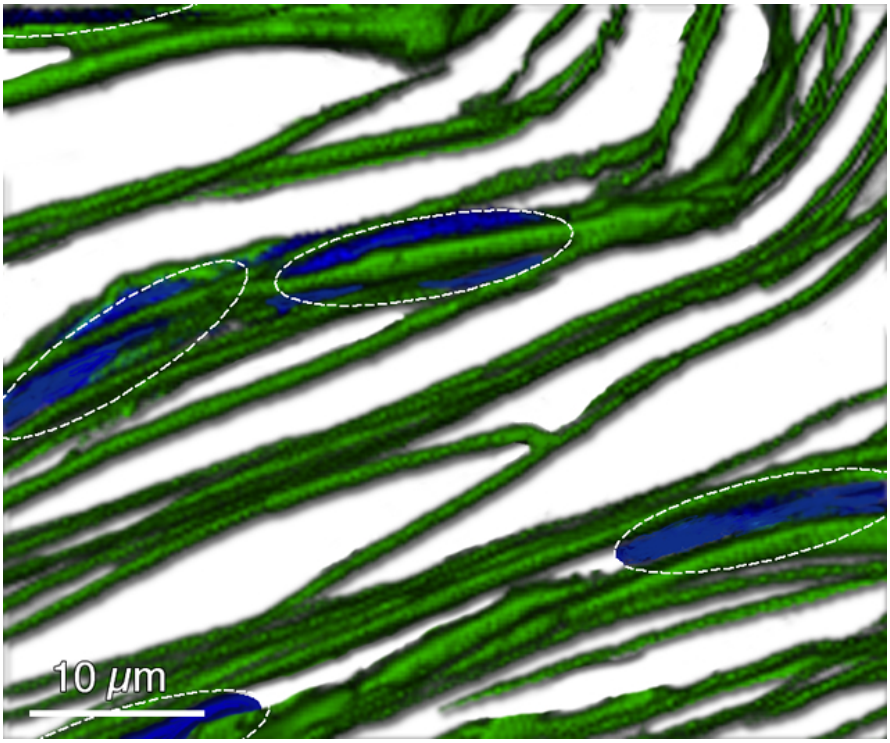

Figure 3.10: 3D reconstruction of elastic fibers and tendon nuclei. Multiple elastic fibers (elastin immunostaining, green) surround arrays of cells (DAPI, blue). Branching of elastic fibers occurs at multiple locations. (Grant et al., 2013) with permission from John Wiley and Sons.

Samples obtained from the midsubstance of bovine tendon had very little variation in elastic fiber organization. However, the distribution likely varies between regions of tendon that are exposed to different mechanical environments, such as the MTJ and OTJ. Ritty et al. (2002) provided evidence for this hypothesis by showing increased concentrations of elastin in regions of tendon that experience large deformations. The occasional lack of colocalization of fibrillin–1 and elastin suggests that there was a range of elastic fiber types present in tendon, including oxytalan fibers. The inclusion of multiple fiber types, each with different mechanical properties, may enhance the ability of tendon to address local

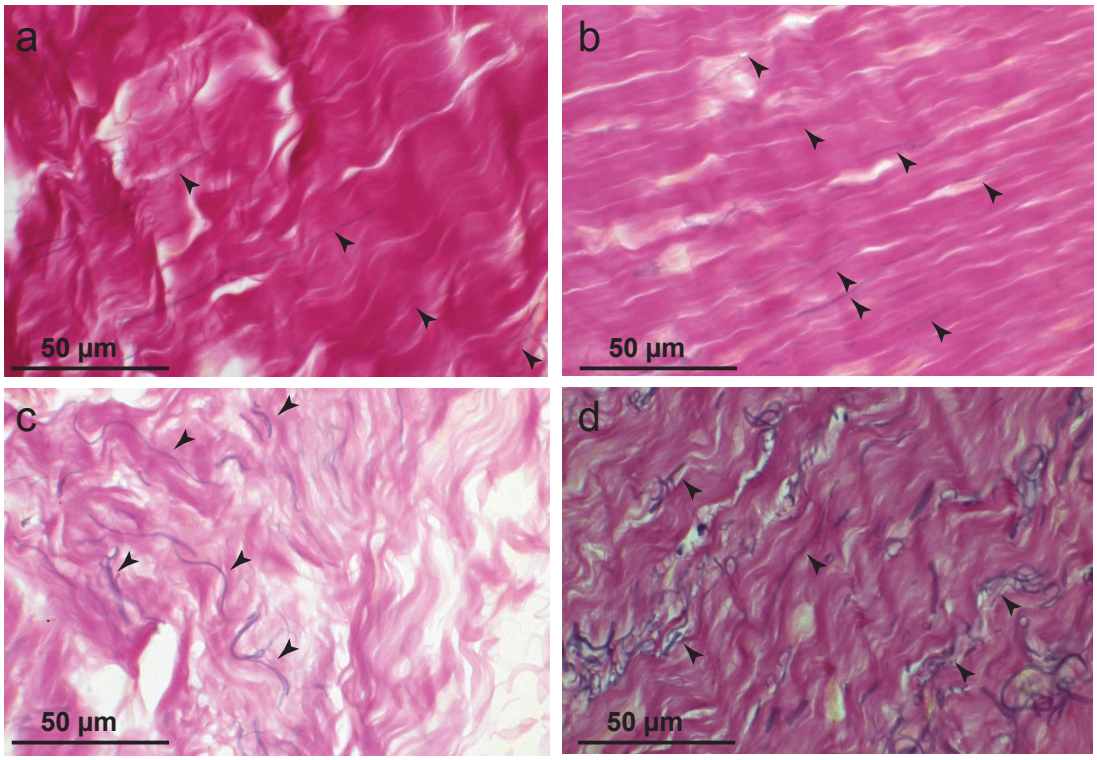

Figure 3.11: Representative elastic fiber organization of healthy and damaged human supraspinatus tendon. (a) Control specimen illustrating elastic fibers aligned parallel to tendon. (b) Sample from patient with small rotator cuff tear. Elastic fibers have a slight increase in visibility. (c) Sample from patient with shoulder impingement. Tissue appears disorganized and there is an increased elastic fiber presence. (d) Sample from patient with large rotator cuff tear showing a dramatic increase in the visibility of elastic fibers.

tissue mechanics. It is also expected that the organization of elastic fibers varies with age, e.g., elastin fragmentation and further studies should be conducted to characterize the corresponding changes.

3.4.2 Elastic Fibers Distributed in the Pericellular Matrix

The PCM likely influences the micromechanical environment of cells and elastic fibers may play a role in maintaining tissue homeostasis through mechanobiological mechanisms. In cartilage and bone, it has been shown that there exists a specialized structure surrounding cells, i.e., the PCM, but the presence of a similar structure in tendon is yet to be fully realized. My results suggest that elastic fibers contribute to the PCM in tendon and that the PCM forms a continuous structure around arrays of cells. The PCM consists of multiple structural molecules and other studies have shown that type VI collagen (Ritty et al., 2003) and perlecan (Hayes et al., 2011) are also deposited in the vicinity of tenocytes.

Human tendon specimens indicated that the elastic fiber organization was significantly disorganized in damaged specimens compared to controls. If elastic fibers do contribute to the micromechanical environment of tenocytes as I have suggested a disruption could significantly impact tissue homeostasis through mechanobiological pathways. Further work is required to determine the impact of a disrupted elastic fiber organization on tendon function.

The elastic fibers that were distributed between tendon fascicles were likely part of the endotenon sheath. In previous studies a similar organization was observed in both ligaments (Smith et al., 2011) and tendons (Caldini et al., 1990). As discussed in Section 2.1.2 the endotenon sheath binds collagen fibrils and provides lubrication between adjacent structures. Tendon has a hierarchical deformation and sliding has been observed between tendon fascicles (Snedeker et al., 2009). The high density of elastic fibers in the endotenon sheath suggests that the structure experiences large deformations. Fibers may also provide mechanical support to

blood vessels that travel between fascicles.

Although elastic fibers serve an important mechanical role in many dynamic tissues, their function may involve the regulation of growth factor availability. Fibrillin–1 has the ability to bind cytokines, such as transforming growth factor beta (TGF–β) (Vehvilainen et al., 2009), which may be released upon damage to the PCM. This process would initiate an important response to tendon damage and encourage tissue remodeling. As introduced in Section 3.1.2. the clinical features of Marfan (fibrillin–1 disorder) and Beals (fibrillin–2 disorder) syndrome include joint hypermobility and joint contractures, respectively. Interestingly, these two genetic disorders have seemingly opposite effects on joint mechanics, which may be the result of growth factor availability during development.

3.4.3 Mechanical Contribution of Elastic Fibers

Previous studies have hypothesized that elastic fibers contribute to the macroscopic mechanical properties of tendon similar to their well–established role in blood vessels. However, my results indicated that elastic fibers had a relatively sparse distribution in tendon. Through a simple rule of mixtures analysis as derived in Appendix A we can better understand the mechanical contribution of various structural molecules to tendon. Using images from this chapter to calculate the area contribution of elastic fibers to the ECM and PCM we can estimate the stiffness contribution using the rule for mixtures analysis. Results from this analysis suggest that elastic fibers do not significantly influence the macroscopic axial elastic modulus of the ECM (<1% stiffness contribution), but do contribute to the axial elastic modulus of the PCM (28% stiffness contribution). Elastic fibers

may influence other mechanical properties, such as viscoelastic effects and further investigation will be required to determine if they contribute to the macroscopic properties of tendon.

3.4.4 Multiphoton Microscopy of Tendon

To the best of my knowledge, MPM has not been used to investigate the elastic fiber organization of tendon. Due to the dense collagen structure it was difficult to visualize elastic fibers within the tissue and there was a trade–off between laser power and tissue integrity. Higher powers ($>$ 15 mW) were found to greatly improve the visualization of elastin, but the tissue became quickly damaged. The SHG signal clearly highlighted collagen fibrils and did not require a high laser power. Currently, IHC provides superior visualization of elastic fibers compared to the TPF signal in tendon, but improvements in imaging techniques using MPM may lead to superior images.

3.5 Conclusion

In conclusion, I found that elastic fibers were heavily distributed around arrays of tenocytes and between tendon fascicles. My interpretation of these results was that elastic fibers contribute to the PCM and endotenon sheath of the tissue. Damaged tendon was found to have a significantly disorganized elastic fiber network, which may influence the mechanical properties of the cellular microenvironment and/or the interaction of tendon fascicles.

Chapter 4

Effect of Elastase on the Structure and Function of Tendon

4.1 Introduction

4.1.1 Use of Enzyme Treatments to Analyze Tissue Mechanics

As shown in Section 3.3.1 elastic fibers have a sparse distribution in tendon, but are highly localized around arrays of cells and between fascicles. In view of this sparse distribution it is not apparent that elastic fibers contribute to the macroscopic mechanical properties of tendon. Researchers have postulated that elastic fibers contribute to the low stress–strain response and elastic recoil of tendon, however additional evidence is required to support or reject this hypothesis. Therefore, this chapter aims to investigate the mechanical role of elastic fibers in tendon using an enzyme treatment in combination with mechanical testing.

There are two major experimental techniques that have been used to measure the mechanical contribution of elastic fibers in dynamic tissues. The first technique involves isolating elastic fibers from the ECM followed by mechanically testing of the elastic fiber network. This can be accomplished through autoclaving specimens to degrade collagen (Melting Temperature (T_M) = 40–63°C) while leaving elastin intact (T_M = 200°C) (Lillie et al., 1994; Pezzin et al., 1976) or through a chemical treatment such as sodium hydroxide in formic acid or cyanide bromide (Vesely, 1997). Although both techniques have been successfully implemented for analyzing blood vessel mechanics, the sparse distribution of elastic fibers in tendon make this technique challenging (data not shown).

The second strategy is to use enzyme treatments to remove elastic fibers from the ECM and then perform mechanical characterization of the tissue. Elastase has been used in multiple studies to analyze the contribution of elastic fibers to the mechanics of various tissues including skin (Oxlund et al., 1988), aortic valves (Lee et al., 2001), esophagus (Fan et al., 2005) and intervertebral disk (Barbir et al., 2010). As a result of the nonspecific degradation of elastase (Banda et al., 1987) recent protocols have introduced protease inhibitors to limit undesired degradation of structural molecules.

4.1.2 Elastase Treatment of Tendon

There have been three major elastase studies conducted on tendon–like tissues to elucidate the mechanical role of elastic fibers. An early study conducted by Reihsner et al. (1991) analyzed the mechanical role of elastic fibers in human palmar aponeuroses. The palmar aponeurosis is a sheet of connective tissue in

the palm of the hand that aids in gripping objects and has a similar structure to tendon. They found that elastase increases the residual strain (ability of tissue to return to unloaded state following removal of load) and hysteresis of the tissue following treatment. The second study was an extension of their previous work and showed that elastase increases the failure strain of both palmar aponeuroses and palmaris tendon while the elastic modulus decreases (Millesi et al., 1995). More recently, Henninger et al. (2013) analyzed the mechanical role of elastic fibers in the medial collateral ligament (MCL). Their results suggest that elastase decreases the stiffness in the toe region, but does not influence the failure strain, elastic modulus, or hysteresis of the tissue. These conflicting results suggest that elastic fibers may serve a different mechanical function in tendon compared to ligament and/or that the elastase treatments used in each study have a different effect on the tissue.

4.1.3 Aims and Objectives

The aim of this chapter was to characterize the change in mechanics, structure, and composition of tendon treated with elastase to better understand the mechanical role of elastic fibers in tendon. The first objective was to analyze the degradation of a collagen–elastin scaffold to evaluate the specificity of the elastase treatment on a simple structure. The second objective was to characterize the quasi–static and viscoelastic response of tendon before and after treatment with elastase. These results would then be compared to previous reports and provide insight into the mechanical contribution of elastic fibers to tendon. The final objective was to analyze the nonspecific degradation of the elastase treatment using imaging and biochemical techniques to better understand the origin of any mechanical changes

in elastase–treated tendon specimens.

4.2 Materials and Methods

4.2.1 Tissue Collection and Preparation

Tails from Sprague Dawley rats (350 ±12 g, 3–6 months n = 12) were obtained from animals that were euthanized for an unrelated study. The skin was decontaminated with 5% ethanol and 10 fascicles (length = 20 cm) were excised from the distal region of each tail under a laminar flow hood within 60 min of sacrifice. The fascicles were placed in Dulbecco's Modified Eagle Medium (DMEM) with 10% fetal calf serum (FCS) and 1% penicillin–streptomycin to maintain tissue integrity.

4.2.2 Enzyme Treatment for Elastin Digestion

A modified elastase protocol from Oxlund et al. (1988) was used to treat tendon specimens. An elastase solution was created by combining 1 U/ml of purified elastase (Sigma E1250) in PBS (pH 8.6) with a trypsin inhibitor (0.1 mg/ml) (Sigma T6414) to reduce degradation of collagen. Three controls were run parallel to the elastase treatment to analyze the influence of the incubation period (fresh control), cell death (DMEM control) and exposure to a buffered solution (PBS control) on tendon structure and function. Fascicles were transferred into chambers of a 36–well plate containing DMEM (n=30), PBS (n=30), or elastase solution (n=30). The fascicles were then placed in an incubator (37°C, 5% CO_2) for 36 h.

4.2.3 Collagen–Elastin Scaffold Preparation

Freeze–dried collagen–elastin scaffolds (n=10) were prepared using type I collagen from bovine Achilles tendon (C9879, Sigma, UK) and elastin from bovine nuchal ligament (E1625, Sigma, UK) to characterize the degradation of elastase with the help of Qi Wang (Department of Materials). A 1:1 collagen–elastin weight ratio suspension was mixed in 0.05 M acetic acid (pH 3.2) (O'Brien et al., 2005) and cast into polytetrafluoroethylene cylindrical molds 15 mm in diameter. The suspension was cooled to -80°C and then placed in a freeze dryer (Christ I–5, UK) for 24 h in a vacuum at 5 Pa. The ice crystals were removed by sublimation, which left porous solid scaffolds. The scaffolds were placed into a 36–well plate and treated with PBS or elastase then incubated (37°C, 5% CO_2) for 36 h. Before and after incubation the scaffolds were imaged using MPM as described in Section 3.2.3 to characterize the organization of collagen and elastin.

4.2.4 Mechanical Testing of Tendon Specimens

A tensile testing machine (Bose, UK) was used to characterize the mechanical properties of treated rat tail tendon fascicles (RTTFs) (Figure 4.1). A PBS bath at room temperature (24°C) was used to hydrate the samples during mechanical testing and custom–built tensile testing clamps were used to grip the RTTFs, which minimized stress concentrations and prevented slippage. The grips consisted of two stainless steel plates with circular cutout for placement of tendons. Specimens were wrapped around acrylic rods and covered with silicon tubing. The wrapped tendons were then placed into the grips and clamped in place with the use of screws.

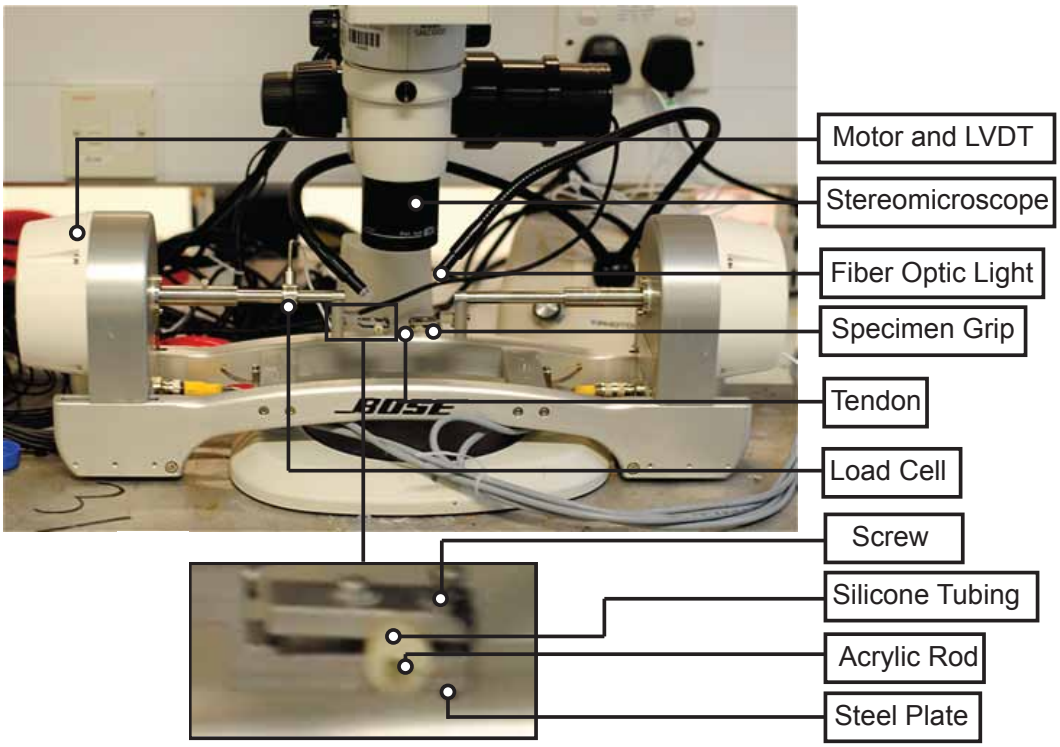

Figure 4.1: Tensile testing machine. Tendon specimens are wrapped around acrylic rods that are surrounded by a silicone sheath and secured by grips. An internal motor is used to apply displacement to the specimen and the force is captured using a load cell. A stereomicroscope is used to analyze the displacement of the tendon and calculate the gauge length of the specimen prior to testing.

The diameter of the RTTFs was measured at six locations along the testing region using a digital micrometer (Keyence, UK) prior to incubation. Between each measurement the specimens were hydrated with PBS to avoid measurement errors due to water loss. The average diameter was used to calculate the cross sectional area assuming the geometry of fascicles to be cylindrical.

Displacement was applied to the tissue to remove slack in the specimen and the starting position was defined as the displacement that induced a stress of 0.25 MPa. The initial gauge length was then measured using a calibrated stereomicroscope

(±0.1 mm)(Zeiss, UK). A triangular displacement corresponding to 5% strain was applied to the specimen for ten cycles to precondition the tissue (Figure 4.2). Following preconditioning the gauge length was measured for a second time at 0.25 MPa and a hysteresis test was conducted by applying a ramped displacement corresponding to 5% strain to the tendon specimen at a rate of 0.05 mm/s followed by a ramped displacement to 0% strain. Next, the gauge length was measured for a final time at 0.25 MPa and the specimen was subjected to ramped displacement to failure at a rate of 0.05 mm/s. The force and grip–to–grip displacement were recorded at 20 points per second in both tests.

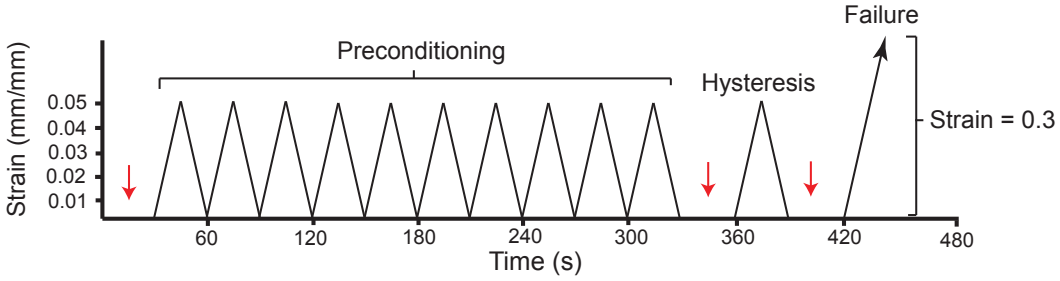

Figure 4.2: Loading profile of tendon. Preconditioning of the tissue is conducted by applying 5% strain to the tissue for 10 cycles. Following precondition, the tissue is subjected to a hysteresis test to 5% strain and a test to failure. Vertical arrows represent the time at which the gauge length is measured and used for strain calculations.

The force and displacement were converted into engineering stress (Force/Area) and strain (Change in Length/Initial Length) and plotted as stress–strain curves in Matlab (Mathworks, UK). The linear modulus, ultimate tensile strength (UTS) and failure strain were calculated for quasi–static tests (Figure 4.3). The linear modulus was calculated using a linear least squares fit to all the data points between 5% and 85% of the UTS. The UTS was defined as maximum stress during

the tensile test and the failure strain was defined as the strain at tendon rupture. The mechanical hysteresis was calculated by dividing the area between the loading and unloading curves (energy dissipated) by the area under the loading portion of the curve (energy input) (Figure 4.4). One–way analysis of variance (ANOVA) with a post hoc Tukey test was used to compare the material constants in Prism (GraphPad, UK).

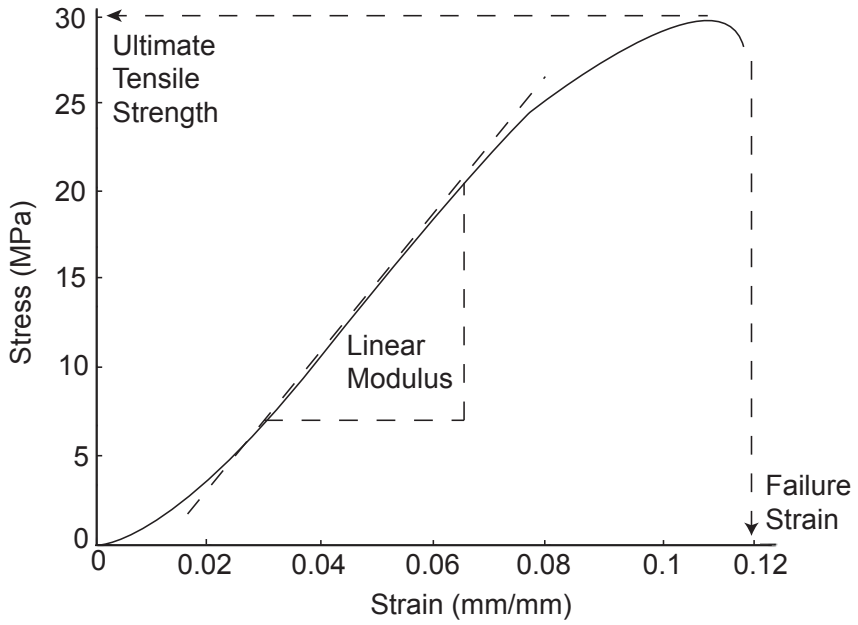

Figure 4.3: Quasi–static tensile test mechanical properties. The linear modulus represents the average slope of the linear portion of the curve. The UTS is defined as the maximum stress and the failure strain occurs at the point of rupture.

4.2.5 Structural Analysis of Tendon Specimens

MPM was used to visualize collagen and elastin structures in tendon specimens using the SHG and TPF signals as described in Section 3.2.3. A 20 mm portion of each RTTF (n=120) was used to quantify the crimp structure of the specimen after

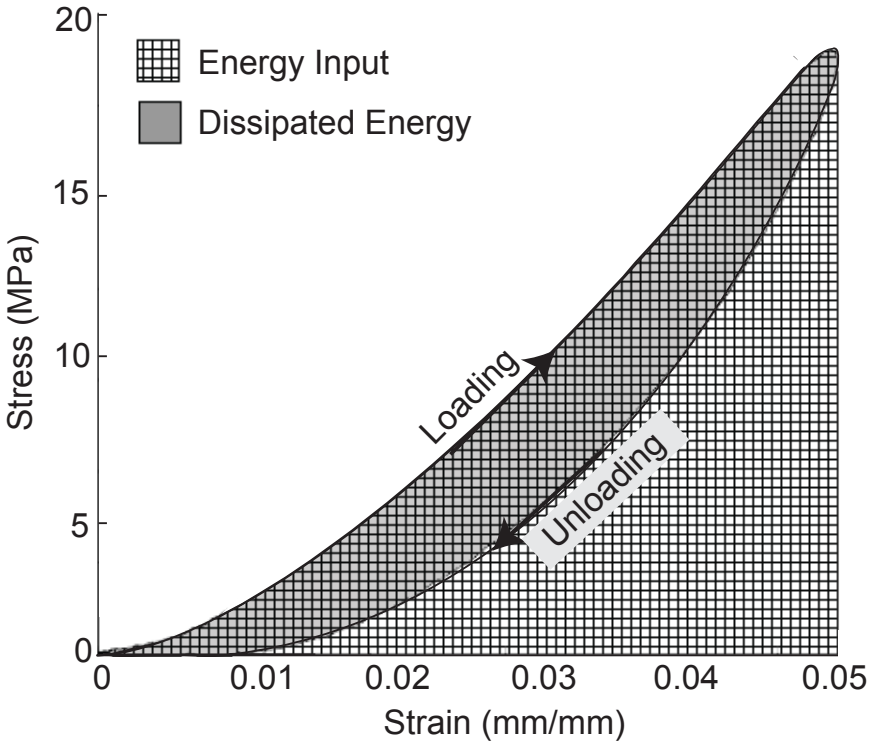

Figure 4.4: Hysteresis test mechanical properties. The energy input is measured by calculating area under the loading portion of the curve and the dissipated energy is measured by calculating the area between the loading and unloading curves.

the corresponding treatment. A tile scan was used to collect four images along the tendon corresponding to a total length of 3.4 mm. The images were imported into Image J and the crimp wavelength and angle were measured manually using the angle and line segment tool. The crimp wavelength was defined as the distance between consecutive crimp peaks and the crimp angle was estimated by measuring the angle formed between the horizontal and tangent line midway between a crimp trough and peak (Figure 4.5).

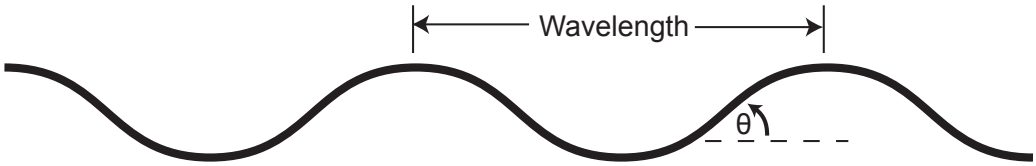

Figure 4.5: Crimp angle and wavelength. Image J is used to manually measure the wavelength and angle of the collagen fibril crimp.

4.2.6 Biochemical Assays of Tendon Specimens

Specimens were subjected to dimethyl methylene blue (DMMB) (Farndale et al., 1986), hydroxyproline (Reddy and Enwemeka, 1996) and elastin (Fastin Elastin Assay Kit, Biocolour, UK) assays to quantify the degradation of GAGs, type I collagen and elastin, respectively. Briefly, tendon specimens were rinsed in PBS, lyophilized and the dry weight recorded. Next tendon specimens were digested, subjected to a colorimetric agent and quantified using a spectrophotometer (Spectramax Plus, UK) in a 96–well plate. For the DMMB assay, papain was used to digest the specimens and chondroitin sulfate (C9819, Sigma Aldrich, UK) was used to create a standard curve. Tendon specimens for the hydroxyproline assay were autoclaved and then digested with chloromine–T reagent and hydroxyproline (H54409, Sigma Aldrich, UK) was used to create a standard curve. Finally, elastin was extracted in tendon specimens using oxalic acid and alpha–elastin (Biocolour, UK) was used to generate a standard curve.

4.3 Results

4.3.1 Degradation of Scaffold with Elastase

Collagen–elastin scaffolds had a random distribution of collagen and elastin as observed with the SHG and TPF signals, respectively (Figure 4.6). Collagen formed smaller fibers than elastin, but both had a fibrous structure. When treated with elastase, the collagen structure appeared unaffected by the treatment, but the elastin was largely degraded.

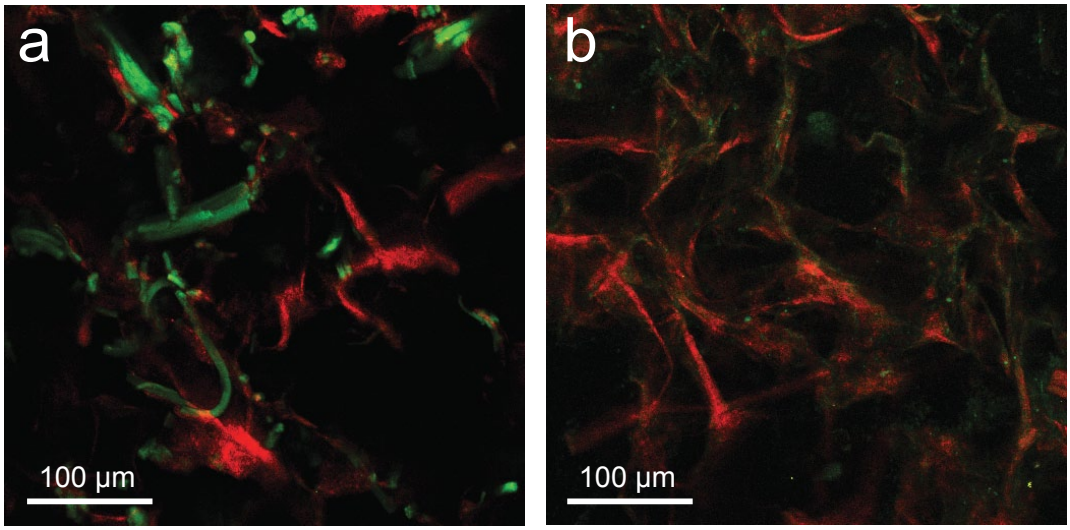

Figure 4.6: Collagen–elastin scaffold degradation. (a) Collagen–elastin scaffold prior to elastase digestion indicating collagen (red) and elastin (green) structure. (b) Scaffold following elastase digestion showing intact collagen (red) and reduction of elastin (green).

4.3.2 Mechanical Properties of Elastase–Treated Tendon

The mechanical response of tendon specimens followed the expected curve for quasi–static and hysteresis tensile tests. Preconditioning led to repeatable results and the mechanical properties of fresh tendons were comparable to those published in the literature (Screen et al., 2004). The majority (98%) of tendons failed at the midpoint of tendon through fiber pullout and sliding did not occur at the grips as observed with a stereomicroscope.

Quasi–static tensile tests indicated that there was a large decrease ($p<0.001$) in the UTS of elastase–treated specimens compared to all controls (Figure 4.7). Elastase–treated tendon ruptured after sustaining a mean maximum stress of 12.8 MPa compared to 30.5 MPa in fresh specimens. The failure strain of PBS incubated specimens increased significantly ($p<0.01$) compared to fresh specimens while elastase–treated specimens decreased compared to DMEM ($p<0.05$) and PBS ($p<0.001$). There was no observable difference ($p>0.05$) in the linear modulus or hysteresis of elastase–treated tendon compared to all controls.

4.3.3 Structural Organization of Elastase–Treated Tendon

The RTTFs emitted a strong SHG signal and the fibril crimp was clearly visible (Figure 4.8). There was little variation in the crimp angle and length of fresh tendon fascicles excised from animals used in this study. DMEM specimens had a similar fibril crimp structure to fresh tendon ($p>0.05$), with a large crimp angle and small crimp wavelength (Figure 4.9). However, PBS and elastase–treated specimens had a loose fibril crimp structure compared to fresh specimens resulting in a significant reduction of the crimp angle and increase in the crimp wavelength

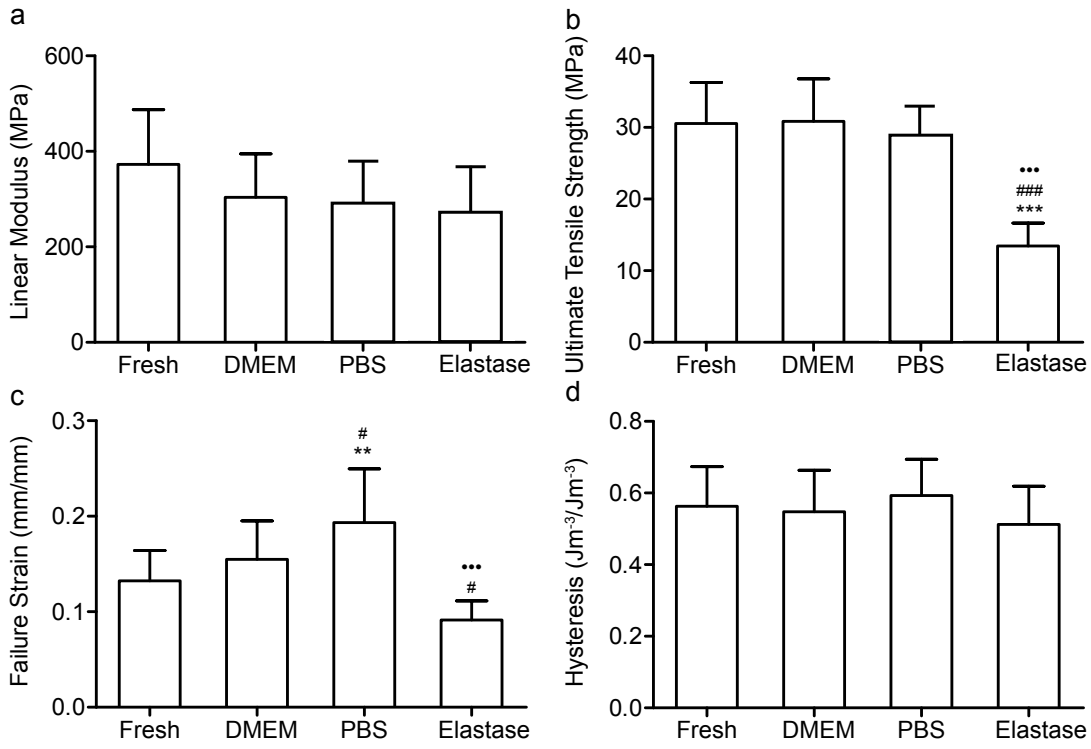

Figure 4.7: Mechanical properties of controls and elastase–treated tendon. (a) There are no significant differences between linear moduli of all specimens. (b) The UTS of elastase–treated tendon is significantly lower than all controls. (c) The failure strain of PBS incubated specimens increases compared to DMEM and fresh controls. Elastase–treated tendon is significantly reduced compared to PBS and DMEM controls. (d) There are no significant differences in the hysteresis of all controls and elastase–treated tendon. (One–way ANOVA, post hoc Tukey test, $\star\star\star p<0.001$, $\star\star p<0.01$, $\star p<0.05$ compared to fresh control; $\#\#\# p<0.001$, $\#\# p<0.01$, $\# p<0.05$ compared to DMEM control; $\bullet\bullet\bullet p<0.001$, $\bullet\bullet p<0.01$, $\bullet p<0.05$ compared to PBS control).

($p<0.001$). Specimens incubated in PBS sustained an increase in diameter compared to fresh and DMEM controls ($p<0.01$), while other treatments did not vary significantly ($p>0.05$) (Figure 4.9).

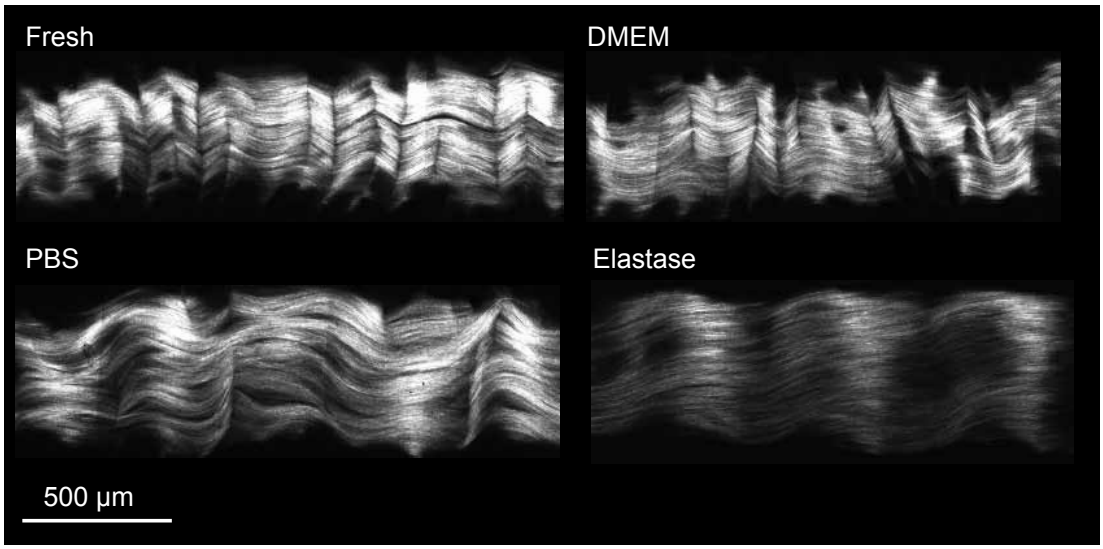

Figure 4.8: Change in fibril crimp of controls and elastase–treated tendon. Representative SHG images depicting fibril crimp organization of controls and elastase–treated tendon specimens. Collagen fibril crimp is tightly organized in fresh and DMEM specimens with the organization becoming more loosely packed in PBS and elastase–treated specimens. There is an observable increase in diameter of PBS and elastase–treated specimens as compared to DMEM and fresh tendon.

4.3.4 Molecular Compositions of Elastase–Treated Tendon

The hydroxyproline, DMMB and elastin assays gave consistent results for the collagen, GAG and elastin content of fresh and treated specimens (Figure 4.10). The hydroxyproline content did not significantly vary across treatments ($p>0.05$). However, the GAG and elastin content was significantly reduced in elastase–treated tendon compared to controls ($p<0.001$).

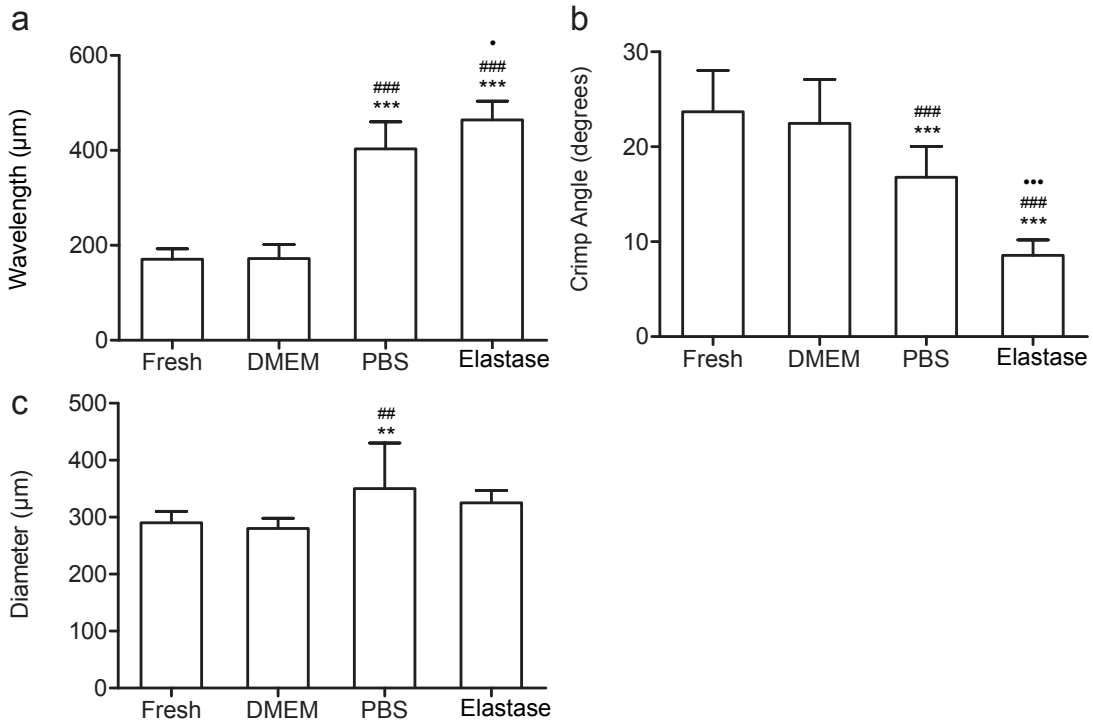

Figure 4.9: Structural organization of controls and elastase–treated tendon. (a) The wavelength of tendon increases significantly for PBS and elastase–treated tendons compared to fresh and DMEM controls. Additionally, elastase–treated tendon has a larger wavelength than PBS controls. (b) The crimp angle significantly decreases in PBS and elastase incubated specimens compared to fresh and DMEM controls. Moreover, elastase–treated tendon has a smaller crimp angle compared to PBS controls. (c) The diameter of PBS incubated specimens is greater than fresh and DMEM controls. (One–way ANOVA, post hoc Tukey test, $\star\star\star$p<0.001, $\star\star$p<0.01, $\star$p<0.05 compared to fresh control; ###p<0.001, ##p<0.01, #p<0.05 compared to DMEM control; $\bullet\bullet\bullet$p<0.001, $\bullet\bullet$p<0.01, $\bullet$p<0.05 compared to PBS control).

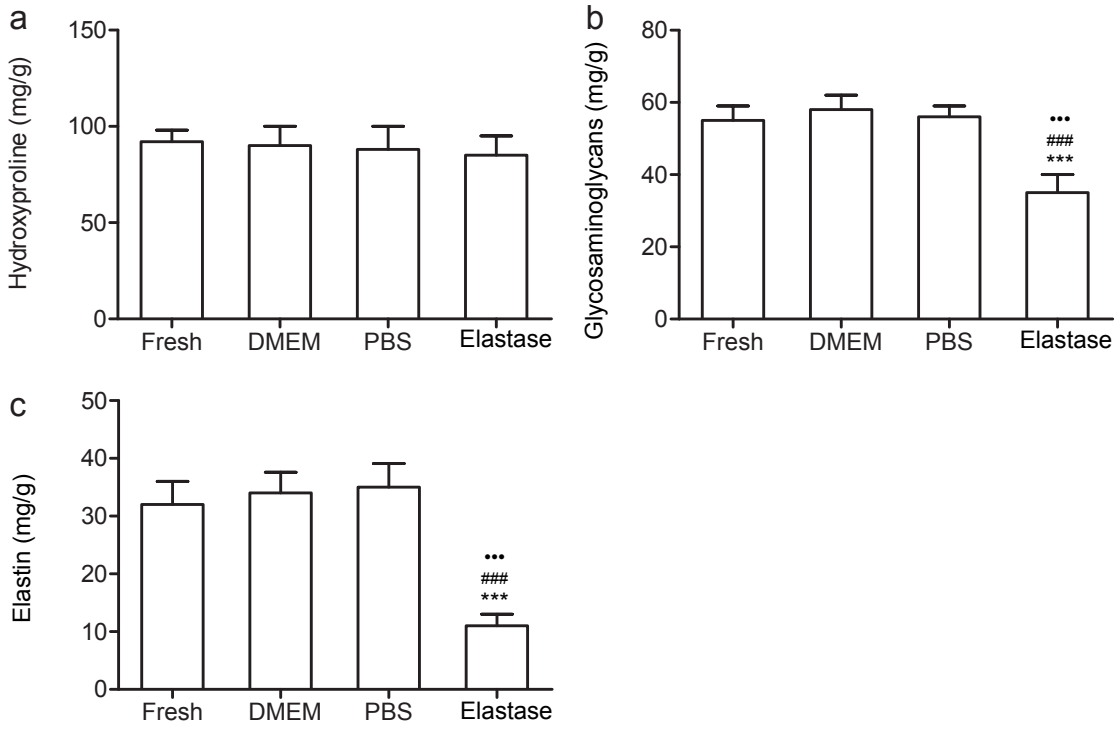

Figure 4.10: Molecular composition of controls and elastase–treated tendon. (a) Hydroxyproline content does not vary significantly between controls and elastase–treated specimens. (b) Elastase–treated tendon has significantly reduced glycosaminoglycan content compared to all controls. (c) Elastase–treated tendon has significantly reduced elastin content compared to all controls. (One–way ANOVA, post hoc Tukey test, $\star\star\star p<0.001$, $\star\star p<0.01$, $\star p<0.05$ compared to fresh control; $\#\#\# p<0.001$, $\#\# p<0.01$, $\# p<0.05$ compared to DMEM control; $\bullet\bullet\bullet p<0.001$, $\bullet\bullet p<0.01$, $\bullet p<0.05$ compared to PBS control).

4.4 Discussion

4.4.1 Mechanical Role of Elastic Fibers in Tendon

In this chapter mechanical testing, MPM and biochemical assays were used to analyze the mechanical, structural and compositional changes of tendon treated with elastase to better understand the mechanical role of elastin in tendon. Mechanical tests indicated that elastase did not affect the linear modulus or hysteresis of tendon, but significantly reduced the UTS and failure strain. Moreover, elastase affected collagen fibril crimp and significantly reduced GAG and elastin content.

Within the literature it has been suggested that elastic fibers contribute to the low stress–strain response and elastic recoil of tendon, which has been primarily derived from elastase experiments and cardiovascular theories (Figure 4.11). However, the current chapter raises concerns about the specificity of elastase and its ability to distinguish the mechanical role of elastic fibers in tendon. Moreover, extrapolating theories from other dynamic tissue is not necessarily applicable for tendon given the large variation in structure and function between tissues.

The composition, organization and loading conditions of tendon vary significantly from that of blood vessels. For example, the human aorta consists of 30% elastin (Lowry et al., 1941) which forms lamellae and experiences circumferential stresses up to 16 kPa (Khanafer et al., 2011), while the human Achilles tendon consists of 2% elastin (Lowry et al., 1941) which is distributed longitudinally and experiences tensile stresses of up to 70 MPa (Magnusson and Kjaer, 2003). Given the large variation between the human aorta and Achilles tendon, elastic fibers may play a different role in each tissue. Generally, elastic fibers are included in

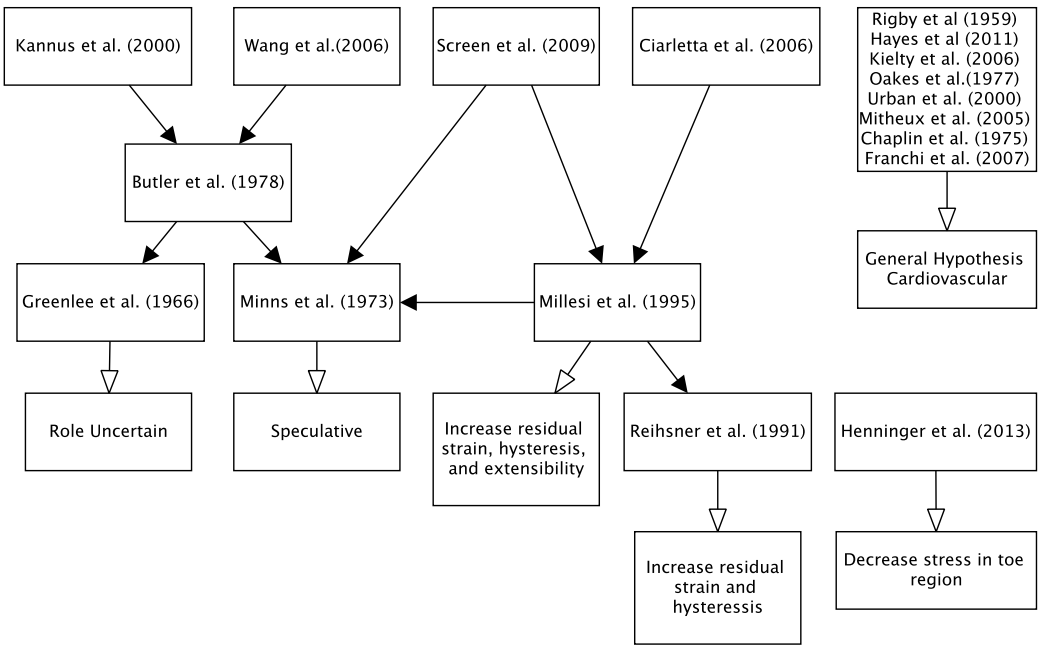

Figure 4.11: Literature involving the mechanical role of elastic fibers in tendon. Solid arrowheads represent citations and open arrowheads represent key findings. (Butler et al., 1978; Chaplin and Greenlee Jr, 1975; Ciarletta et al., 2006; Franchi et al., 2007; Greenlee et al., 1966; Hayes et al., 2011; Henninger et al., 2013; Kannus, 2000; Kielty, 2006; Millesi et al., 1995; Minns et al., 1973; Mithieux and Weiss, 2005; Oakes and Bialkower, 1977; Reihsner et al., 1991; Rigby et al., 1959; Screen and Evans, 2009; Urbán and Boyd, 2000; Wang, 2006)

tissues that experience large deformations because they are capable of withstanding large strains. However, tendon rarely exceeds strains greater than 5% under physiological conditions, which is significantly lower than that of blood vessel, lung tissue, or skin. Consequently, the function of longitudinally oriented elastic fibers in tendon is not evident.

The theory suggesting that elastic fibers contribute to the low stress–strain response of tendon was first established by Lanir (1978), which was based on experimental studies conducted on skin, arteries and the nuchal ligament. The key component of the model was that elastic fibers had a straight orientation that bound crimped collagen fibrils. This organization would cause elastic fibers to be loaded prior to collagen fibrils and induce undulation of crimp with the application of tissue strain. However, in Section 3.3.1 I showed that elastic fibers had a crimped organization with similar wavelength and amplitude to that of collagen fibrils. Using this structural data I would expect that collagen fibrils and elastic fibers would be loaded at the same time during tendon deformation. Therefore, my structural results do not provide support for this theory.

Additional support for the theory that elastic fibers contribute to fibril crimp was provided by an elastase experiment that showed undulation of crimp following elastase treatment (Oakes and Bialkower, 1977). I have confirmed that elastase significantly reduces fibril crimp in tendon, but attribute this result to both the removal of elastin as well as the nonspecific degradation of the ECM, including GAGs. Fibril crimp is likely dependent on the structural integrity of the ground substance that surrounds collagen fibrils and not solely a function of elastin.

The second mechanical contribution that elastic fibers have been suggested to provide in tendon is elastic recoil. However, the term elastic recoil is not well

defined within the tendon literature and has been extrapolated from respiratory mechanics theory. In the respiratory system elastic recoil is defined as the ability of inflated lungs to return to their normal resting volume. In other words, elastic recoil is directly proportional to lung stiffness. When applying this definition to tendon we see that it is unlikely that the low proportion of elastic fibers would significantly contribute to tendon stiffness. The simple rule of mixtures model derived in Appendix A and discussed in Section 3.4.3 indicates that elastic fibers are not expected to contribute to the elastic modulus of tendon in the axial direction. Therefore, it is unlikely that elastic fibers contribute to elastic recoil in tendon given their sparse distribution.

4.4.2 Nonspecific Degradation and Tissue Swelling of Tendon

As indicated in the structural and degradation analyses, tendon is subjected to nonspecific degradation when exposed to elastase. Elastase is a powerful enzyme that can degrade a host of structural molecules in the ECM and has been shown to decrease GAG content by 32–92%, while having a limited effect on type I collagen (Barbir et al., 2010; Jacobs et al., 2011; Smith et al., 2008). I found that elastase decreased GAG content by 36% and elastin content by 60% while having an insignificant effect on type I collagen. Therefore, the results of a mechanical test following an elastase treatment should be interpreted as the degradation of multiple ECM structural molecules rather than elastin alone.

My results also indicated that incubating tendon specimens in PBS caused the tissue to swell. The diameter increased by 16% and the fibril crimp was more

loosely organized than fresh or DMEM treated tendon. Previous studies have shown that the inter–fibril spacing of tendon increases after incubation in PBS and that there is a significant increase in the water content (Han et al., 2000; Lujan et al., 2009; Screen et al., 2006). However, the mechanical properties of collagen fibrils have been shown be unaltered by PBS (Svensson et al., 2010). My results indicated that PBS–incubated specimens failed at large strains, which confirms previous findings (Chimich et al., 1992) and may be indicative of increased fibril sliding.

4.5 Conclusion

In conclusion, I investigated the contribution of elastic fibers to the mechanical properties of tendon. I found that elastase did not affect the linear modulus or hysteresis of tendon, but significantly reduced the UTS and failure strain. Although elastase was efficient at degrading elastin in simple collagen–elastin scaffolds, the degradation profile of tendon indicated that non–elastin structural molecules were affected by the treatment. Therefore, results of an elastase treatment should be interpreted as the effect of elastase on the structure and function of tendon and not necessarily the role of elastic fibers in tendon. The current theory that elastic fibers contribute to the low stress–strain response and elastic recoil of tendon requires further evidence and additional studies are required to determine its exact role, which may include non–mechanical functions.

Chapter 5

Deformation of Collagen Fibrils and Tenocytes

5.1 Introduction

5.1.1 Microscopy in Combination with Mechanical Testing

In previous chapters I have shown that arrays of tenocytes are enclosed by a specialized structure called the PCM, which is composed of a unique combination of structural molecules, including elastic fibers (Section 3.3.2). From this structural data I conjectured that the PCM plays a key role in mediating force transmission from the ECM to cells, therefore, influencing the mechanobiological response of tendon. To further investigate this hypothesis I combine mechanical testing and microscopy in this chapter to analyze the displacement of tendon cells in tissue exposed to load. This technique can be used to better understand the underlying mechanisms responsible for tendon and cell–level deformation.

Mechanical testing in combination with microscopy was pioneered by Viidik (1972) to analyze the recession of fibril crimp in excised tendon specimens exposed to load. Following the introduction of this novel method, numerous immunohistochemical and optical techniques have been developed that are capable of characterizing the complex interaction of structural molecules in tissue. Arnoczky et al. (2002) were the first to embrace this technology in tendon by combining confocal microscopy with mechanical testing. Through staining and measuring the deformation of cell nuclei they found that local tissue strain led to an increase in nuclear deformation. Studies have also measured the displacement of cells in order to characterize the deformation of the ECM in two dimensions (2D) (Screen et al., 2002) and three dimensions (3D) (Khodabakhshi et al., 2013) and have reported that shear, twisting and deflection contribute to tendon deformation.

An alternative technique that has been used to study ECM deformation is accomplished by photobleaching a grid onto tissue and analyzing the relative deflection of the grid pattern with applied load. This technique was first introduced by Bruehlmann et al. (2005) and later used by Cheng and Screen (2007) to show that tissue strain in tendon has an inhomogeneous distribution. Additional studies have also investigated deformation of the primary cilium (Lavagnino et al., 2011) and collagen fibrils (Goulam Houssen et al., 2011) in tendon using IHC and MPM, respectively. Currently, there is much room for further development of this technique by combining immunostaining and microscopic techniques to analyze the interaction of structural molecules in tissue. Of particular interest is the interaction of the ECM and cells, which is a key factor in understanding mechanobiological stimulation. Additionally, through the collection of large tile–scanned images a better understanding of the overall displacement of the ECM and cells can be achieved,

which, to the best of my knowledge has yet to be presented in the literature.

5.1.2 Previous Microtensile Testing Machine Designs

Presently, there does not exist a commercially available MTM for use with light or confocal microscopes. As a result, multiple custom–built designs have been presented in the literature, which generally consist of five major components: (1) stepper motor to apply displacement to the tissue; (2) grips to bind excised specimens; (3) linear variable differential transformer (LVDT) to measure grip–to–grip displacement; (4) load cell to measure force transmitted through tissue; and (5) a data acquisition unit (DAQ) to collect voltages from the LVDT and load cell.

5.1.3 Aims and Objectives

The aim of this research was to better understand the displacement of tenocytes in relation to collagen fibril organization by combining confocal/multiphoton microscopy with mechanical testing. This data was used to elucidate the micromechanical mechanisms responsible for tendon deformation and to better understand how they influenced cell–level deformation. The first objective involved designing and manufacturing a custom–built MTM for use with a confocal/multiphoton microscope in order to measure cell displacement and fibril deformation in tendon. The second objective was to use the MTM in combination with microscopy to characterize the displacement of tendon cells in tissue using large tile–scanned images. More specifically, the movement of cells was used to determine if the displacement was representative of a planar or helical structure, which has been a highly debated topic in the literature and important for understanding the mi-

crostructural deformation of tendon. Moreover, tile–scanned images were used to create deformation gradients that provided insight into the overall movement of cells at larger strains. The third objective was to analyze the elongation of nuclei under physiological conditions to evaluate the validity of nuclear deformation acting as a mechanosensor in tendon.

5.2 Materials and Methods

5.2.1 Design Specifications of Microtensile Testing Machine

The major design constraint associated with the MTM was the vertical distance between the condenser and microscope stage (Figure 5.1). Detailed measurements of the microscope were calculated by capturing scaled images from a variety of angles using a Nikon D3000 digital camera (Nikon, USA). The dimensions were used to model the microscope environment in AutoCAD (Autodesk, USA) and the MTM was designed with respect to the reconstructed environment to ensure optimal fit.

The major design specifications for the MTM were as follows:

1. The device must fit inside the microscope incubation chamber and fit securely over the objective lens.

2. The device must be capable of applying small displacements to the tissue ($<$100 μm) while measuring small loads ($<$0.1 N).

3. The grips must securely bind specimens to prevent slippage while ensuring that stress concentrations do not build up at the ends of tendon.

4. The tissue must be positioned as close as possible to the objective lens to optimize image resolution and allow for high magnification imaging.

To accommodate these conditions, commercially available load cells and linear actuators were investigated and key measures compared. Multiple grip designs were proposed and discussed with technicians in the Institute of Biomedical Engineering (IBME) workshop to determine their feasibility. Finally, the capabilities of various DAQs and software programs were analyzed.

Following acquisition of the necessary components, calibration of the instrumentation was conducted. A calibration curve was produced for the load cell by balancing fixed weights (250, 500, 750, and 1,000 g) from the device and calculating the linear load–voltage relationship. Precision of the linear actuator was measured by inputting a fixed grip displacement and comparing the input to the measured displacement under a calibrated stereomicroscope (Nikon, UK).

5.2.2 Mechanical Testing in Combination with Imaging Protocol

Following design and manufacturing of the MTM the following protocol was used to analyze the microstructural deformation of tendon. Tendon fascicles (n=20) were excised from rat tails and the diameter was measured using the techniques described in Sections 4.2.1 and 4.2.4. The fascicles were individually placed into chambers of a six–well plate and cell nuclei stained using DAPI in DMEM for 20 min (Invitrogen, UK). The wells were covered with wrapping film (Parafilm, UK) to prevent dehydration and the plate was covered with aluminum foil to avoid photobleaching. A standard glass cover slip (No. 1.5, 25 x 75 mm) was adhered

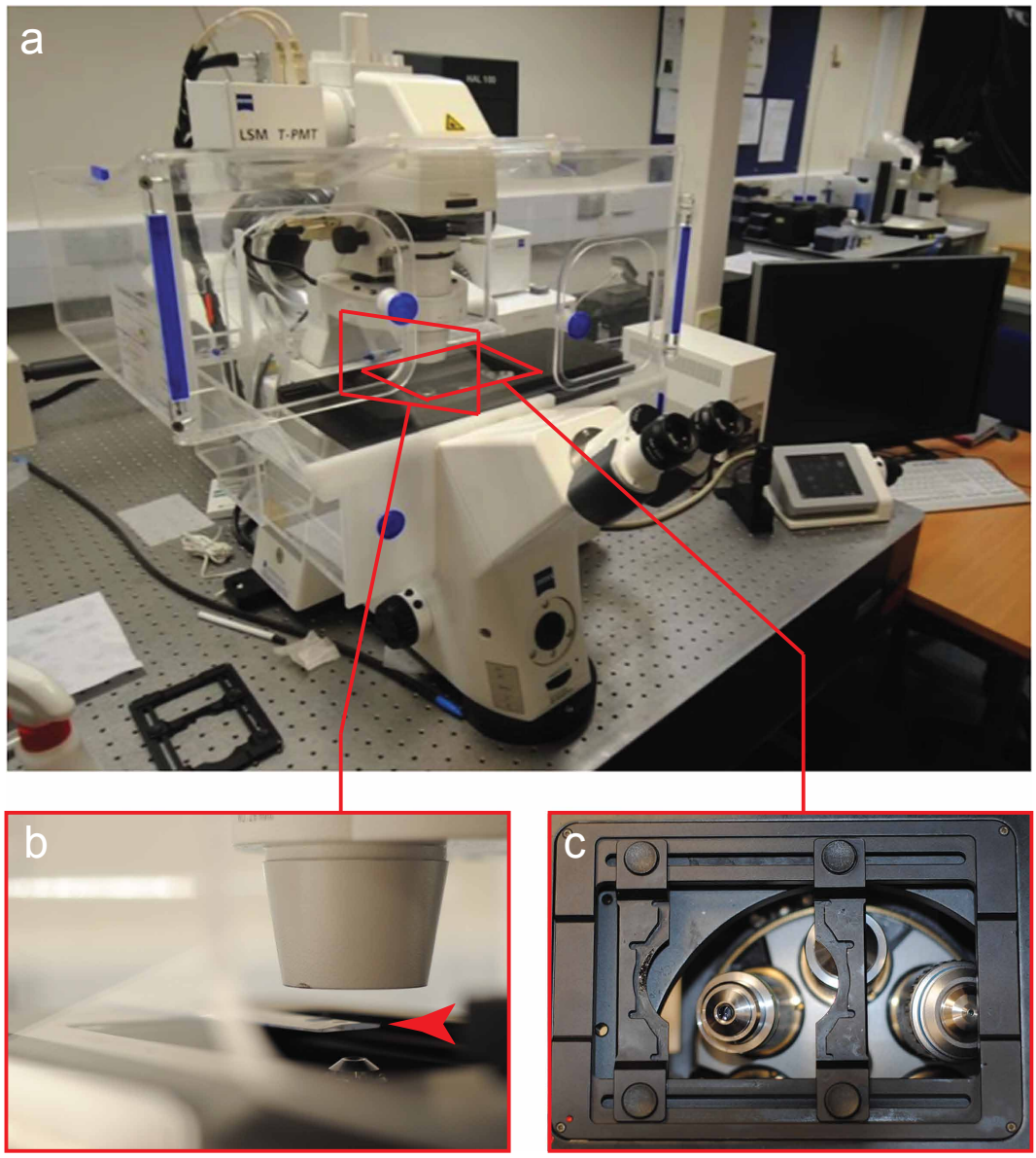

Figure 5.1: Microscope environment for MTM (a) Inverted confocal microscope for use with tensile testing machine. (b) Side view indicating the distance between the condenser and objective lens. The horizontally oriented ruler (arrowhead) represents the height of the microscope stage. (c) Top view of objective lenses depicting the size of the opening in the microscope stage.

to the bottom of the testing machine using silicon glue (Fixogum, UK). Following staining, the tendons were placed into grips and the gauge length was measured using a a calibrated microscope at 2.5x magnification (±0.1 mm, Zeiss, UK). Three drops of DMEM were added to the tissue to prevent dehydration of the specimen and preconditioning was conducted according to Section 4.2.4 (Figure 5.2). The specimens were placed adjacent to the cover slip by adjusting the vertical position of the grips to optimize image resolution.

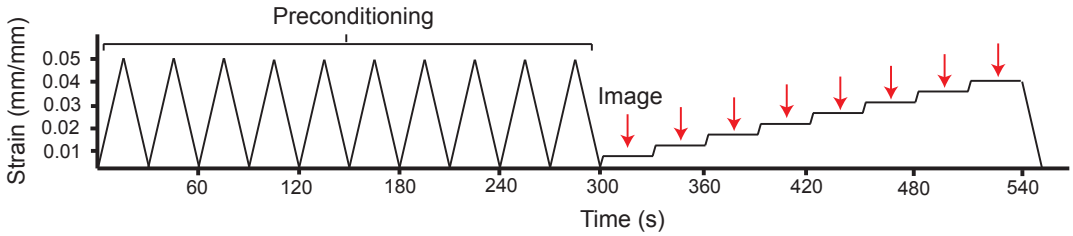

Figure 5.2: Load profile for microscopic analysis. Ten preconditioning cycles are conducted on the tissue prior to imaging. Arrows represent the start of imaging at each strain level.

Confocal in combination with multiphoton microscopy was used to simultaneously capture cell nuclei and collagen fibril structure during mechanical tests. The detailed microscopic techniques for the confocal and multiphoton analysis are found in Section 3.2.3. Briefly, the DAPI and SHG channels were captured simultaneously at a depth of 20 μm from the surface of the tissue. Prior to the mechanical test, a rectangle was photobleached onto the tissue adjacent to the region of interest using the multiphoton laser at 50% power. The photobleached rectangle was visible on the channel associated with the DAPI stain and was used as a reference datum for alignment of images (Figure 5.3). At 0.5% strain intervals tile scans were collected to generate images 1 mm in length. A strain rate of 0.05

mm/s was used to stretch the tissue to the predefined displacement using the linear actuator controlled by LabView software (National Instruments, UK) (Appendix D). Prior to imaging the tissue was allowed to stabilize for 30 s to accommodate for stress–relaxation mechanisms (Defrate and Li, 2007). The load, displacement and time stamp were recorded at 20 points per second.

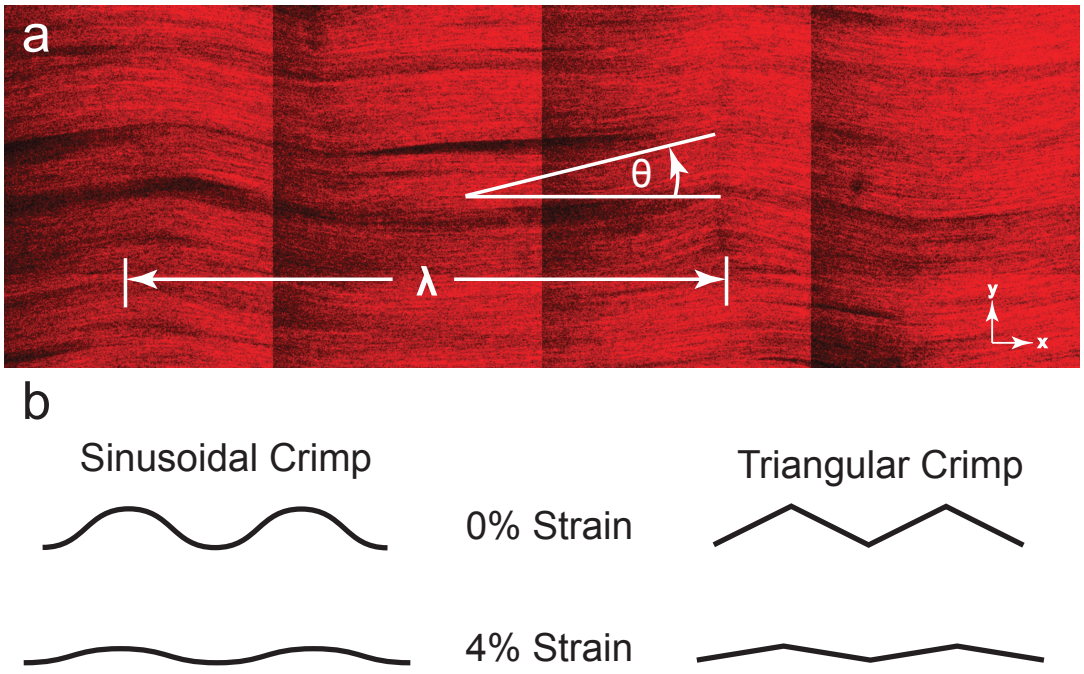

Figure 5.3: Alignment of microscopic images. Edge of photobleached rectangle (arrowhead) appears as a straight line prior to application of tissue displacement. In strained tendon the rectangle deforms leading to curved edge. The images are aligned using the rectangular edge before (solid line) and after (dashed line) deformation.

5.2.3 Automated Characterization of Cell Displacement

Following collection of force–displacement measurements and structural images, the two data sets were synchronized using the time–stamps collected during testing.

The force was calculated using the average load measurement over the duration of the imaging period. The stress was calculated assuming a circular cross–sectional area of the fascicle and the strain with respect to the gauge length measured after preconditioning. The strain was measured using the grip–to–grip displacement throughout the test.

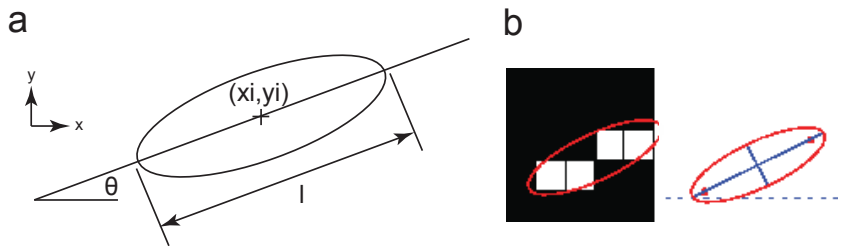

Figure 5.4: Characterization of cell nuclei. (a) Diagram indicates the alignment (θ), centroid position (xi, yi) and the long axis length (l) of nuclei calculated at each subsequent strain. (b) Figures depict how ellipse is fit to pixels using the 'regionprops' function.

The stress–strain curves from the mechanical tests were plotted in Matlab and images imported into Image J. The tile–scanned images were exported into Photoshop (Adobe, USA) and aligned using the photobleached rectangle as a reference datum. Images were aligned by overlapping the edge of the photobleached rectangle in subsequent images. There was no change in vertical position, so only the horizontal direction was aligned. As a result of the rectangle deforming with tissue stain, the alignment that maximized overlap between the two lines as determined by eye was used (Figure 5.3). The aligned images were imported into Matlab and used to analyze structural features of tenocytes at various strains. Blue channel images highlighted the nuclear DAPI stain and were used to analyze the centroid position, long axis length and orientation of nuclei in the tissue (Figure 5.4). An

automated script was generated in Matlab to measure parameters using the 'regionprops' function in the image processing toolbox (Appendix C). Briefly, the 'regionprops' function fit ellipses to groups of adjoined pixels and then calculated parameters that defined the shape of the ellipses. The SHG images were used to calculate the location of the fibril crimp peak at each strain using the measurement tool in Image J. The nuclear alignment and elongation were then referenced with respect to the crimp position in order to allow for comparison between samples.

5.2.4 Modeling Deformation of Collagen Fibril Waveforms

As a comparative measure, 2D triangular and sinusoidal theoretical models were derived at each strain to predict the change in cell alignment along tendon in each respective waveform. The triangular waveform was intended to represent a planar structure and the sinusoidal waveform a helical organization projected in 2D. The initial crimp amplitude and wavelength were measured in Image J using SHG images in order to define triangular and sinusoidal curves (Figure 5.5). A detailed derivation for the change in alignment of cells in both waveforms is shown in equations (5.1) through (5.14).

I start with a general sinusoidal equation (5.1) to define the curve prior to deformation. A_1 and λ_1 represents the amplitude and wavelength of the initial waveform, respectively. Similarly equation (5.2) defines the curve following deformation.

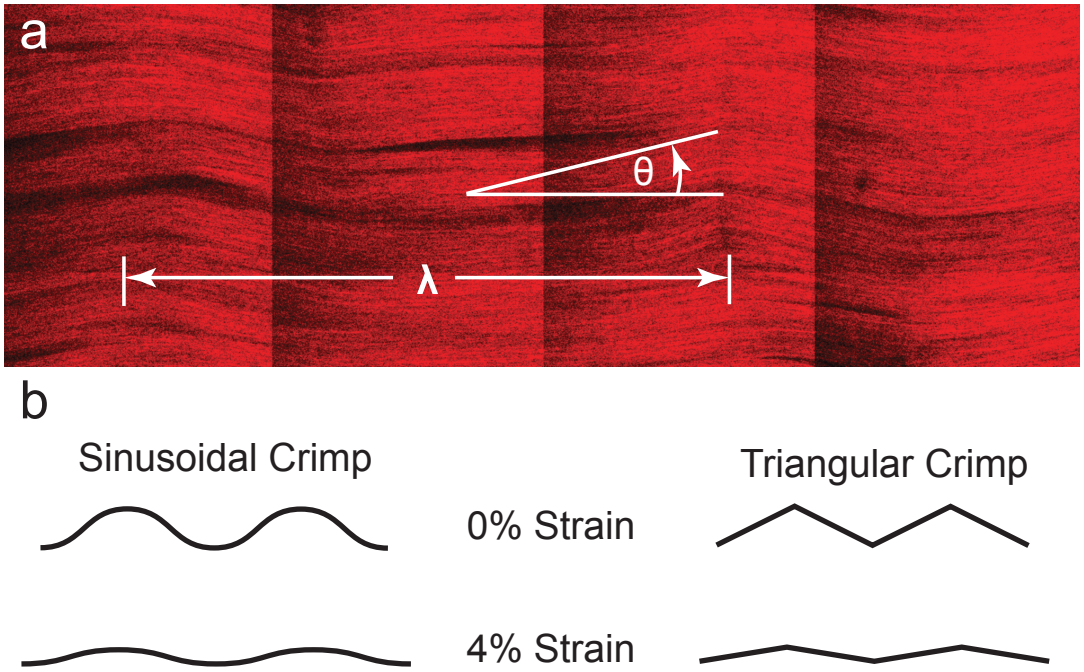

Figure 5.5: Simulation of sinusoidal and triangular crimp waveform deformation. (a) The SHG signal (red) is used to measure the wavelength and amplitude of the fibril crimp. Dark and light areas are the result of tile–scanned image acquisition. (b) The measured parameters are used to define a sinusoidal or triangular crimp in two dimensions and the deformation is simulated to calculate the change in alignment.

$$f_{s_1}(x) = A_1 sin(\frac{2\pi}{\lambda_1}x) \tag{5.1}$$

$$f_{s_2}(x) = A_2 sin(\frac{2\pi}{\lambda_2}x) \tag{5.2}$$

The first derivative of both sinusoidal equations is shown in equations (5.3) and (5.4) and is used to calculate the change in slope of the curve along the horizontal direction.

$$f'_{s_1}(x) = \frac{2A_1\pi}{\lambda_1} cos(\frac{2\pi}{\lambda_1}x) \tag{5.3}$$

$$f'_{s_2}(x) = \frac{2A_2\pi}{\lambda_2} cos(\frac{2\pi}{\lambda_2}x) \tag{5.4}$$

In order to solve equations (5.3) and (5.4) the wavelength and amplitude following deformation are required. I assume that the wavelength increases by a factor of 4% with the application of 4% tissue strain (5.5) and that the length of the curve remains constant (5.6). These assumptions were made because the nonlinear region of the stress–strain curve has been shown to be the result of straightening of fibril crimp and not the extension of collagen fibrils (Fratzl et al., 1998).

$$\lambda_2 = 1.04\lambda_1 \tag{5.5}$$

$$L_{s_1} = L_{s_2} \tag{5.6}$$

To derive the length of the curve before and after deformation in equation (5.6), the length integral function is used (5.7) . The first derivative before (5.3) and after (5.4) deformation are substituted into (5.7) and used to calculate the length of the curve over a single wavelength.

$$L = \int_a^b \sqrt{1 + [f'(x)]^2} dx \tag{5.7}$$

$$L_{s_1} = \int_0^{\lambda_1} \sqrt{1 + (\frac{2A_1\pi}{\lambda_1} cos(\frac{2\pi}{\lambda_1} x))^2} dx \tag{5.8}$$

$$L_{s_2} = \int_0^{\lambda_2} \sqrt{1 + (\frac{2A_2\pi}{\lambda_2} cos(\frac{2\pi}{\lambda_2} x))^2} dx \tag{5.9}$$

The change in amplitude of the triangular waveform is calculated similarly to the sinusoidal curve. The wavelength is assumed to increase by 4% with the application of tissue strain (5.5). The length of the waveform is assumed to be constant (5.10) and is calculated using the Pythagorean theorem before (5.11) and after (5.12) deformation.

$$L_{t_1} = L_{t_2} \tag{5.10}$$

$$L_{t_1} = 2\sqrt{(2A_1)^2 + (\frac{\lambda_1}{2})^2} \tag{5.11}$$

$$L_{t_2} = 2\sqrt{(2A_2)^2 + (\frac{\lambda_2}{2})^2} \tag{5.12}$$

Next, I calculate the change in slope of the waveform by deriving the first derivative before (5.13) and after (5.14) deformation. Because the waveform is

linear, the first derivative reduces to a constant that alternates between positive and negative values.

$$f'_{t_1}(x) = \begin{cases} +\frac{4A_1}{\lambda_1}, & \text{if } x > (4n-1)\frac{\lambda}{4} \text{ and } x < (4n+1)\frac{\lambda}{4} \\ -\frac{4A_1}{\lambda_1}, & \text{otherwise} \\ & \text{for n=0,1,2,..} \end{cases} \tag{5.13}$$

$$f'_{t_2}(x) = \begin{cases} +\frac{4A_2}{\lambda_2}, & \text{if } x > (4n-1)\frac{\lambda}{4} \text{ and } x < (4n+1)\frac{\lambda}{4} \\ -\frac{4A_2}{\lambda_2}, & \text{otherwise} \\ & \text{for n=0,1,2,..} \end{cases} \tag{5.14}$$

Finally through equating the waveform length before and after deformation the amplitude and wavelength are calculated and used to measure the change in alignment of nuclei.

5.3 Results

5.3.1 Microtensile Testing Machine Design

The main components of the MTM design included a linear actuator, load cell, and grips (Figure 5.6). The linear actuator was a model T–NA0A850 from Zaber (USA) and was chosen for its high–precision stepper motor. The device was able to apply displacements less than 1 μm and sustain a thrust force of up to 50 N.

The tip of the actuator had a threaded M3 shaft, which secured the left grip in place.

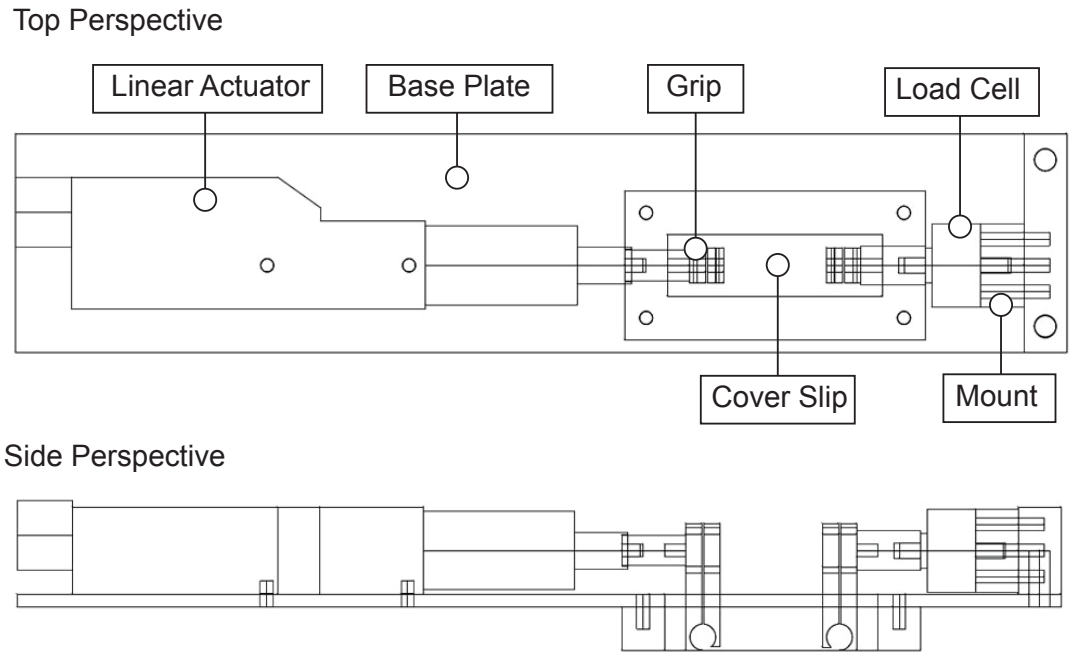

Figure 5.6: MTM design highlighting key components. A linear actuator is used to apply displacement to grips and the load cell measures the force. The grips are adjustable in the vertical direction to allow for placement of the specimen adjacent to the cover slip. The base and mount supports the components and are anodized to reduce reflection of laser light.

The grips were based on the design described in Section 4.2.4, which were highly efficient at clamping tendons and minimizing slippage. The newly designed grips were oriented in the vertical direction to avoid obstruction of the objective lens. The grips consisted of two stainless steel plates clamped together by a screw. The screw fed through a slotted opening, which allowed for vertical adjustment of the grips. The grips were situated in a rectangular opening in the base, which was enclosed by a cover slip. The cover slip was held in place by synthetic glue, which

formed a watertight seal and allowed for hydration of tissue.

The load cell was a model WMC–5 from Interface (UK) and had a maximum load capacity of 22 N. It was chosen for the design because of its high accuracy ($\pm$0.033 N) and small dimensions. It was secured to the base through an adjustable mount, which oriented the load cell in a non–obstructive orientation when placed under the microscope. The load cell was connected to an SY038V load cell amplifier (Interface, UK), which increased the output voltage between $\pm$10.00 V.

The linear actuator was connected to a laptop (Dell, UK) via a USB cable and the load cell and amplifier through a National Instruments (UK) 6008 DAQ (Figure 5.7). Labview was used to control the linear actuator in addition to collecting force and displacement data from the load cell and linear actuator, respectively.

5.3.2 Effectiveness of Microtensile Testing Machine

The MTM was effective at stretching tendons under an inverted confocal/multiphoton microscope. Specimens were situated in close approximation to the objective lens allowing for the collection of high–resolution images. There was sufficient horizontal travel to allow for complete rupture of specimens during quasi–static tensile tests. Throughout the tests, grips securely bound tendons and did not appear to introduce significant stress concentrations as indicated by rupture occurring at the midpoint of the specimen in all tests. The load cell accurately measured the force throughout the test and the linear actuator was capable of applying micron–level displacements to specimens. The adhered coverslip formed a watertight seal and ensured that tissue specimens were fully hydrated throughout mechanical tests.

The load cell was successfully calibrated using the set of weights. Moreover,

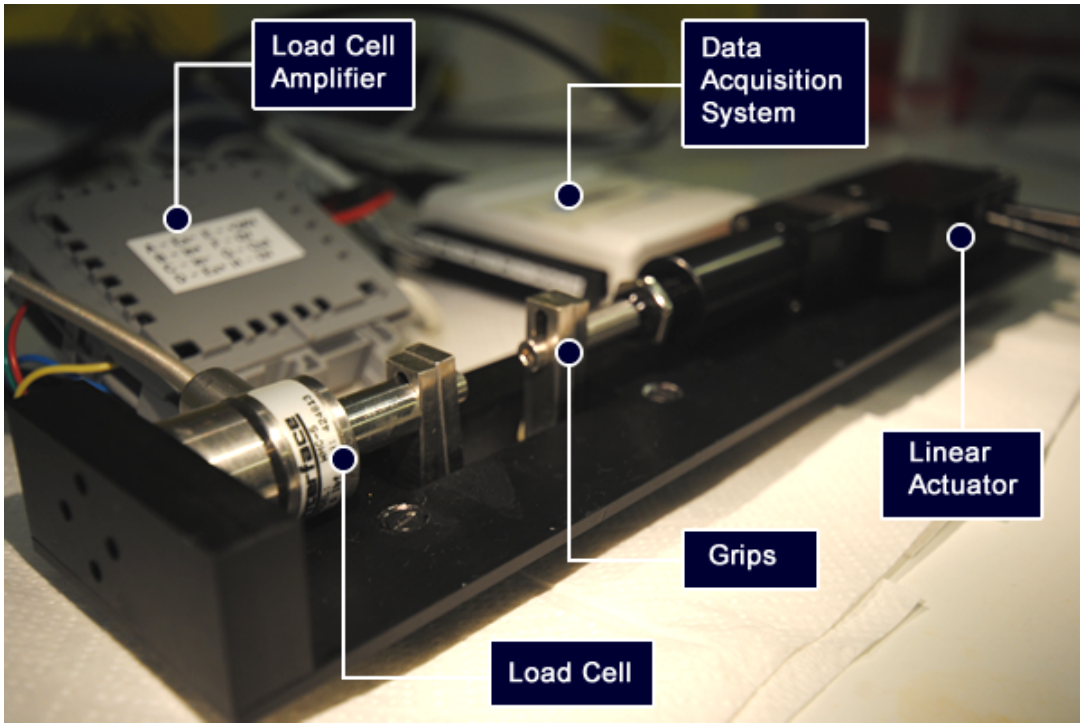

Figure 5.7: MTM apparatus. Force is measured with the load cell, then enhanced by the amplifier and collected with the DAQ. Labview is used to control the linear actuator and record data from the load cell.

displacements from the linear actuator had a high level of correlation with the stereomicroscope measurements (R^2=0.999) (data not shown).

5.3.3 Stress–Relaxation Response of Tendon During Imaging

The stress measurements captured throughout the tensile test clearly depicted the stress–relaxation response of tendon (Figure 5.8). The peak stress at each displacement was comparable to the values measured in quasi–static tests at equivalent strains (Section 4.3.2). An increase in displacement led to a more pronounced

stress–relaxation response with the curve becoming steeper. For strains less than 4% the stress decreased by a maximum of 5.0% during imaging. At 10% tissue strain the stress had the greatest relaxation response and decreased by 7.5% during imaging. However, the position of nuclei did not appear to change throughout imaging following a rest period of 30 s.

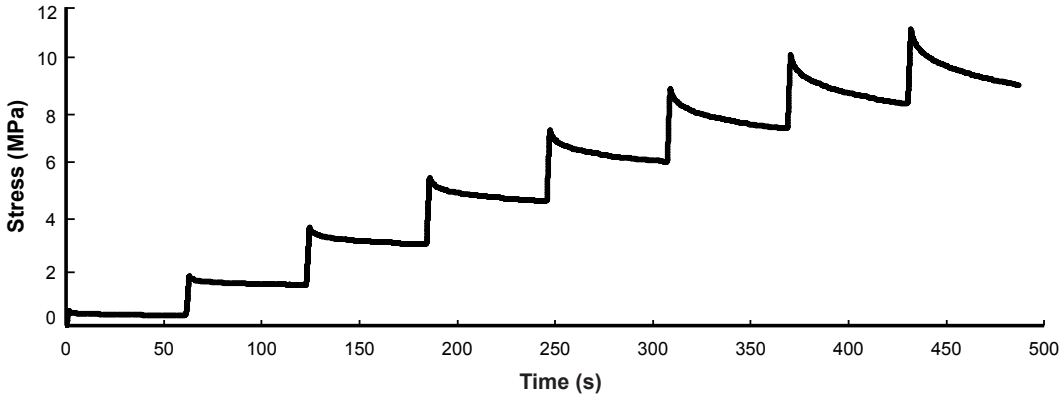

Figure 5.8: Representative stress–relaxation response of tendon over the course of a mechanical test (0–4% strain). Each peak represents an additional 0.5% strain applied to the tissue at intervals of 60 s. Imaging was initiated 30 s after reaching the desired strain level.

5.3.4 Cell–Level Displacement of Tenocytes in the Toe Region

The DAPI stain clearly highlighted cell nuclei and penetrated deep into tissue. The tissue remained hydrated throughout the test and there were no signs of photodamage during imaging (including photobleached region). There was no observable slippage at the grips and the specimen remained in focus throughout imaging. The cell–level displacement measurements for strains less than 4% corresponded

to complete removal of the fibril crimp as observed with the SHG signal.

The custom–written automated image analysis protocol was successful at detecting nuclei and quantifying their major axis length, centroid position and alignment (Figure 5.9). The change in alignment of nuclei was found to be most similar to the derived sinusoidal relationship with respect to the horizontal position along tendon at tissue strains less than 4% (Figure 5.10). The measurements (n = 10 tendons, n = 200 nuclei) were consistent between specimens.

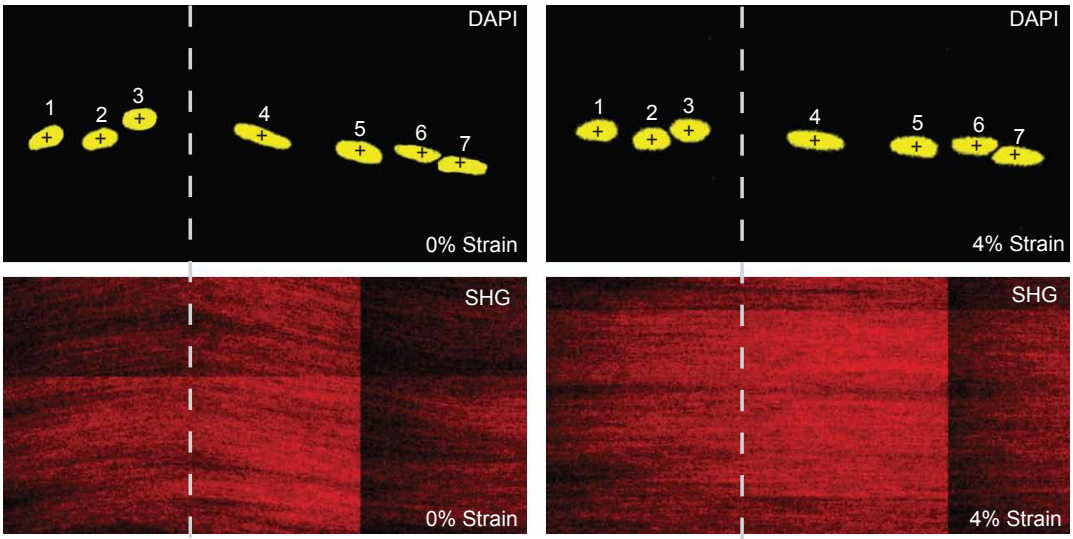

Figure 5.9: Automated characterization of nuclei in tendon specimen. Dashed line represents the position of the fibril crimp peak before and after deformation. Centroid position of nuclei are marked (+) and indicate change in alignment between 0 and 4% strain. Dark and light areas on SHG images are the result of tile–scanned image acquisition.

5.3.5 Cell–Level Displacement of Tenocytes at Large Strains

Grip–to–grip strains greater than 4% caused the fibril crimp to completely disappear. There was very little change in alignment of nuclei as arrays of cells

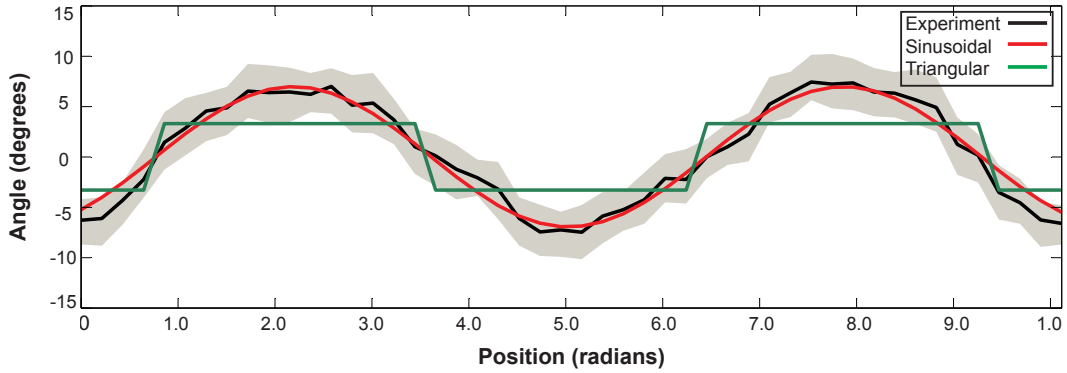

Figure 5.10: Change in alignment of nuclei with respect to the horizontal position of tendon. The mean change in alignment from experimental measurements is indicated by the black line and is surrounded by a gray area representing the standard deviation. The red curve represents the predicted change in alignment of a sinusoidal waveform and the green line a triangular waveform.

straightened under load. However, the displacement of nuclei increased as indicated by a change in centroid position compared to their previous position. At an approximate angle of 30° there existed a boundary that separated cells moving in opposite directions (Figure 5.11). Cells to the right of the boundary had a positive x and negative y displacement in comparison to cells on the left, which had a negative x and positive y displacement. Comparison between the deformation of all specimens indicated that the overall cell displacement had a similar profile. Separation of nuclei within arrays of cells was represented by a change in x–displacement of adjacent displacement vectors. Between 0 and 10% tissue strain there was a mean increase in displacement between cells of 3.25% (±0.62%).

The elongation of nuclei increased with applied strain and had a linear response above 4% strain (Figure 5.12). Prior to the removal of fibril crimp the major axis length of nuclei had a large variation with both positive and negative changes measured. Following crimp recruitment, elongation of nuclei was much more consistent

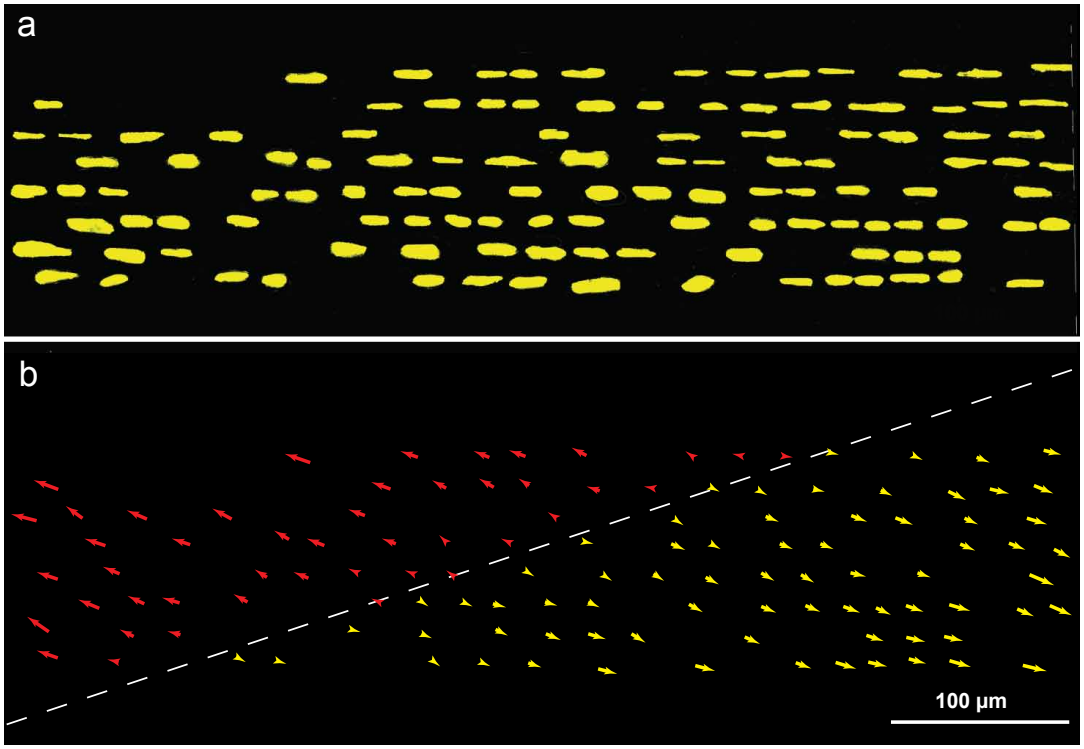

Figure 5.11: Representative displacement profile for nuclei in tendon. (a) DAPI stain at 4% tissue strain indicating alignment of nuclei. (b) Displacement vectors between 4 and 10% strain tracing the change in position of nuclei. Cells with a positive x–displacement are colored yellow and negative red. Dotted line represents transition from positive to negative horizontal orientation of vectors.

and all observations had a positive change in major axis length.

5.4 Discussion

5.4.1 Microtensile Testing Machine and Imaging Protocol

In this chapter the design of a MTM for use with an inverted confocal/multiphoton microscope was presented. The device consisted of a high–precision linear actuator, load cell, and custom–grips and was capable of applying micron–level dis-

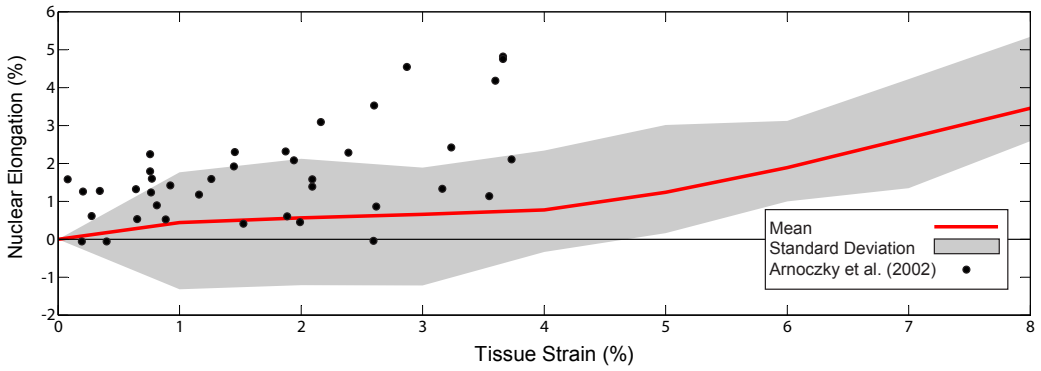

Figure 5.12: Change in major axis length of nuclei with the application of tissue strain. Prior to fibril recruitment there is a much larger variation in measurements (gray area). Results are compared to those reported by Arnoczky et al. (2002).

placements to tissue and measuring the transmitted force. The MTM worked in unison with a confocal/multiphoton microscope and allowed for detailed collection of microstructural images. The proposed design satisfied the design constraints defined in Section 5.2.1. Following testing, an automated image analysis program successfully measured the centroid position, elongation and orientation of nuclei in captured images allowing for characterization of nuclei–level deformations.

The MTM was comparable to previous devices, but included two major design improvements. First, the linear actuator allowed for the application of micron–level displacements to tissue, achieving a level of precision not previously reported. Previous devices (Arnoczky et al., 2002; Goulam Houssen et al., 2011; Screen et al., 2002) have used stepper motors coupled to worm gears to apply tissue displacement, but were limited by the size of the gear pitch. Being able to apply micron–level displacements to tissue was key to elucidating subtle changes to microstructural components. The second major improvement to the MTM was the grip design. The silicon sheath that surrounded tendons protected specimens

from stress concentrations previously reported in the literature (Weiss and Gardiner, 2001). This allowed for structure–function analyses at high strains while preventing tissue rupture at the grips.

Following collection of microscopic images, the automated image analysis procedure was used to characterize the displacement and deformation of nuclei allowing for accurate characterization of large data sets collected during testing. The combination of tile scans with automated characterization of nuclei and simultaneous imaging of collagen fibril organization provided detailed characterization of cell and ECM displacement across large portions of tendon.

The main limitation of the MTM design was the ability of the grips to hold tendon specimens adjacent to the cover slip at large strains ($> 8\%$). Specimens lifted slightly off the surface of the cover slip and made analyzing the tissue with high magnification oil or water immersion lenses difficult because the image resolution decreased significantly. However, non–immersion air lenses (20x) were capable of capturing clear images and provided sufficient magnification for the measurements reported in this chapter.

5.4.2 Microstructural Organization of Tendon

Through use of the MTM in combination with DAPI staining and SHG imaging I was able to characterize the displacement of nuclei relative to the position of fibril crimp. Through comparison of the experimental alignment measurements with theoretical sinusoidal and triangular models I found that the displacement of nuclei correlated well with the sinusoidal waveform.

Within the literature there has been a dynamic debate regarding the mi-

crostructural organization of tendon as having either a planar crimp (Diamant et al., 1972; Gathercole and Keller, 1991; Hulmes, 2002; Kastelic et al., 1978; Raspanti et al., 2005) or helical structure (De Campos Vidal and Mello, 2009; Feitosa et al., 2006; Franchi et al., 2010; Freed and Doehring, 2005; Ker, 2007). The organization is not fully understood because results vary depending on imaging modality, species and anatomical location being analyzed. There is much interest in the structure of fibril crimp because diseased tendon experiences notable variation in crimp angle and periodicity (Tuite et al., 1997). Moreover, fibril crimp has been suggested to act as a shock absorber, protecting tendon from impact loading (O'Brien, 1997).

The change in alignment of nuclei in the current chapter suggests that tendon has a sinusoidal organization in 2D, which may be representative of a 3D helical waveform at the fibril level. Further evidence supporting a helical organization is observed when capturing images from a variety of angles in different tendon specimens. Regardless of the orientation of the tendon, fibril crimp is always visible and has a consistent structure suggesting that the organization is not planar (data not shown). Therefore, my results support the hypothesis that tendon has a helical organization based on nuclear displacement measurements.

5.4.3 Displacement and Deformation of Tendon Nuclei

Following the removal of fibril crimp at approximately 4% strain, arrays of cells straightened in unison with collagen fibrils. Cell spacing increased with load and nuclei experienced significant elongation. Displacement gradients indicated that there was a transverse component involved in cell displacement. Moreover, the

displacement field showed reflection of symmetry in a plane at approximately 30° to the tendon long axis.

The increased elongation and separation of nuclei is expected in response to the application of tissue displacement given previous results (Arnoczky et al., 2002; Screen et al., 2004). At low strains (<4%) there was a slight increase in the mean long axis length of nuclei, but individual measurements unexpectedly ranged from -1% to 2%. The observed decrease in nuclear length was likely the consequence of measuring the long axis length of a 3D structure in 2D. With the application of load, select nuclei would move into the plane reducing the apparent long axis length in 2D.

The symmetry of the displacement field observed at high strains was not expected given results presented in the literature (Screen et al., 2004). The distribution was indicative of fascicle twisting with vectors pointing in opposite directions along an oblique line. Prior to each mechanical test, fascicles were inspected along the length of tendon to ensure that they were not twisted between the grips. However, variation in the loading position of the tendon may have led to a slight rotary response. Cheng and Screen (2007) and Khodabakhshi et al. (2013) suggest that tendon deformation may involve a twisting mechanisms, which correlates well with the current results. These findings highlight the importance of understanding the variation in the strain profile across large areas of tissue. For example, if the upper left portion of a specimen was analyzed all of the cells would appear to be traveling up and to the left (Figure 5.11). However, if the center of the specimen was analyzed a portion of the cells would appear to be traveling up and to the left, while others would appear to be traveling down and to the right.

5.5 Conclusion

In conclusion, I established a technique that was capable of simultaneously measuring the position of cells and collagen fibrils in a tendon exposed to load. Using this technique, I found that the displacement of cells was indicative of a sinusoidal organization in 2D and that nuclei experienced significant elongation under physiological conditions. From these results, a hypothesized that tendon has a helical organization and that nuclear deformation may act as a mechanosensor. These results improve our understanding of the loading environment of tenocytes which may contribute to tendon disease and regeneration.

Chapter 6

Microstructural Finite Element Model of Tendon

6.1 Introduction

6.1.1 Computational Tendon Models

In previous chapters I hypothesized that the PCM plays an important role in the transmission of force from the ECM to cells. I showed that applied tissue strain led to an elongation of nuclei that had the potential to initiate a mechanobiological response in tendon. However, the mechanical mechanisms responsible for force transmission are not well understood. Therefore, I created a microstructural finite element model of tendon to analyze cell–level displacement using newly derived structural images and mechanical observations from previous chapters.

Theoretical models provide quantification of parameters that cannot be easily measured in physical experiments. These models help us understand basic

biological mechanisms and predict changes involved in tissue health and disease. Mechanical models aim to describe the complex mechanisms responsible for tissue deformation.

Modeling the mechanical response of hierarchical tissues is challenging due to the complex interaction of structural molecules. For example, tendon consists of at least four hierarchical levels of organization and has a nonlinear, anisotropic, inhomogeneous, viscoelastic response with the ability to withstand large deformations. Consequently, numerous mechanical models have been presented in the literature to improve our understanding of tendon mechanics.

Mechanical models can be broadly categorized into two groups: phenomenological and mechanistic models (Figure 6.1). Phenomenological models describe the overall mechanical behavior of tissue and do not provide insight into the deformation mechanisms of the structure. The most commonly used phenomenological model is of exponential form.

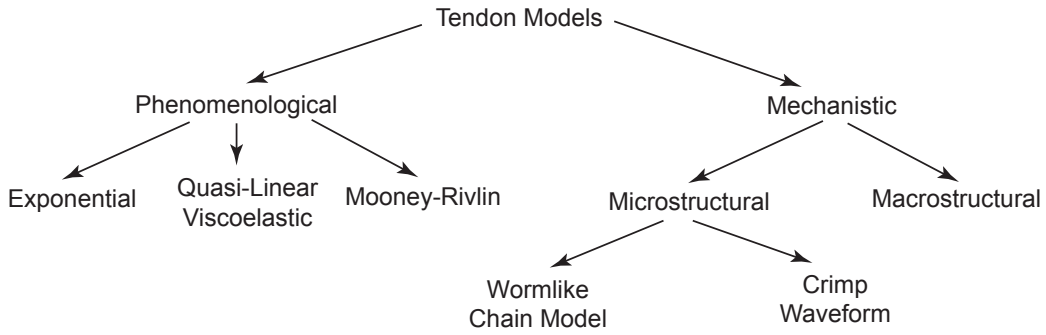

Figure 6.1: Categorization of mechanical tendon models. The model presented in this chapter falls within the microstructural category.

Structural models aim to describe the interaction of physical components in tissue to clarify deformation mechanisms. To date, the majority of models have

been 2D or limited to isotropic constraints in 3D. Early models aimed to describe the nonlinear stress–strain response of tendon (Diamant et al., 1972), but recent models have investigated additional structure–function mechanisms. Through 3D microstructural models, researchers have investigated interfibril matrix interactions (Fessel and Snedeker, 2010), helical structures (Reese et al., 2010) and fluid flow in tendon (Adeeb et al., 2004).

The most relevant model presented in the literature involving the micromechanical environment of tenocytes is an axisymmetric poroelastic model that analyzed the influence of fluid shear stress on membrane strain (Lavagnino et al., 2008). Collagen fibrils were modeled as spring elements and cells were embedded into the tissue structure as a submodel. It was suggested that fluid shear stress was capable of inducing a mechanobiological response through deformation of the cell membrane. The model thoroughly described the influence of fluid flow on cell–level force, but did not aim to describe the contribution of matrix strain on cell deformation. To the best of my knowledge, a tendon model analyzing the transmission of force from the ECM to cells has yet to be published in the literature.

6.1.2 Aims and Objectives

The aim of this chapter was to construct and validate a 3D finite element model of tendon capable of quantifying the deformation of cells due to matrix strain. This information could then be used to predict the mechanobiological response of the tendon to load using *in vitro* cell stimulus data presented in the literature. The first objective was to characterize the microstructural organization of tendon using TEM and MPM images in order to generate an accurate geometry for the

model. The second objective was to analyze the influence of collagen fibril and PCM stiffness on tissue–level stress and cell–level strain in tendon.

6.2 Materials and Methods

6.2.1 Geometric Characterization of Tendon Microstructure

The first step in generating the finite element model was to characterize the microstructural organization of tendon. This was accomplished by analyzing tendon specimens using TEM and MPM techniques. Images collected using MPM were used to define the organization of cells within crimped collagen fibrils and TEM images were used to characterize the size of collagen fibrils and tenocytes.

Rat tail tendons (n=10) were excised from tails as previously described (Section 4.2.1). Immediately following excision, tendons were cut in half and placed in either DMEM for MPM imaging or a fixative for TEM imaging. Confocal and MPM techniques were used to analyze fibril crimp and cell position as previously described in Sections 3.2.3 and 5.2.3.

The microstructural organization of tendon was analyzed using TEM with the help of Dr David Furgeson (John Radcliffe Hospital). RTTFs for TEM imaging were fixed in 4% glutaraldehyde in a phosphate buffer (pH 7.3) for 24 h at 4°C. The tissue was then post–fixed in osmium tetroxide for 60 min, dehydrated in increasing concentrations of ethanol and treated with propylene oxide for 24 h. The tissue was embedded in an epoxy resin (EMix, UK) and baked in an oven at 60°C for 48 h. Sections of 90 nm thickness were cut and stained with 2% uranyl

acetate and lead citrate and then analyzed with a JEM 100CX electron microscope (JEOL, UK).

Following imaging, TEM and MPM images were imported into Matlab for analysis. The automated protocol described in Section 5.2.3 was used to measure the position of cells in MPM images and the fibril and cell diameter in TEM images (Figure 6.2). The fibril crimp, wavelength and amplitude were estimated using the position of peaks and troughs in SHG images.

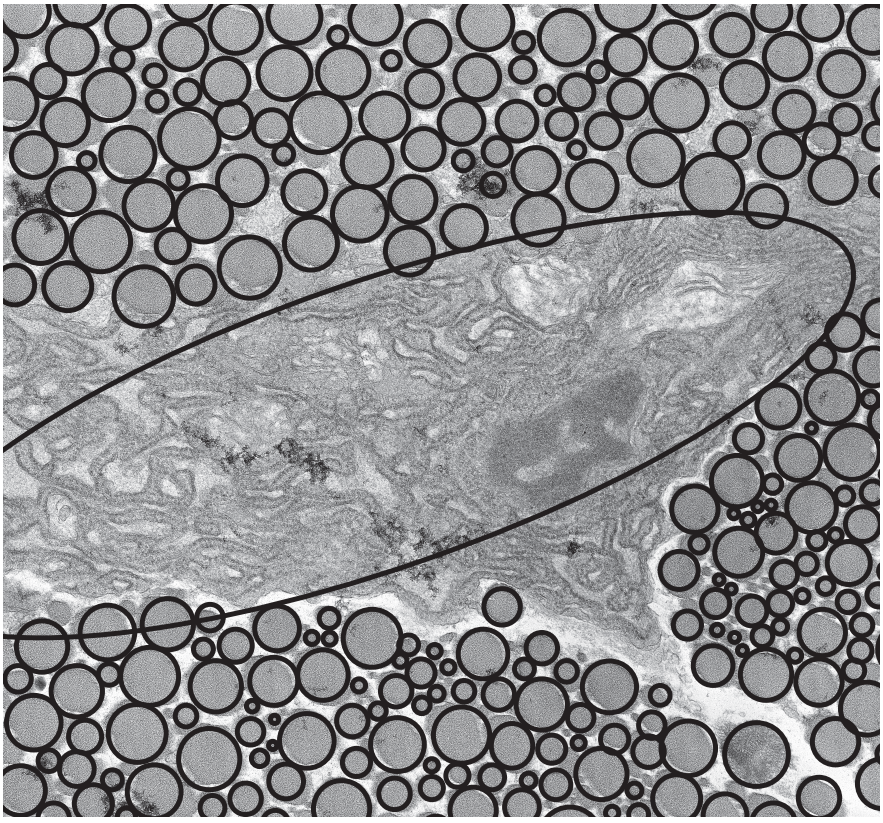

Figure 6.2: Characterization of collagen fibrils and tenocytes. Solid circles highlight the boundary of collagen fibrils and a tendon cell in TEM image. Collagen fibrils have a circular geometry and tenocytes an approximate elliptical geometry.

6.2.2 Finite Element Model Definition

The finite element model consisted of six major parts that were defined in Abaqus (SIMULIA, UK): collagen fibrils, ground substance, PCM, tenocyte, actin filaments and cell nuclei. The dimensions of all elements were extracted from MPM/TEM images excluding the PCM, which collapsed under TEM fixation. Alternatively, the PCM size was acquired from values reported in the literature using nondestructive techniques, such as freeze-fracture rotary electron microscopy (Ritty et al., 2003).

Given the evidence provided in Section 5.3.4, the model was assumed to have a helical geometry. The wavelength and helical pitch of fibrils were derived from the average measurements of SHG images (Table 6.1). Fibrils ran continuously along a 400 μm length and were situated within the ground substance, separated by 250 nm spacing (Figure 6.3). The model consisted of 130 collagen fibrils distributed in three circular arrays. The ground substance consisted of a hollow cylindrical geometry with subtracted helices for placement of collagen fibrils. The PCM and cells were distributed within the center of the ground substance. Cells were aligned along an identical helix to fibrils and had a longitudinal spacing of 5 μm between cells. Nuclei were placed at the centroid of tenocytes.

The elastic modulus of each element was acquired from the literature, however, the reported values varied significantly between studies (Table 6.1). The mean value for each measurement was used to define a base model, which was followed by a sensitivity study to quantify the influence of mechanical properties on measured parameters.

All materials were assumed to be linear elastic, isotropic and had a Poisson's

Table 6.1: Geometry and Material Properties of Finite Element Model Parts

Part	Geometry	Dimensions	Elastic Modulus
Collagen Fibril[1]	Cylindrical Helix	500 nm Diameter Pitch 200 μm Radius 30 μm	0.1 - 4 GPa
Ground Substance[2]	Hollow Cylinder	45 μm Outer Diameter 40 μm Inner Diameter 400 μm Length	0.1 - 1 MPa
Pericellular Matrix[3]	Spring Elements	10 - 15 μm Length	10 - 100 kPa*
Tendon Cell[4]	Sphereoid	20 μm Width 50 μm Length	1 - 10 kPa
Actin Filaments[5]	Spring Elements	7.5 - 15 μm Length	1 - 10 kPa*
Nucleus[6]	Sphereoid	5 μm Width 20 μm Length	0.1 - 5 kPa

1. (Heim et al., 2006; Lorenzo and Caffarena, 2005; van der Rijt et al., 2006). 2. (Ault and Hoffman, 1992; Reese et al., 2010). 3. (Alexopoulos et al., 2003; Guilak and Mow, 2000; Jaalouk and Lammerding, 2009). 4. (Guilak and Mow, 2000; Gupta and Haut Donahue, 2006). 5. (Howard, 2001). 6. (Guilak and Mow, 2000). *Indicates a representative elastic modulus. Spring element stiffness and number of spring elements are modified to represent the reported elastic modulus.

ratio of 0.3. These assumptions were made because the major aim of the model was to analyze the geometric deformation of the structure at low strains. Given these assumptions, constitutive equations ((6.1) – (6.4)) were used to define the material using Hooke's Law.

$$\epsilon_x = \frac{1}{E}(\sigma_x - \nu\sigma_y - \nu\sigma_z) \tag{6.1}$$

$$\epsilon_y = \frac{1}{E}(\sigma_y - \nu\sigma_x - \nu\sigma_z) \tag{6.2}$$

$$\epsilon_z = \frac{1}{E}(\sigma_z - \nu\sigma_x - \nu\sigma_y) \tag{6.3}$$

$$\gamma_{xy} = \frac{1}{G}\tau_{xy} \tag{6.4}$$

Where ϵ represents the strain, σ the stress, ν the Poisson's ratio, E the elastic modulus, γ the shear strain, τ the shear stress and G the bulk modulus. The bulk modulus is related to the elastic modulus and Poisson's ratio through (6.5).

$$G = \frac{E}{2(1+\nu)} \tag{6.5}$$

Combining (6.1) – (6.5), the constitutive equation for all materials is defined by matrix (6.6).

$$\begin{bmatrix} \epsilon_x \\ \epsilon_y \\ \epsilon_z \\ \gamma_{yz} \\ \gamma_{xz} \\ \gamma_{xy} \end{bmatrix} = \begin{bmatrix} \frac{1}{E} & -\frac{\nu}{E} & -\frac{\nu}{E} & 0 & 0 & 0 \\ -\frac{\nu}{E} & \frac{1}{E} & -\frac{\nu}{E} & 0 & 0 & 0 \\ -\frac{\nu}{E} & -\frac{\nu}{E} & \frac{1}{E} & 0 & 0 & 0 \\ 0 & 0 & 0 & \frac{1}{G} & 0 & 0 \\ 0 & 0 & 0 & 0 & \frac{1}{G} & 0 \\ 0 & 0 & 0 & 0 & 0 & \frac{1}{G} \end{bmatrix} \times \begin{bmatrix} \sigma_x \\ \sigma_y \\ \sigma_z \\ \tau_{yz} \\ \tau_{xz} \\ \tau_{xy} \end{bmatrix} \tag{6.6}$$

Collagen fibrils and the ground substance were meshed with C3D8R hexahedral elements using the sweep command. Fibrils were partitioned in the longitudinal direction at 0.5 μm intervals to improve seeding of the mesh. Cells and nuclei were also partitioned at 0.5 μm intervals and meshed using C3D8R hexahedral elements.

A fixed displacement corresponding to 4% overall strain was applied to fibrils and the ground substance at one end of the model while the opposing end was fixed in the x, y and z directions. The outer surface of collagen fibrils was fixed to the ground substance and no sliding occurred. Tissue stress, cell–level strain, and nuclear elongation were quantified throughout the simulation. The average stress (Force/Area) of the cross section was measured in order to compare results with stress–strain data collected in physical experiments presented in Section 4.3.2. The average elongation of nuclei was measured by subtracting the position of poles and was compared to nuclear extension results presented in Section 5.3.5. Finally, the average strain of cells was calculated to better understand cell–level deformation in tendon. The step size used for experiments was 0.01 and simulation took on average 20 min to converge.

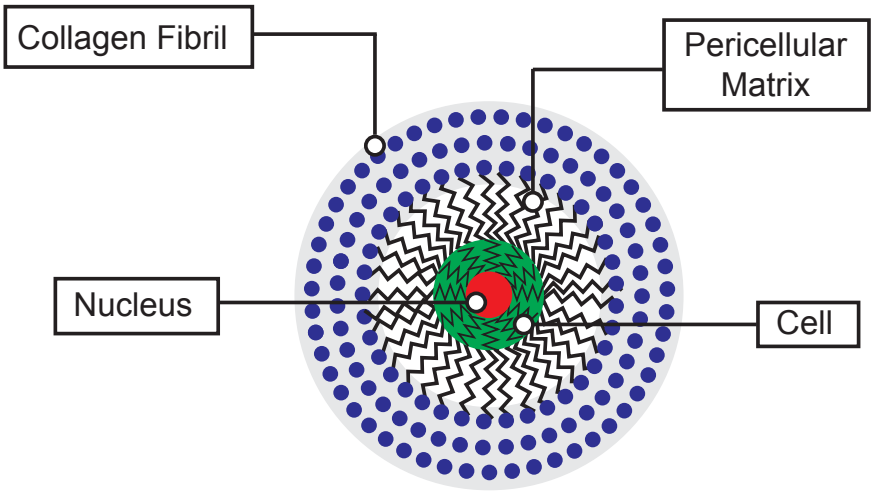

Figure 6.3: Cross–sectional schematic of finite element model. Fibrils were deposited within the ground substance and spring elements connected the innermost layer of fibrils to the cell membrane and the cell membrane to the nuclear membrane.

6.2.3 Sensitivity Analysis of Elastic Modulus

The largest uncertainty associated with the model was the mechanical properties of the model parts extracted from the literature. Given the large variation in reported values, a sensitivity analysis was conducted to determine the influence of element stiffness on the model output. More specifically, the range of elastic moduli for each element was divided into five values and then applied to the model while holding all other values at base levels. For example, a fibril stiffness of 0.1, 1, 2, 3 and 4 GPa was applied to the model and corresponded with the 0.1–4 GPa range. The stress–strain response, cell–level displacement and nuclear elongation were then compared for the range of input values.

A mesh sensitivity analysis was conducted to determine the optimal number of elements to achieve a sufficient level of accuracy while minimizing computational

time. The number of elements of each component was varied between 10 and 8,000 and the maximum stress of each part was used for optimization.

6.3 Results

6.3.1 Geometry and Assembly of Finite Element Model

The geometry of the helical model resembled the structure of tendon captured with confocal and multiphoton microscopy (Figure 6.4). In longitudinal projections the model appeared to have a sinusoidal waveform with cells distributed parallel to collagen fibrils. In transverse projections fibrils and cells intersected the cutting plane and resembled TEM images.

6.3.2 Overall Stress–Strain Response of Tendon Model

The helical model had a nonlinear stress–strain response, which coincided with the straightening of collagen fibrils. The stress–strain relationship correlated well with experimental data and increasing the fibril stiffness led to an increase in the slope of the stress–strain curve (Figure 6.5). An elastic modulus between 1 and 2 GPa most closely fit the experimental results.

The ground substance stiffness also influenced the stress–strain response (Figure 6.6). Increasing the elastic modulus led to a steeper curve, but to a lesser extent than collagen fibrils. It was found that the PCM, cell, actin and nuclear elastic moduli did not impact the overall stress–strain response within the reported values.

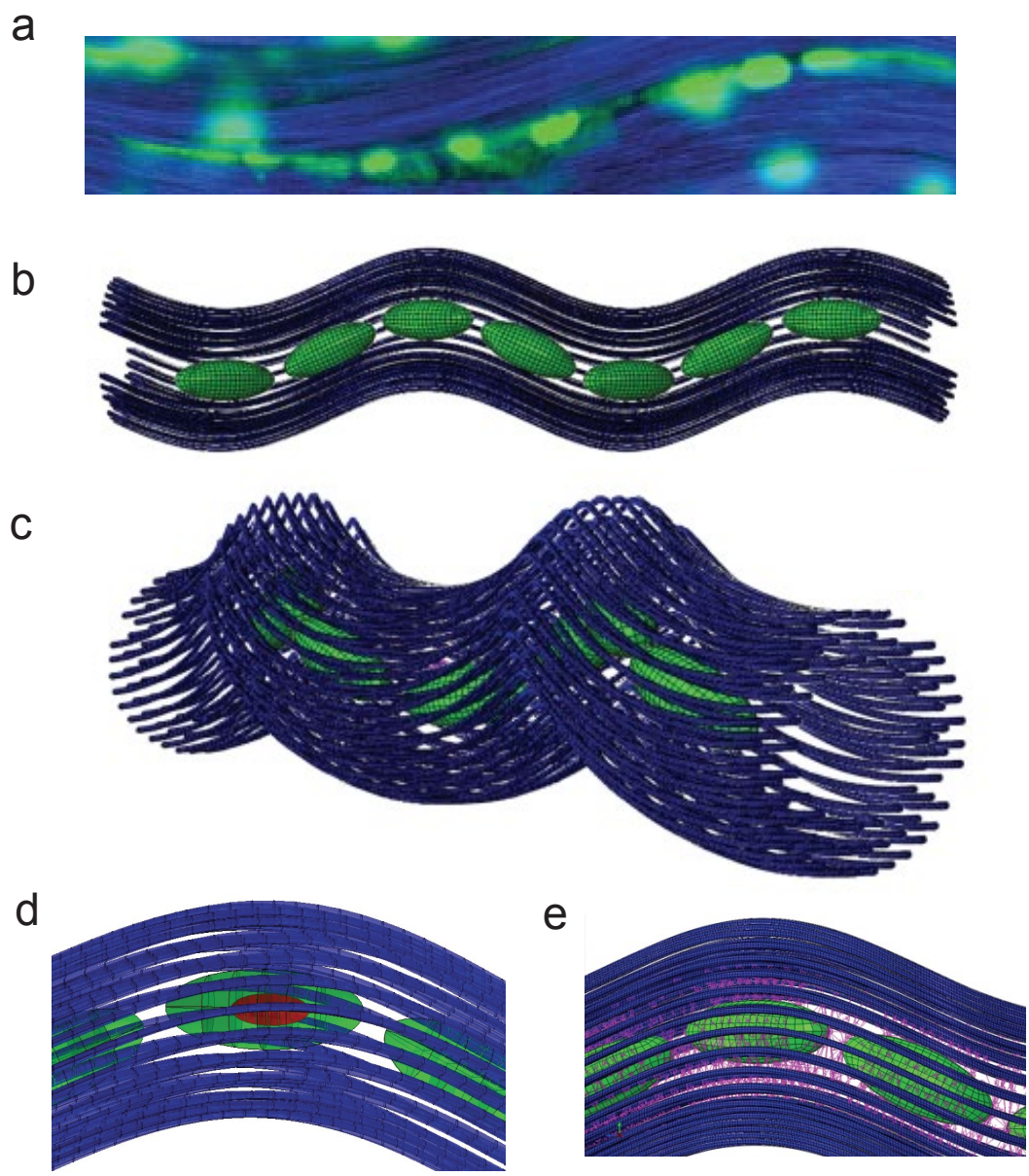

Figure 6.4: Assembly of finite element model. (a) Array of tenocytes (DAPI) that are distributed within collagen fibrils as acquired from confocal and multiphoton microscopy. (b) Side projection of model showing sinusoidal waveform. (c) Isometric projection of model depicting a crimped morphology as a result of the small helical radius. (d) Tendon cells (green) and nucleus (red) embedded in collagen fibril matrix. (e) Pericellular matrix (purple) is represented by spring elements connecting innermost collagen fibril layer to the surface of the cell.

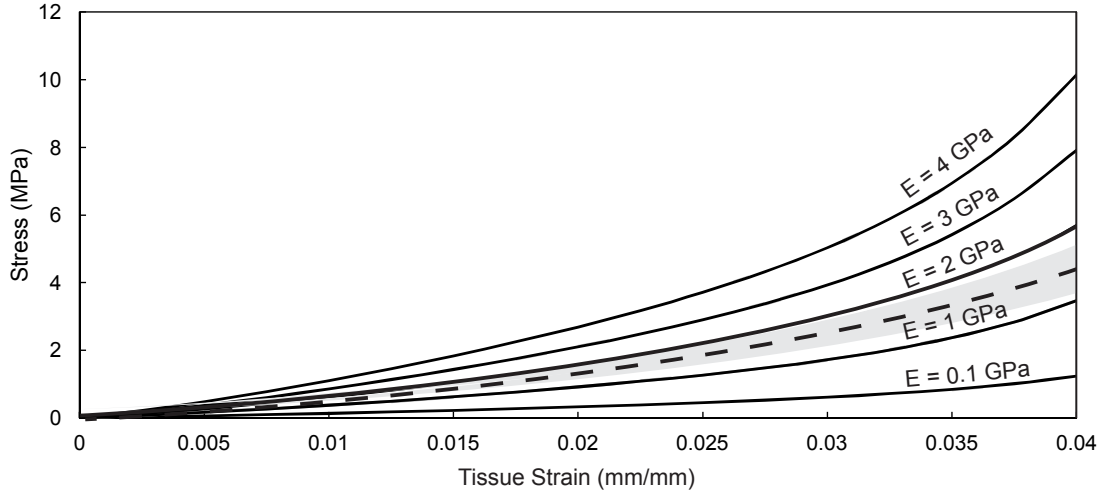

Figure 6.5: Influence of fibril stiffness on the stress–strain response. Results from the finite element model (solid lines) and mean experimental tensile test (dotted line, Section 5.3.5) correlate well. The gray area surrounding experimental results represents the standard deviation (n=10). An increase in fibril stiffness leads to a greater slope.

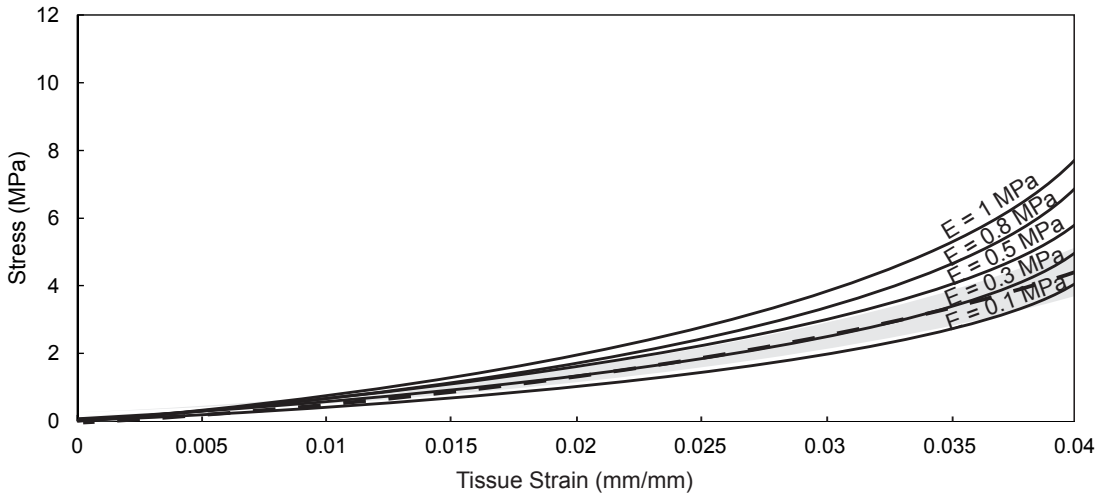

Figure 6.6: Influence of ground substance stiffness on the stress–strain response. An increase in elastic moduli leads to a steeper stress–strain curve of tendon. Results of finite element model (solid lines) correlates well with mean experimental tensile test (dotted line, Section 5.3.5). The gray area surrounding experimental results represents the standard deviation (n=10).

6.3.3 Cell-Level Deformation of Tendon Model

The deformation of cells was governed by the geometric deformation of fibrils and the ground substance causing deformation of the PCM. Cell–level strain had a linear relationship with respect to tissue strain and became steeper with increasing PCM stiffness (Figure 6.7). Within the range of the PCM elastic moduli, the cell–level strain at 4% tissue strain varied between 0.4 and 3.8% strain.

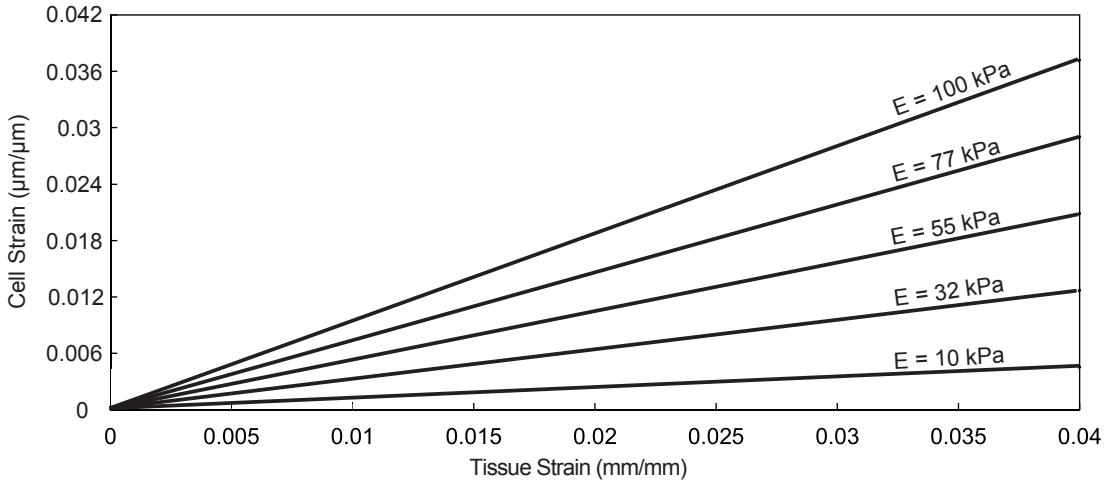

Figure 6.7: Influence of PCM stiffness on cell–level strain. Cell strain has a linear relationship with respect to tissue strain. Increasing the PCM elastic modulus increases the strain experienced by tendon cells.

Geometric deformation of cells caused elongation of cell nuclei (Figure 6.8). The long axis elongation had a linear relationship with the application of tissue strain. Increasing the stiffness of the cells, actin and nuclei within the prescribed range had little influence on the nuclear elongation (data not shown).

The mesh sensitivity analysis for all parts indicated that the maximum measured stress, strain and elongation increased with number of elements and stabi-

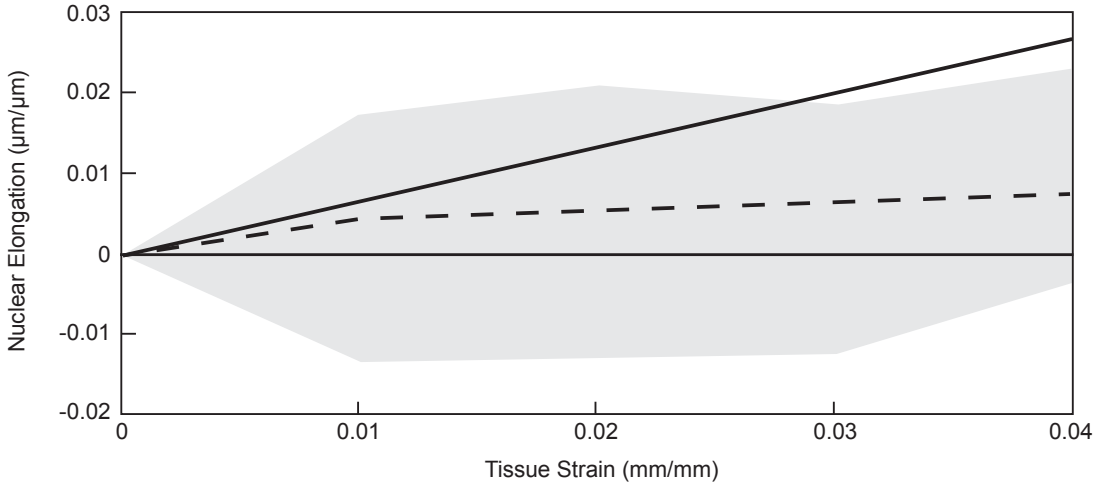

Figure 6.8: Elongation of nuclei with the application of tissue strain. The response has a linear relationship (solid line) and is greater than measured experimental values in 2D (dotted line is mean elongation, gray area is standard deviation) (Section 5.3.5.).

lized when reaching a sufficient mesh density. For example, the maximum stress of collagen fibrils stabilized at approximately 1,000 elements (Figure 6.9). Similarly, it was found that a mesh size of 1,500 was sufficient for the ground substance, 200 for cells and 100 for nuclei.

6.4 Discussion

6.4.1 Geometry and Mechanical Response of Tendon Model

The 3D helical microstructural model was capable of reproducing the nonlinear stress–strain response of tendon. The results correlated well with experimental data and a fibril stiffness between 1 and 2 GPa led to the smallest deviation when compared to experimental measurements. It was also expected that the

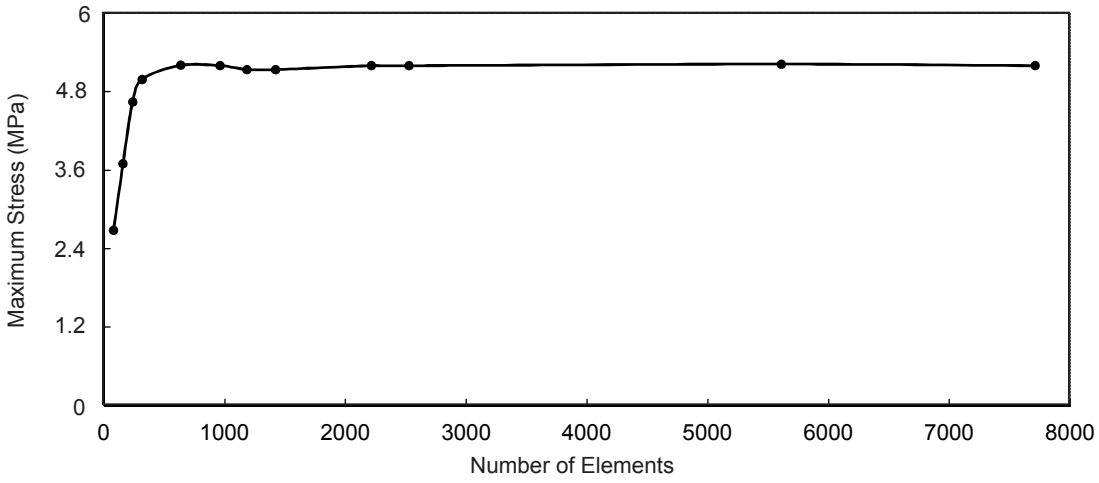

Figure 6.9: Representative mesh sensitivity curve for collagen fibrils. A mesh consisting of approximately 1,000 elements reaches a sufficient level of accuracy.

stress–strain response would vary with respect to the helical radius and pitch. However, I did not investigate this relationship because my aim was to model RTTFs, which had a consistent structural organization. Previously, it has been shown that increasing the helical pitch increases the slope of the stress–strain curve (Reese et al., 2010).

The apparent organization of the model was influenced by the position of the viewing plane. For example, a side projection depicted a sinusoidal waveform whereas an isometric projection depicted a triangular waveform. This suggests that previous characterizations of tendon as having a planar crimped structure may have been the result of a 2D analysis of a 3D helical structure. Future studies investigating the detailed 3D organization can be conducted using serial section techniques.

There has been much interest in modeling the toe region of the stress–strain curve of tendon and previous studies have addressed the nonlinear response by

modifying either the fibril geometry or fibril recruitment mechanism of tendon. Early studies modeled fibril geometry using hinged elements (Diamant et al., 1972) or sinusoidal beams (Lanir, 1978) connected together by spring elements. As force is applied to the model, the spring elements resist deformation until the crimped structure straightens. The physical structure that represents spring elements has been suggested to be elastic fibers, although structural evidence has not been provided. More recent studies have modeled the nonlinear region of the curve using 3D cylindrical helices (Freed and Doehring, 2005; Reese et al., 2010).

An alternative method for representing the nonlinear region of the stress–strain curve has been achieved by modeling fibrils of various lengths. The overall stiffness of the model increases as additional fibrils are loaded yielding a nonlinear response (Viidik, 1968). A similar approach was used by Cacho et al. (2007) who modeled fibrils of the same length, but with a random crimp angle. As tendon deforms, fibrils are sequentially loaded from the smallest crimp angle to the largest, again yielding a nonlinear response.

Through detailed structural characterization of tendon with MPM and TEM I did not observe evidence of structural molecules connecting together fibrils. Moreover, images indicated that fibrils had a consistent amplitude and wavelength suggesting that deformation mechanisms do not involve sequential fibril recruitment or connected planar structures. However, the helical model was capable of reproducing the stress–strain response and nuclear elongation observed in tendon. Therefore, I believe that the deformation mechanism of tendon involves a helical response at the microstructural level.

As introduced in Section 2.2.4 previous experimental observations have suggested that tendon deformation involves a series of a mechanisms. In particu-

lar, through use of synchrotron X–ray diffraction (XRD) techniques, Fratzl et al. (1998) suggested that collagen molecules are only exposed to 40% of the total strain applied to tissue. Therefore, it is expected that interfibril and interfascicle cross–links contribute to tendon deformation. My model assumes that there is complete bonding between collagen fibrils and the ground substance and that no fibril sliding occurs. Therefore, my model may overestimate the amount of strain that is applied to collagen fibrils. However, sliding mechanisms were found to significantly influence the linear region of the stress–strain curve, but had little effect on the nonlinear region (Fratzl et al., 1998), so errors due to fibril sliding in the current model are expected to be small.

6.4.2 Role of the Pericellular Matrix in Cell–Level Deformation

The finite element model with PCM was capable of reproducing the nuclear deformation of tenocytes as observed in experimental results. The largest contributing factor to cell–level strain was the elastic modulus of the PCM. These results suggest that the PCM plays a key role in influencing the micromechanical environment of tendon cells.

Previous studies on PCM function have focused on cartilage and bone and have highlighted the significance of the PCM in health and disease. In cartilage, the PCM has been shown to amplify chondrocyte compressive strains (Guilak et al., 1999; Han et al., 2004) while providing stress shielding for cells (Alexopoulos et al., 2005). Fluid flow within the PCM has also been shown to mechanically stimulate bone cells (Han et al., 2004; You et al., 2001), chondrocytes (Julkunen et al., 2009)

and tendon cells (Lavagnino et al., 2008).

Although previous models have highlighted the mechanical contribution of the PCM in cartilage and bone, the structure and loading environment is significantly different from that of tendon. Cartilage and bone cells are independently surrounded by a PCM and are largely exposed to compressive forces. In contrast, the PCM of tendon surrounds arrays of cells and the tissue is predominately exposed to tensile forces. Therefore, extrapolating results from previous models and drawing conclusions about tendon PCM may not be suitable due to the large differences in tissue structure and function.

Results from the parametric analysis provide insight into the role of the PCM in tendon deformation. If tendon lacked a PCM and cells were directly attached to fibrils this organization could be modeled under the current scheme using a PCM stiffness equivalent to the cell stiffness. Because the reported elastic modulus of cells is at least 10 times smaller than that of the PCM (Table 6.1), cell–level strain would decrease significantly as shown in Figure 6.7. For example, the maximum cell stiffness reported in the literature (10 kPa) would lead to a 0.5% cellular strain within the nonlinear region. Given the range of reported values required to stimulate tendon cells, a model lacking the PCM would lead to insufficient cell–level strain required to elicit a mechanobiological response. Therefore, similar to cartilage and bone, tendon PCM may serve the important role of amplifying mechanical signals. It should be noted that the current model does not include the influence of fluid flow on cell strain and future models should aim to include both matrix and fluid stress.

6.4.3 Nuclear Deformation of Tendon Cells

Cellular deformation and nuclear elongation were predicted in the model under physiological conditions. The predicted nuclear elongation correlated relatively well with experimental results and had a linear relationship with applied tissue strain. This finding provides support for the proposed matrix–cytoskeleton mechanotransduction pathway as discussed in Section 2.3.1.

Multiple studies have investigated the influence of mechanical stimulus on biological function. Studies involving tendon and ligament cells have shown that the magnitude of loading (Yang et al., 2004), rate of loading (Barkhausen et al., 2003) and location of cells within the tissue (Hsieh et al., 2000) influence the mechanobiological response. Mechanical loading causes changes in type III (Lee et al., 1999) and type I (Howard et al., 1998) collagen production in addition to changes in the synthesis and secretion of fibronectin, matrix metalloproteinases (MMPs) and tissue inhibitor of metalloproteinase (TIMPs) (He et al., 2004). The magnitude of strain applied to cells was in the 3–6% range and the rate of loading varied between 0.5–1 Hz.

Given the reported strain values required to elicit a response in tendon, my model predicts that cells would undergo mechanobiological stimulation. However, predicting the specific molecules that would be synthesized is not possible given the availability of mechanobiological data. As further mechanobiological studies are conducted, including 3D stimulus, results can be used in combination with the current model to predict compositional and structural changes to tendon.

6.5 Conclusion

In conclusion, I proposed a finite element model that was capable of predicting cell–level deformation within the nonlinear region of the stress–strain curve. Results indicated that a helical organization was capable of reproducing the stress–strain curve and the PCM influenced cell–level strain. These findings suggest that the nonlinear region of the curve is the result of a helical organization and that the PCM acts as an amplifier of mechanical stimulus.

Chapter 7

Discussion

7.1 Summary and Future Directions

7.1.1 Overall Summary of Thesis

The aim of this thesis was to elucidate the microstructural deformation response of tendon. Emphasis was placed on the mechanical microenvironment of tenocytes, which was hypothesized to be a key factor in maintaining tissue homeostasis through mechanobiological mechanisms. A common theme present throughout the thesis was the role of elastic fibers in tendon because of their poorly understood function. Through detailed collection and analysis of novel structural images and mechanical properties I was able to improve the current understanding of tendon structure and function, particularly at the microstructural level.

7.1.2 Organization of Elastic Fibers in Tendon

The aim of the third chapter was to characterize the distribution of elastic fibers in healthy and damaged tendon to better understand their function. Through use of histological and immunostaining techniques I found that elastic fibers had a sparse distribution, but were highly localized around arrays of tenocytes and between fascicles. My interpretation of these results was that elastic fibers formed part of the PCM and the endotenon sheath. Moreover, I predicted that elastic fibers would significantly contribute to the mechanics of the PCM, which may serve an important mechanical role in musculoskeletal tissues. Damaged tendon biopsies had an increased visibility of elastic fibers and a heavily disrupted elastic fiber network.

There are multiple experiments that can be conducted to improve our understanding of elastic fiber function in healthy and damaged tendon. First, the organization of elastic fibers is likely dependent on the tendon type, location (OTJ, MTJ, Midsubstance) and age of the specimen and experiments should be conducted to better understand the associated changes. Of particular interest is a comparison between the local mechanical environment of the tissue and the corresponding elastic fiber organization. From my results (Section 3.3.2) I would expect that the elastic fiber density of the PCM would be dependent on the forces experienced by cells.

The second aspect to be further explored is the organization and concentration of elastic fibers in diseased tissue. I showed that elastic fibers had a severely disrupted network and increased visibility in damaged tissue (Section 3.3.3). Additional techniques (e.g., western blotting and quantitative polymerase chain re-

action (qPCR)) can be used to quantify the change in elastic fiber synthesis and distribution in diseased tissue. It would be interesting to determine if the increased visibility of elastic fibers observed in damaged specimens is the result of increased synthesis of elastic fibers or solely improved visibility of fibers due to ECM degradation. Moreover, qPCR could help elucidate the synthesis of elastic fibers in damaged tendon to determine if cells are capable of replacing elastin at later stages of life. Changes to other PCM structural molecules can also be analyzed to determine the consequences of tendinosis on PCM integrity.

7.1.3 Effect of Elastase on the Structure and Function of Tendon

The aim of the fourth chapter was to analyze the effect of elastase on the mechanics, structure and composition of tendon to better understand the mechanical role of elastic fibers in tendon. Using mechanical testing, MPM and biochemical assays I found that elastase caused nonspecific degradation of the ECM. More specifically elastase decreased the crimp angle of collagen fibrils and led to degradation of GAGs. Consequently, I hypothesized that changes to the UTS and failure strain observed in elastase treated specimens were likely the result of nonspecific degradation of the ECM. Therefore, previous and current mechanical observations that have been derived from elastase treatments should be interpreted as the result of widespread ECM degradation rather than the removal of only elastic fibers.

Although elastase causes nonspecific degradation to the ECM it may prove useful in understanding the consequences of damage to tissue mechanics. There are a variety of enzymes that have been used to analyze the mechanical con-

tribution of structural molecules to tissue mechanics including GAGs and type I collagen. Incubating tissue specimens in various enzymes and quantifying the change in composition and structure may lead to new links between structural molecules and the mechanical properties of tissue. Rather than relying on the specificity of the enzyme, biochemical assays should be conducted to determine the specific degradation profile of the corresponding treatment. Moreover, a detailed medium sensitivity study should be conducted given the unexpected tissue swelling observed in PBS incubated specimens. By varying the ionic concentration of solutions and incubating tendon specimens, the influence of fluid properties on tendon structure and function can be achieved. This may be particularly relevant for tendons that are lubricated by synovial fluid and wrapped by a synovial sheath.

A second area that can be further explored is the influence of elastase on tendon compared to tendon fascicles. Excised tendon fascicles lack an endotenon sheath and are not exposed to interfasciclular interactions. I found that the endotenon sheath consists of a dense distribution of elastic fibers that likely contributes to the mechanics of the local structure (Section 3.3.2). Therefore, differences in the mechanical properties between tendon and tendon fascicles incubated in elastase may improve our understanding of the mechanical contribution of the endotenon sheath. However, detailed characterization of the degradation will need to be conducted to evaluate the removal of structural molecules from the ECM and endotenon sheath.

The final area of interest that may prove useful is investigating the release of elastase by neutrophils during tendinitis. Neutrophils have been shown to naturally produce elastase in a number of inflammatory diseases (Starkey, 1976), which is thought to improve tissue remodeling. I have shown that small concentrations of

elastase cause significant changes to tissue composition, structure and mechanics and therefore, release of elastase may have a large influence on tendon integrity. Particularly, the change in elastase production with respect to tissue loading could lead to a fuller understanding of mechanobiological mechanisms in tendon disorders.

7.1.4 Deformation of Collagen Fibrils and Tenocytes

The aim of the fifth chapter was to examine the deformation mechanisms of tendon to better understand structure–function relationships of the tissue and cell–level deformation. A MTM was designed for a confocal/multiphoton microscope and used to track the position of collagen fibrils and cells during tendon deformation. Through a custom–written automated image analysis program the position, alignment and elongation of cells was derived and compared to results of theoretical triangular and sinusoidal waveforms. I found that cell–level displacement was representative of a sinusoidal waveform and that cell nuclei experienced significant elongation under physiological conditions. From these results I postulated that tendon had a helical structure and that nuclear deformation could elicit a mechanobiolgoical response.

The combination of microscopy and mechanical testing is a powerful technique that can be used to elucidate structure–function relationships of tissue. In tendon, there are several mechanisms that are poorly understood but are prime candidates for analysis with this technique. For example, the deformation of the cell membrane can be investigated to better understand force transmission from the ECM to the cell. By staining the cell membrane, focal adhesion complexes, actin and

the nucleus the ECM–cell mechanobiological pathway may be better understood.

Structure–function analyses may prove useful in elucidating the micromechanical consequences of tissue damage. Mechanical testing in combination with MPM can be used to analyze collagen fibril deformation of tendon with various degrees of damage. Tissue damage can be initiated using mechanical (e.g., laceration) or biochemical (e.g., MMPs) techniques. Changes to cell–level deformation may provide insight into the consequences of tissue damage on mechanobiological mechanisms.

I investigated the quasi–static loading of tendon, but the origin of viscoelastic deformation mechanisms is poorly understood. Microscopy and mechanical testing can be used to analyze the micromechanical mechanisms responsible for the stress–relaxation and creep responses in tendon. More specifically, MPM can be used to analyze the change in type I collagen fibril organization during viscoelastic mechanical tests to better understand the micromechanical mechanisms responsible for the dynamic response of tendon. Knowledge of the viscoelastic mechanisms will be key to understanding tendon function under physiological conditions, which involves dynamic loading.

7.1.5 Microstructural Finite Element Model of Tendon

The aim of the sixth chapter was to generate a microstructural model of tendon to better understand force transmission from the ECM to cells. TEM and MPM were used to characterize the microstructural organization of collagen fibrils, the ground substance and the PCM in tendon. These structural images in combination with mechanical properties from the literature were used to define the organization and material properties of the model. A parametric analysis was conducted on key

parameters and used to determine the influence of various properties on tendon deformation. I found that a helical organization was capable of replicating the stress–strain response of tendon. Moreover, it was shown that cells experienced notable deformation, which was dependent on the stiffness of the PCM. I hypothesized that the PCM played a key role in amplifying forces that would be required to elicit a mechanobiolgiocal response in tendon under physiological conditions.

Force transmission from the ECM to cells represents a means of inducing a mechanobiolgiocal response in tendon. In addition to the ECM–cell pathway there are other mechanisms that have been suggested to contribute to cell function. Of particular relevance is the influence of fluid flow on cell membrane deformation during loading of tendon. The PCM is less densely packed and appears more porous than the ECM and therefore, may encourage fluid to flow around arrays of tendon cells. Fluid flow would increase membrane strain and potentially deform mechanosensitive structures such as the primary cilium, which would lead to mechanobiological responses in tendon. Future studies should incorporate fluid flow into the current model to better understand the loading environment of tendon cells.

The nonlinear portion of the stress–strain curve was modeled in this thesis, but it has been suggested that physiological stresses can reach the linear region of the stress–strain curve. Consequently, future studies should extend the current model to analyze micromechanical mechanisms at higher strains. In order to model tendon at large strains additional micromechanical mechanisms will need to be defined to described the mechanical response of the tissue. Sliding has been shown to play a significant role at larger strains (Section 2.2.4), thus the interaction between collagen fibrils and the ground substance must be defined. In addition

to MPM, other imaging techniques, such as Brillouin scattering, elastography and Raman spectroscopy, may prove useful in defining these mechanisms.

Finally, this model can be used to analyze the consequences of tissue damage on transmission of force from the ECM to cells. Using microscopic techniques such as MPM and TEM the detailed organization of healthy and damage tendon may be characterized. Images can then be used to define the organization of the finite element model and elucidate the influence of damage on cell–level deformation.

7.1.6 Future Research Projects

From the discussion above it is apparent that there are multiple areas that can be further explored to better understand the microstructural deformation of tendon. To summarize the discussion I propose three specific research projects below that build on findings presented in this thesis and have the potential to lead to novel insight regarding tendon structure and function. Each project description includes an aim followed by a brief discussion as to why I think it is of particular relevance.

- **Aim: Characterize the organization of elastic fibers in bovine flexor tendon and bovine extensor tendon.** Flexor tendon experiences large loads and has been suggested to have an energy storage role. Extensor tendon experiences small loads and has been suggested to have a positional function. I have reported the elastic fiber organization of bovine flexor tendon and showed that it is mainly distributed in the endotenon sheath and pericellular matrix. However, this organization may be significantly different from that of bovine extensor tendon and a comparison between the two tendon types will likely to improve our understanding of elastic fiber function in the tissue.

- **Aim: Define the mechanical properties of tendon fascicles and tendon proper treated with elastase.** I have reported the change in mechanical properties of tendon fascicles treated with elastase. However, tendon fascicles lack an endotenon sheath, which I have shown to have high concentrations of elastic fibers. Consequently, treating entire tendons with elastase and comparing the change in mechanical properties to that of tendon fascicles will likely lead to novel insight into the role of elastic fibers in the endotenon sheath.

- **Aim: Observe the deformation of the cell membrane, focal adhesion complexes and actin filaments in tendon under load.** I was able to characterize the displacement and deformation of cell nuclei in tendon exposed to load. However, there are many other cellular structures that can be observed, which will help elucidate cell-level loading of tendon. RTTF structures can be highlighted with a variety of cellular stains and I have recently stained the membrane of tenocytes (data not shown) with a cell-membrane stain (Invitrogen, UK). Through staining of the cell membrane, focal adhesion complexes, actin filaments and nuclei, force transmission from the ECM to nuceli may be observed. These findings will aid in understanding mechanobiological loading of tendon.

7.1.7 Use of Mechanobiology for Treatment of Tendon Disorders

As introduced in Section 1.1, a firm understanding of mechanobiology is required to design effective tissue–engineered treatment strategies. The mechanical envi-

ronment of cells is key to maintain cell phenotypes and promoting healthy production of ECM structural molecules. Results from this thesis suggest that tissue–engineered constructs should aim to mimic the PCM of healthy tendon. This may be accomplished by generating a micro–architecture that is similar to that of healthy tendon and including structural molecules that provide appropriate local mechanical properties.

In addition to tissue–engineered constructs this research may improve diagnosis of tendon disorders. Disruption of the ECM and/or PCM is expected to influence the mechanobiolgical response of the tissue and may influence a myriad of factors including cell phenotype and metabolism. Molecules in the PCM may act as targets for pharmacological strategies that aim to restore function following acute injury or tendinosis.

Appendix A

Rule of Mixtures Extracellular and Pericellular Matrix

To investigate the mechanical role of elastic fibers in tendon two simple rule of mixtures composite models are proposed. The ECM is assumed to be composed of collagen fibrils and elastic fibers embedded in a ground substance and the PCM consists of elastic fibers embedded in a type VI collagen matrix (Figure C.1).

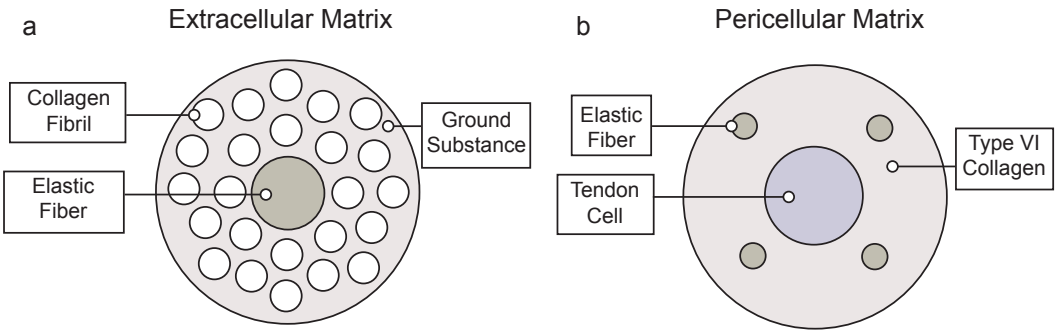

Figure C.1 Rule of mixtures schematic for tendon ECM and PCM. (a) The ECM model consists of collagen fibrils and elastic fibers distributed in the ground substance. (b) The PCM model consists of elastic fibers distributed in a type VI collagen matrix.

The assumptions associated with the models are that fibers are uniformly dis-

tributed in the matrix, there is complete bonding between fibers and the matrix and that both the fibers and matrix are linear elastic materials. With these assumptions in place, the stiffness contribution of each component is derived using static equilibrium conditions.

First, two basic definitions for the stress (1) and elastic modulus (2) of the material are defined.

$$\sigma = \frac{F}{A} \tag{1}$$

$$E = \frac{\sigma}{\epsilon} \tag{2}$$

Next, if all components of the ECM are loaded in parallel, the total force carried by the material (F_{ECM}) is equal to the sum of the force in the collagen fibrils (F_f), the elastic fibers (F_e) and force in the ground substance (F_g) as show in (3). Similarly, the force of the PCM composite (F_{PCM}) is equal to the force of the elastic fibers (F_e) and the force of the type VI collagen matrix (F_m) as shown in (4).

$$F_{ECM} = F_f + F_e + F_g \tag{3}$$

$$F_{PCM} = F_e + F_m \tag{4}$$

Substituting (2) into (1) followed by (3) I derive (5). Similarly, subbing (2) into (1) followed by (4) I derive (6).

$$E_{ECM}\epsilon_{ECM}A_{ECM} = E_f\epsilon_f A_f + E_e\epsilon_e A_e + E_g\epsilon_g A_g \tag{5}$$

$$E_{PCM}\epsilon_{PCM}A_{PCM} = E_e\epsilon_e A_e + E_m\epsilon_m A_m \tag{6}$$

Assuming that complete bonding occurs between components, the strain in all components is of equal value as shown in (7) and (8).

$$\epsilon_{ECM} = \epsilon_f + \epsilon_e + \epsilon_g \tag{7}$$

$$\epsilon_{PCM} = \epsilon_e + \epsilon_m \tag{8}$$

Under these conditions, I derive the stiffness contribution of each component, which takes the form of (9) and (10).

$$\frac{F_f}{F_{ECM}} = \frac{E_f A_f}{E_f A_f + E_e A_e + E_g A_g} \tag{9}$$

$$\frac{F_e}{F_{PCM}} = \frac{E_e A_e}{E_e A_e + E_m A_m} \tag{10}$$

In order to solve (9) and (10) I require the cross sectional area contribution and elastic modulus of all components. Using TEM images of tendon from Section 6.2.1 I estimate the area occupied by collagen fibrils and the ground substance within the ECM. The area occupied by type VI collagen is calculated using a PCM width of 10 μm and assuming a circular distribution around cells. Next, I use

immunostained images of elastic fibers to calculate the number of elastic fibers in the ECM and PCM. The area contribution of elastic fibers is calculated assuming that each fiber has a diameter of 800 nm (Lorber, 1989). The stiffness of collagen fibrils (Heim et al., 2006), elastic fibers (Fung, 1993), ground substance (Ault and Hoffman, 1992) and type VI collagen (Guilak and Mow, 2000) are extracted from the literature.

TEM images (Figure 2.3) indicate that collagen fibrils make up the majority of tendon ECM (Table C.1). The ground substance has the second largest area contribution and elastic fibers the least making up approximately 2% of the area. Due to the large elastic modulus of collagen fibrils they contribute to nearly 100% of ECM stiffness. For the PCM model elastic fibers are found to be responsible for 28% of the overall stiffness, but only contribute to 3% of the area. Type VI collagen forms 97% of the area and contributes to 72% of the stiffness of the PCM.

Table C.1: Rule of Mixtures Summary for Tendon

Extracellular Matrix

Element	Stiffness (Pa)	Area Contribution	Stiffness Contribution
Collagen Fibril	$1.0x10^9$	88%	99.9%
Ground Substance	$1.0x10^6$	10%	0.013%
Elastic Fiber	$3.5x10^5$	2.0%	0.0008%

Pericellular Matrix

Element	Stiffness (Pa)	Area Contribution	Stiffness Contribution
Type VI Collagen	$3.0x10^4$	97%	72%
Elastic Fiber	$3.5x10^5$	3.0%	28%

Appendix B

The following engineering drawings describe the detailed dimensions of the parts that make up the microtensile testing machine. All dimensions are in mm.

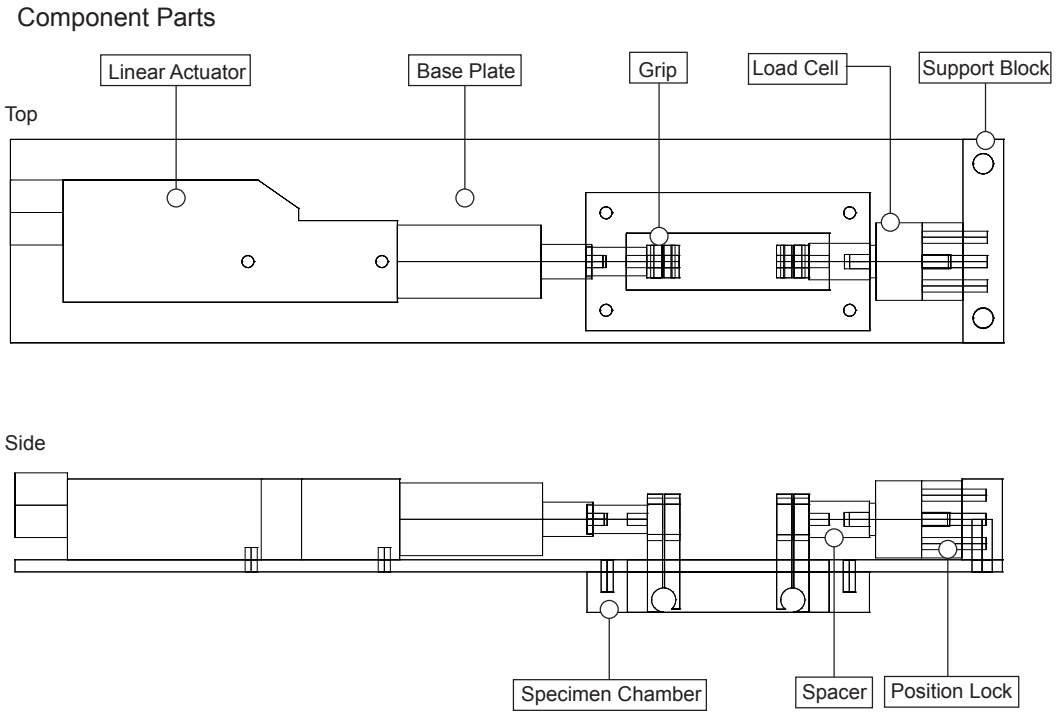

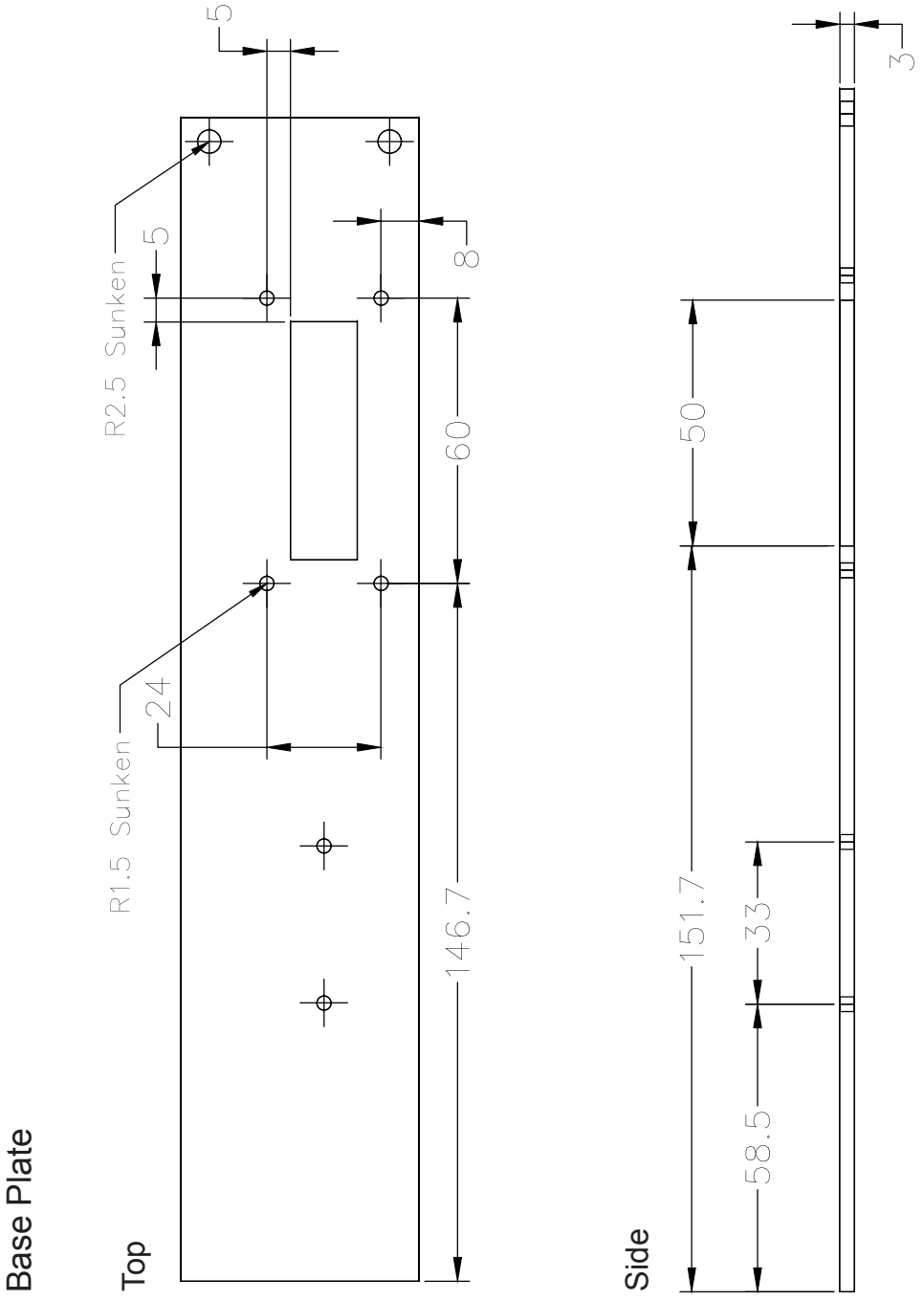
Base Plate
Top
Side
5
3
8
5
R2.5 Sunken
60
24
R1.5 Sunken
146.7
50
151.7
33
58.5

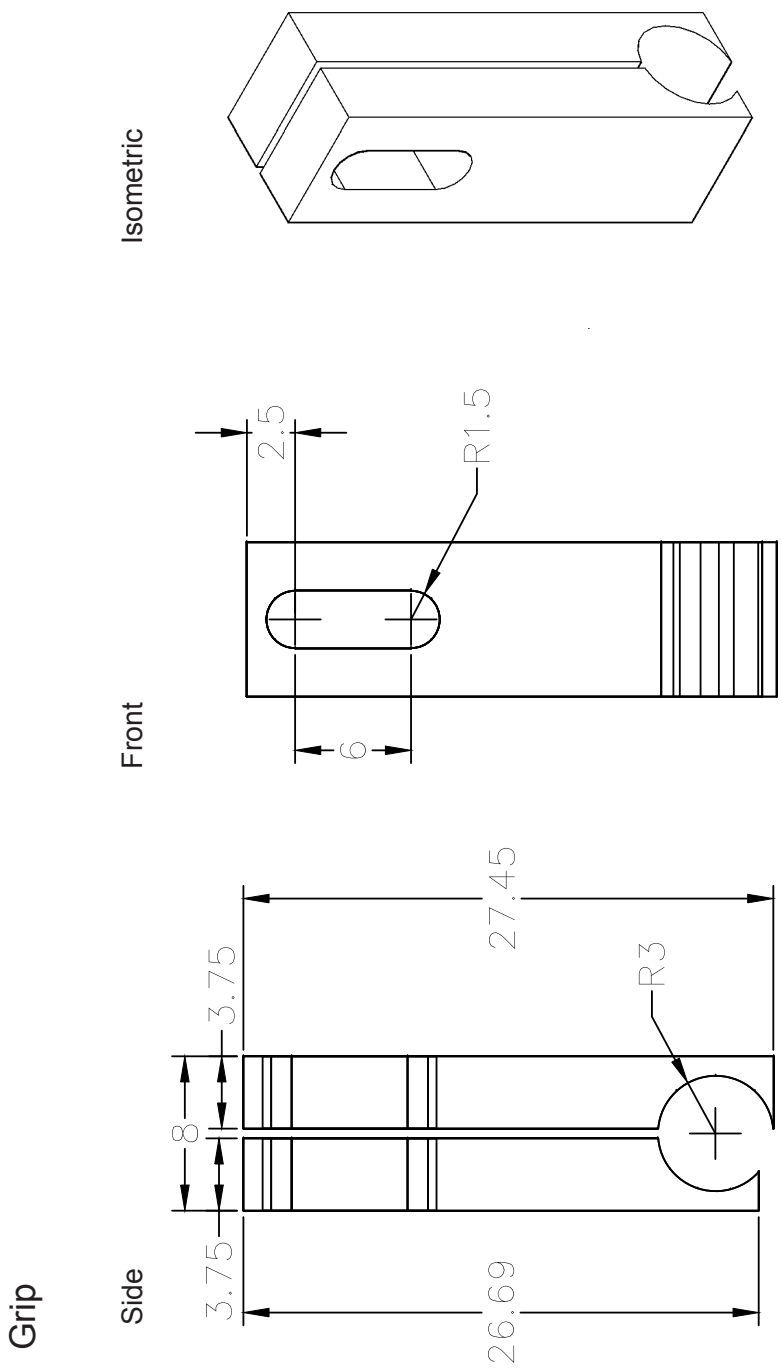
Grip
Isometric
Front
Side
2.5
R1.5
6
27.45
3.75
R3
8
3.75
26.69

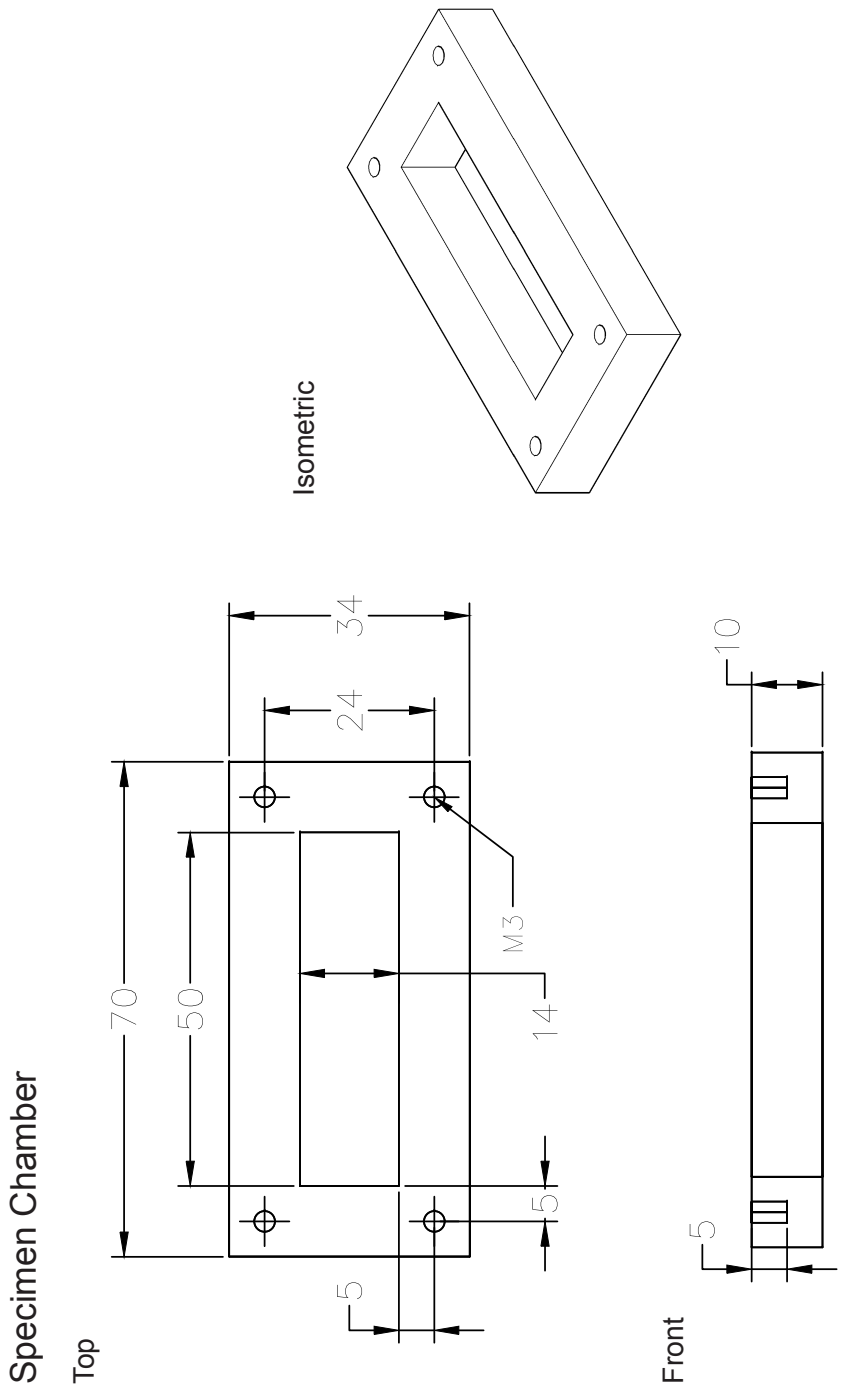
Specimen Chamber
Top
Isometric
Front
34
24
70
50
M3
14
5
5
10
5

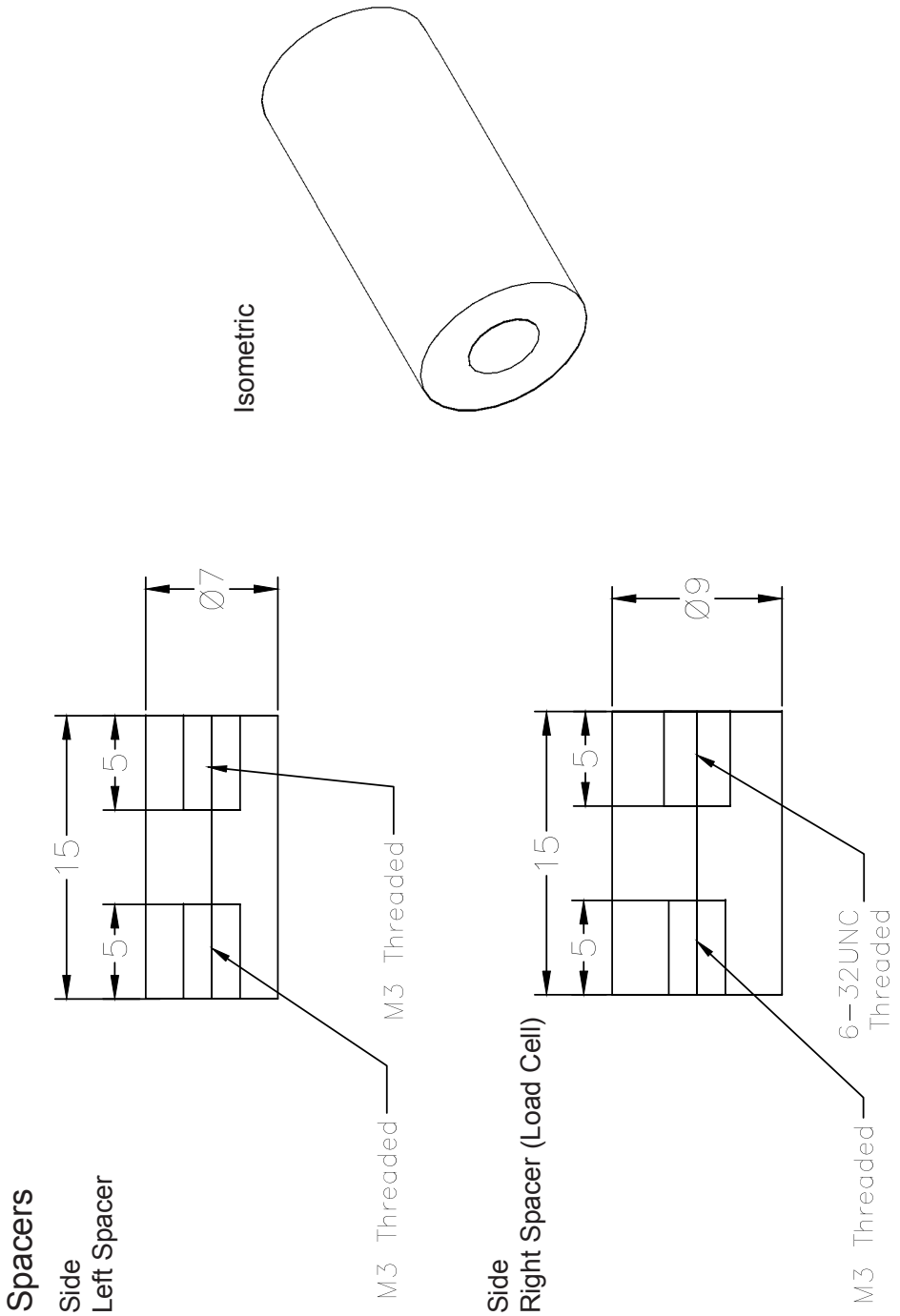
Isometric
Spacers
Side
Left Spacer
Ø7
15
5
5
M3 Threaded
M3 Threaded
Side
Right Spacer (Load Cell)
Ø9
15
5
5
6-32UNC
Threaded
M3 Threaded

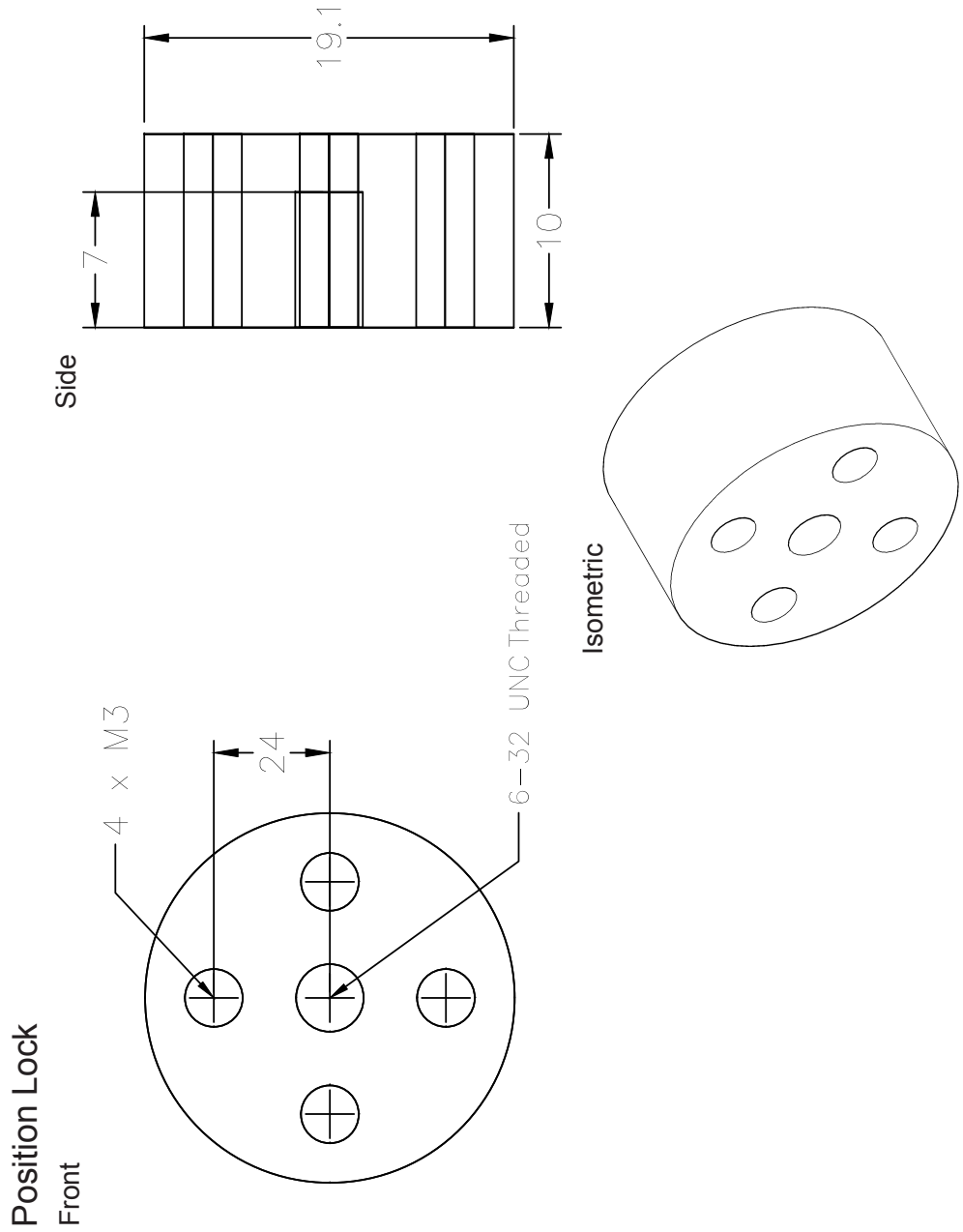
19.1
7
10
Side
Isometric
4 x M3
24
6-32 UNC Threaded
Position Lock
Front

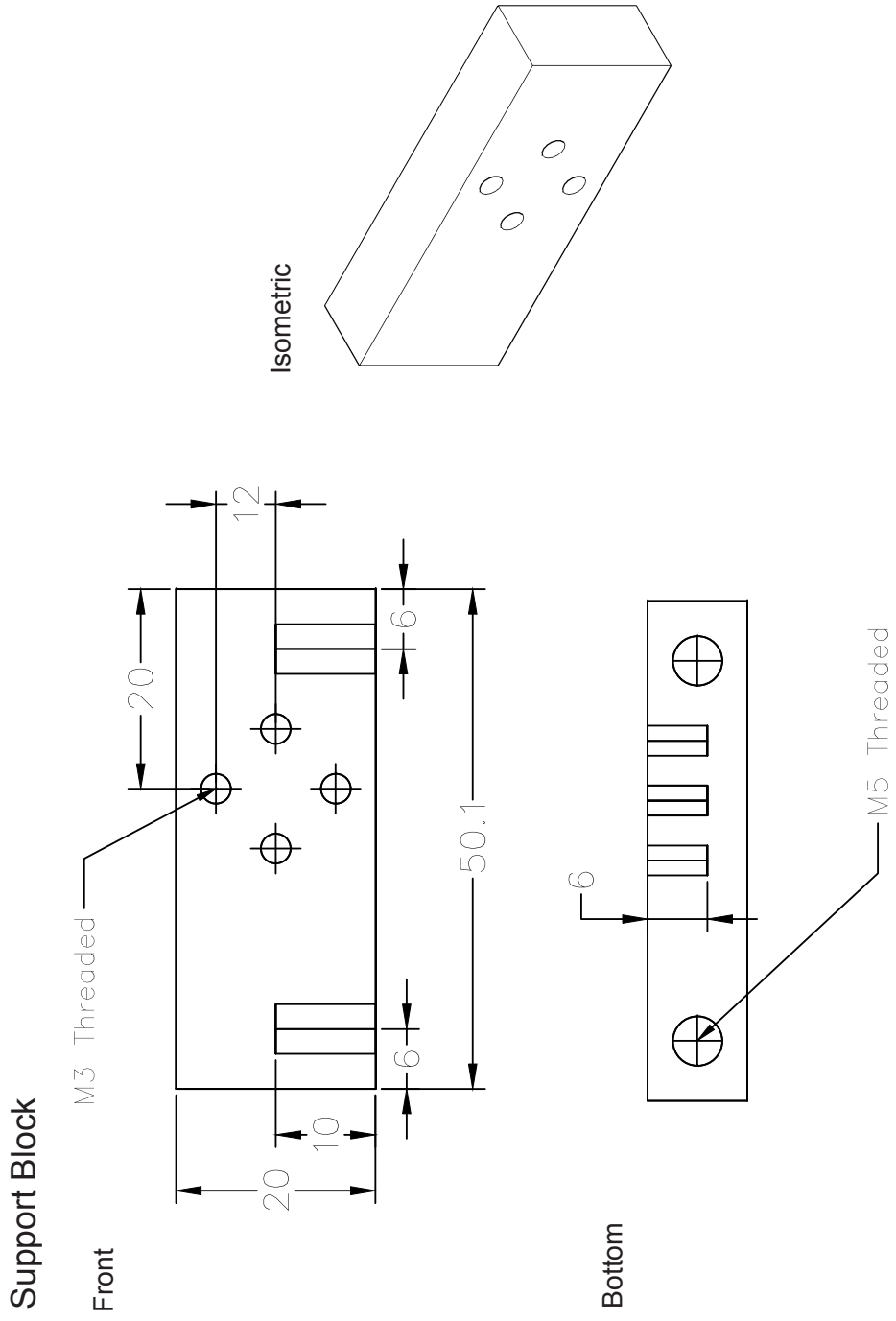
Support Block
Isometric
Front
Bottom
M3 Threaded
M5 Threaded
12
20
6
50.1
6
10
20
6

Appendix C

The following Matlab functions are used to calculate the centroid position, long axis length and alignment of nuclei in structural images. The 'alignment' program measures the properties using the 'regionprops' function and the 'vislabels' program is used to label and visualize cells.

```
function [output] = alignment(cells)
%This function accepts an image of cells as input and outputs the
%centroid, orientation, and major axis length

%Import image and label cells
a=imread(cells);    %Import Image
b=im2bw(a);         %Convert to black and white
vislabels(b)        %Label cells using vislabels function

%Measure and extract area, centroid, oreientatoin, and major axis length
c=regionprops(b,'Area','MajorAxisLength','Orientation','Centroid');
d=[c.Area];             %Extract area measurements
e=[c.Centroid];         %Extract centroid position
f=[c.Orientation];      %Extract orientation
g=[c.MajorAxisLength];  %Extract major axis length

%Set search window for area that represents cells
h=find((d>=100)&(d<=2000));

m=1;
o=1;

%Extract centroid x-position all areas
for i=1:2:length(e),
    x1(m)=e(i);
    m=m+1;
end
```

```
%Extract relevant controid x-positions based on defined area window
for i=1:length(h),
    x(i)=x1(h(i));
    i=i+1;
end

%Extract centroid y-position all areas
for i=2:2:length(e),
    y1(o)=e(i);
    o=o+1;
end

%Extract relevant controid y-positions based on defined area window
for i=1:length(h),
    y(i)=y1(h(i));
    i=i+1;
end

%Extract orientation measurement
for i=1:length(h),
    or(i)=f(h(i));
    i=i+1;
end

%Extract major axis length
for i=1:length(h),
    ma(i)=g(h(i));
    i=i+1;
end

%Output all measure parameters into single matrix
[output]=[x',y',or',ma'];
```

```
function vislabels(L)
%Visualize labels of connected components
%   Steven L. Eddins
%   Copyright 2008 The MathWorks, Inc.

% Form a grayscale image such that both the background and the
% object pixels are light shades of gray.  This is done so that the
% black text will be visible against both background and foreground
% pixels.

background_shade = 200;
foreground_shade = 240;
I = zeros(size(L), 'uint8');
I(L == 0) = background_shade;
I(L ~= 0) = foreground_shade;

% Display the image, fitting it to the size of the figure.
imageHandle = imshow(I, 'InitialMagnification', 'fit');

% Get the axes handle containing the image.  Use this handle in the
% remaining code instead of relying on gca.
axesHandle = ancestor(imageHandle, 'axes');

% Get the extrema points for each labeled object.
s = regionprops(L, 'Extrema');

% Superimpose the text label at the left-most top extremum location
% for each object.  Turn clipping on so that the text doesn't
% display past the edge of the image when zooming.
hold(axesHandle, 'on');
for k = 1:numel(s)
   e = s(k).Extrema;
   text(e(1,1), e(1,2), sprintf('%d', k), ...
      'Parent', axesHandle, ...
      'Clipping', 'on', ...
      'Color', 'b', ...
      'FontWeight', 'bold');
end
hold(axesHandle, 'off');
```

Appendix D

The following LabView block diagram is used to collect load and displacement measurements throughout mechanical tests with the microtensile testing machine.

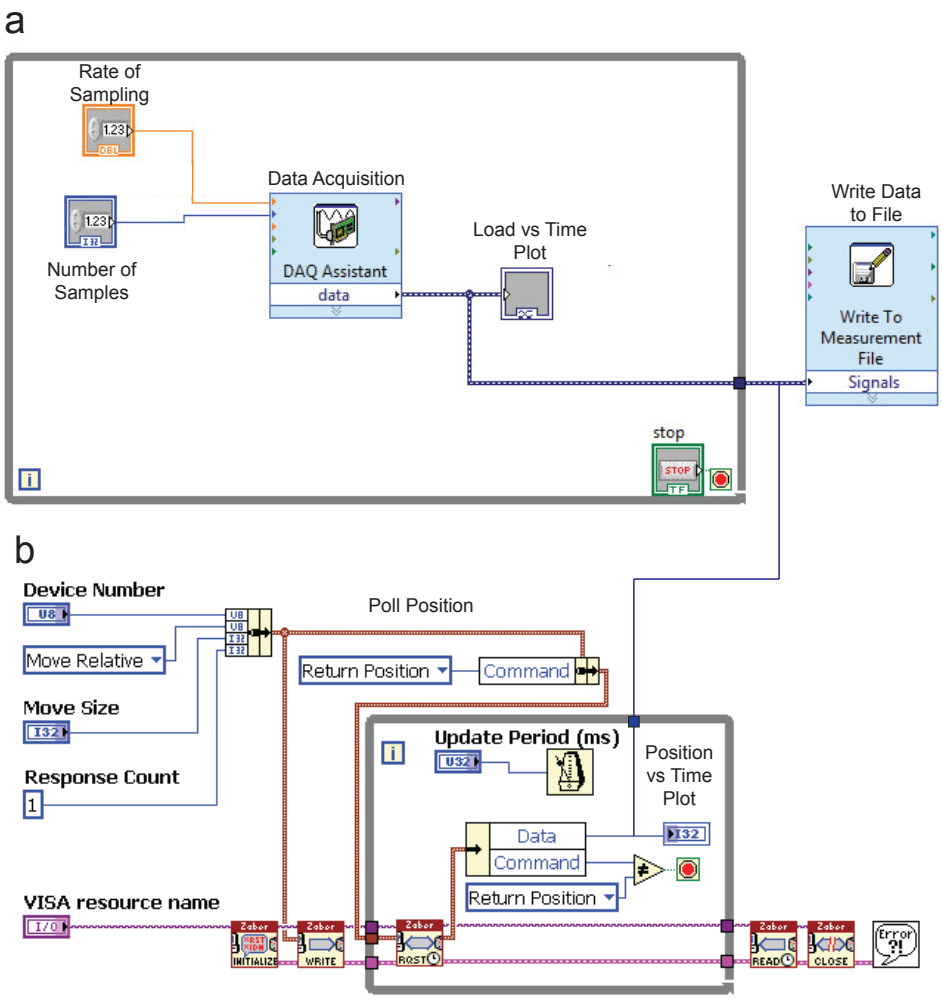

References

Aaron, B. and Gosline, J. (1981). Elastin as a randomnetwork elastomer: A mechanical and optical analysis of single elastin fibers. *Biopolymers*, 20(6):1247–1260.

Adeeb, S., Ali, A., Shrive, N., Frank, C., and Smith, D. (2004). Modelling the behaviour of ligaments: a technical note. *Computer methods in biomechanics and biomedical engineering*, 7(1):33–42.

Alexander, R. M. (1984). Elastic energy stores in running vertebrates. *American Zoologist*, 24(1):85–94.

Alexopoulos, L. G., Haider, M. A., Vail, T. P., and Guilak, F. (2003). Alterations in the mechanical properties of the human chondrocyte pericellular matrix with osteoarthritis. *Journal of Biomechanical Engineering*, 125(3):323–333.

Alexopoulos, L. G., Setton, L. A., and Guilak, F. (2005). The biomechanical role of the chondrocyte pericellular matrix in articular cartilage. *Acta Biomaterialia*, 1(3):317–325.

Ameye, L. and Young, M. F. (2002). Mice deficient in small leucine-rich proteoglycans: novel in vivo models for osteoporosis, osteoarthritis, ehlers-danlos syndrome, muscular dystrophy, and corneal diseases. *Glycobiology*, 12(9):107–116.

Arnoczky, S. P., Lavagnino, M., Whallon, J. H., and Hoonjan, A. (2002). In situ cell nucleus deformation in tendons under tensile load; a morphological analysis using confocal laser microscopy. *Journal of Orthopaedic Research*, 20(1):29–35.

Åström, M. and Rausing, A. (1995). Chronic achilles tendinopathy: A survey of surgical and histopathologic findings mats. *Clinical orthopaedics and related research*, 316:151–164.

Ault, H. and Hoffman, A. (1992). A composite micromechanical model for connective tissues: Part ii—application to rat tail tendon and joint capsule. *Journal of biomechanical engineering*, 114(1):142–146.

Banda, M. J., Werb, Z., and McKerrow, J. H. (1987). Elastin degradation. *Methods in Enzymology*, 144:288–305.

Barbir, A., Michalek, A. J., Abbott, R. D., and Iatridis, J. C. (2010). Effects of enzymatic digestion on compressive properties of rat intervertebral discs. *Journal of Biomechanics*, 43(6):1067–1073.

Barkhausen, T., van Griensven, M., Zeichen, J., and Bosch, U. (2003). Modulation of cell functions of human tendon fibroblasts by different repetitive cyclic mechanical stress patterns. *Experimental and Toxicologic Pathology*, 55(2):153–158.

Benjamin, M., Kaiser, E., and Milz, S. (2008). Structure-function relationships in tendons: A review. *Journal of Anatomy*, 212(3):211–228.

Bennett, M., Ker, R., Imery, N., and Alexander1, R. (1986). Mechanical properties of various mammalian tendons. *Journal of Zoology*, 209(4):537–548.

Birch, H. L. (2007). Tendon matrix composition and turnover in relation to functional requirements. *International Journal of Experimental Pathology*, 88(4):241–248.

Bruehlmann, S., Kelly, E., and Duncan, N. (2005). In situ tendon damage occurs within the interfibril matrix. In *Orthopaedic Research Society Proceedings*, page 389.

Butler, D., Grood, E., Noyes, F., and Zernicke, R. (1978). Biomechanics of ligaments and tendons. *Exercise and sport sciences reviews*, 6:125.

Butler, D. L., Kay, M. D., and Stouffer, D. C. (1986). Comparison of material properties in fascicle-bone units from human patellar tendon and knee ligaments. *Journal of biomechanics*, 19(6):425–432.

Cacho, F., Elbischger, P. J., Rodriguez, J. F., Doblare, M., and Holzapfel, G. A. (2007). A constitutive model for fibrous tissues considering collagen fiber crimp. *International Journal of Non–Linear Mechanics*, 42(2):391–402.

Caldini, E. G., Caldini, N., De-Pasquale, V., Strocchi, R., Guizzardi, S., Ruggeri, A., and Montes, G. S. (1990). Distribution of elastic system fibres in the rat tail tendon and its associated sheaths. *Acta Anatomica*, 139(4):341–348.

Chaplin, D. and Greenlee Jr, T. (1975). The development of human digital tendons. *Journal of Anatomy*, 120:253.

Chen, J., Xu, J., Wang, A., and Zheng, M. (2009). Scaffolds for tendon and ligament repair: review of the efficacy of commercial products. *Expert Review of Medical Devices*, 6(1):61–73.

Cheng, V. W. T. and Screen, H. R. C. (2007). The micro-structural strain response of tendon. *Journal of Materials Science*, 42:8957–8965.

Chimich, D., Shrive, N., Frank, C., Marchuk, L., and Bray, R. (1992). Water content alters viscoelastic behaviour of the normal adolescent rabbit medial collateral ligament. *Journal of Biomechanics*, 25(8):831–837.

Ciarletta, P., Micera, S., Accoto, D., and Dario, P. (2006). A novel microstructural approach in tendon viscoelastic modelling at the fibrillar level. *Journal of Biomechanics*, 39(11):2034–2042.

Cook, C. and McDonagh, M. (1996). Force responses to constant-velocity shortening of electrically stimulated human muscle-tendon complex. *Journal of Applied Physiology*, 81(1):384–392.

Curwin, S. and Stanish, W. D. (1984). *Tendinitis: its etiology and treatment*. Collamore Press Lexington.

Danto, M. I. and Woo, S. L. (1993). The mechanical properties of skeletally mature rabbit anterior cruciate ligament and patellar tendon over a range of strain rates. *Journal of Orthopaedic Research*, 11(1):58–67.

De Campos Vidal, B. and Mello, M. L. S. (2009). Structural organization of collagen fibers in chordae tendineae as assessed by optical anisotropic properties and fast fourier transform. *Journal of Structural Biology*, 167(2):166–175.

Defrate, L. and Li, G. (2007). The prediction of stress-relaxation of ligaments and tendons using the quasi-linear viscoelastic model. *Biomechanics and Modeling in Mechanobiology*, 6(4):245–251.

Diamant, J., Keller, A., Baer, E., Litt, M., and Arridge, R. (1972). Collagen; ultrastructure and its relation to mechanical properties as a function of ageing. *Proceedings of the Royal Society of London. Series B. Biological Sciences*, 180(1060):293–315.

Duance, V., Restall, D., Beard, H., Bourne, F., and Bailey, A. (1977). The location of three collagen types in skeletal muscle. *FEBS letters*, 79(2):248–252.

Edwards, D. (1946). The blood supply and lymphatic drainage of tendons. *Journal of anatomy*, 80(3):147–152.

Evans, E., Benjamin, M., and Pemberton, D. (1990). Fibrocartilage in the attachment zones of the quadriceps tendon and patellar ligament of man. *Journal of anatomy*, 171:155–162.

Fan, Y., Zhao, J., Liao, D., and Gregersen, H. (2005). The effect of digestion of collagen and elastin on histomorphometry and the zero-stress state in rat esophagus. *Digestive Diseases and Sciences*, 50(8):1497–1505.

Farndale, R., Buttle, D., and Barrett, A. (1986). Improved quantitation and discrimination of sulphated glycosaminoglycans by use of dimethylmethylene blue. *Biochimica et Biophysica Acta (BBA)-General Subjects*, 883(2):173–177.

Feitosa, V. L. C., Reis, F. P., Esquisatto, M. A. M., Joazeiro, P. P., Vidal, B. C., and Pimentel, E. R. (2006). Comparative ultrastructural analysis of different regions of two digital flexor tendons of pigs. *Micron*, 37(6):518–525.

Fenwick, S. A., Hazleman, B. L., and Riley, G. P. (2002). The vasculature and its role in the damaged and healing tendon. *Arthritis research*, 4(4):252–260.

Fessel, G. and Snedeker, J. (2010). Equivalent stiffness after glycosaminoglycan depletion in tendon–an ultra-structural finite element model and corresponding-experiments. *Journal of Theoretical Biology*, 268:77–83.

Franchi, M., Fini, M., Quaranta, M., De Pasquale, V., Raspanti, M., Giavaresi, G., Ottani, V., and Ruggeri, A. (2007). Crimp morphology in relaxed and stretched rat achilles tendon. *Journal of Anatomy*, 210(1):1–7.

Franchi, M., Ottani, V., Stagni, R., and Ruggeri, A. (2010). Tendon and ligament fibrillar crimps give rise to left-handed helices of collagen fibrils in both planar and helical crimps. *Journal of Anatomy*, 216(3):301–309.

Fratzl, P., Misof, K., Zizak, I., Rapp, G., Amenitsch, H., and Bernstorff, S. (1998). Fibrillar structure and mechanical properties of collagen. *Journal of Structural Biology*, 122(1):119–122.

Freed, A. D. and Doehring, T. C. (2005). Elastic model for crimped collagen fibrils. *Journal of Biomechanical Engineering*, 127(4):587–593.

Fung, Y. (1993). *Biomechanics: mechanical properties of living tissues*. Springer-Verlag, New York.

Gathercole, L. J. and Keller, A. (1991). Crimp morphology in the fibre-forming collagens. *Matrix*, 11(3):214–234.

Goulam Houssen, Y., Gusachenko, I., Schanne-Klein, M. C., and Allain, J. M. (2011). Monitoring micrometer-scale collagen organization in rat-tail tendon upon mechanical strain using second harmonic microscopy. *Journal of Biomechanics*, 44(11):2047–2052.

Grant, T. M., Thompson, M. S., Urban, J., and Yu, J. (2013). Elastic fibres are broadly distributed in tendon and highly localized around tenocytes. *Journal of Anatomy*, 222(6):573–579.

Green, E. M., Mansfield, J. C., Bell, J. S., and Winlove, C. P. (2014). The structure and micromechanics of elastic tissue. *Interface focus*, 4(2).

Greenlee, T. K., Ross, R., and Hartman, J. L. (1966). The fine structure of elastic fibers. *Journal of Cell Biology*, 30(1):59–71.

Guilak, F., Jones, W. R., Ting-Beall, H. P., and Lee, G. M. (1999). The deformation behavior and mechanical properties of chondrocytes in articular cartilage. *Osteoarthritis and Cartilage*, 7(1):59–70.

Guilak, F. and Mow, V. C. (2000). The mechanical environment of the chondrocyte: A biphasic finite element model of cell-matrix interactions in articular cartilage. *Journal of Biomechanics*, 33(12):1663–1673.

Gupta, H. S., Seto, J., Krauss, S., Boesecke, P., and Screen, H. R. C. (2010). In situ multi-level analysis of viscoelastic deformation mechanisms in tendon collagen. *Journal of Structural Biology*, 169(2):183–191.

Gupta, P. A., Putnam, E. A., Carmical, S. G., Kaitila, I., Steinmann, B., Child, A., Danesino, C., Metcalfe, K., Berry, S. A., Chen, E., Delorme, C. V., Thong, M. K., Adès, L. C., and Milewicz, D. M. (2002). Ten novel fbn2 mutations in congenital contractural arachnodactyly: Delineation of the molecular pathogenesis and clinical phenotype. *Human Mutation*, 19(1):39–48.

Gupta, T. and Haut Donahue, T. L. (2006). Role of cell location and morphology in the mechanical environment around meniscal cells. *Acta biomaterialia*, 2(5):483–492.

Han, S., Gemmell, S., Helmer, K., Grigg, P., Wellen, J., Hoffman, A., and Sotak, C. (2000). Changes in adc caused by tensile loading of rabbit achilles tendon: evidence for water transport. *Journal of Magnetic Resonance*, 144(2):217–227.

Han, Y., Cowin, S. C., Schaffler, M. B., and Weinbaum, S. (2004). Mechanotransduction and strain amplification in osteocyte cell processes. *Proceedings of the National Academy of Sciences of the United States of America*, 101(47):16689–16694.

Hayes, A., Lord, M., Smith, S., Smith, M., Whitelock, J., Weiss, A., and Melrose, J. (2011). Colocalization in vivo and association in vitro of perlecan and elastin. *Histochemistry and cell biology*, 136(4):437–454.

He, Y., Macarak, E. J., Korostoff, J. M., and Howard, P. S. (2004). Compression and tension: differential effects on matrix accumulation by periodontal ligament fibroblasts in vitro. *Connect Tissue Res*, 45(1):28–39.

Heim, A. J., Matthews, W. G., and Koob, T. J. (2006). Determination of the elastic modulus of native collagen fibrils via radial indentation. *Applied physics letters*, 89:181902.

Henninger, H. B., Underwood, C. J., Romney, S. J., Davis, G. L., and Weiss, J. A. (2013). Effect of elastin digestion on the quasistatic tensile response of medial collateral ligament. *Journal of Orthopaedic Research*, 31(8):1226–1233.

Hess, G. P. (1989). Prevention and treatment of overuse tendon injuries. *Sports Medicine*, 8(6):371–384.

Howard, J. (2001). *Mechanics of motor proteins and the cytoskeleton*. Sinauer Associates.

Howard, P. S., Kucich, U., Taliwal, R., and Korostoff, J. M. (1998). Mechanical forces alter extracellular matrix synthesis by human periodontal ligament fibroblasts. *Journal of periodontal research*, 33(8):500–508.

Hsieh, A. H., Tsai, C. M.-H., Ma, Q.-J., Lin, T., Banes, A. J., Villarreal, F. J., Akeson, W. H., and Paul Sung, K.-L. (2000). Time-dependent increases in type-iii collagen gene expression in medial collateral ligament fibroblasts under cyclic strains. *Journal of Orthopaedic Research*, 18(2):220–227.

Hulmes, D. (2002). Building collagen molecules, fibrils, and suprafibrillar structures. *Journal of Structural Biology*, 137(1):2–10.

Ingber, D. (2006). Cellular mechanotransduction: putting all the pieces together again. *The FASEB journal*, 20(7):811–827.

Jaalouk, D. E. and Lammerding, J. (2009). Mechanotransduction gone awry. *Nature Reviews Molecular Cell Biology*, 10(1):63–73.

Jacobs, N. T., Smith, L. J., Han, W. M., Morelli, J., Yoder, J. H., and Elliott, D. M. (2011). Effect of orientation and targeted extracellular matrix degradation on the shear mechanical properties of the annulus fibrosus. *Journal of the Mechanical Behavior of Biomedical Materials*, 4(8):1611–1619.

Järvinen, T. A., Järvinen, T. L., Kannus, P., Józsa, L., and Järvinen, M. (2004). Collagen fibres of the spontaneously ruptured human tendons display decreased thickness and crimp angle. *Journal of orthopaedic research*, 22(6):1303–1309.

Józsa, L. G. and Kannus, P. (1997). *Human tendons: anatomy, physiology, and pathology*. Human Kinetics Champaign.

Julkunen, P., Wilson, W., Jurvelin, J. S., and Korhonen, R. K. (2009). Composition of the pericellular matrix modulates the deformation behaviour of chondrocytes in articular cartilage under static loading. *Medical and Biological Engineering and Computing*, 47(12):1281–1290.

Kadler, K., Holmes, D., Trotter, J., and Chapman, J. (1996). Collagen fibril formation. *Biochemical Journal*, 316:1–11.

Kannus, P. (1997). Tendons–a source of major concern in competitive and recreational athletes. *Scandinavian journal of medicine and science in sports*, 7(2):53–54.

Kannus, P. (2000). Structure of the tendon connective tissue. *Scandinavian Journal of Medicine and Science in Sports*, 10(6):312–320.

Kannus, P. and Jozsa, L. (1991). Histopathological changes preceding spontaneous rupture of a tendon: A controlled study of 891 patients. *Journal of Bone and Joint Surgery - Series A*, 73(10):1507–1525.

Kannus, P., Jozsa, L., J§rvinen, T. A. H., J§rvinen, T. L. N., Kvist, M., Natri, A., and J§rvinen, M. (1998). Location and distribution of non-collagenous matrix proteins in musculoskeletal tissues of rat. *Histochemical Journal*, 30(11):799–810.

Kastelic, J., Galeski, A., and Baer, E. (1978). The multicomposite structure of tendon. *Connective Tissue Research*, 6(1):11–23.

Ker, R. F. (2007). Mechanics of tendon, from an engineering perspective. *International Journal of Fatigue*, 29(6):1001–1009.

Khan, K. M., Cook, J. L., Bonar, F., Harcourt, P., and Östrom, M. (1999). Histopathology of common tendinopathies: Update and implications for clinical management. *Sports Medicine*, 27(6):393–408.

Khanafer, K., Duprey, A., Zainal, M., Schlicht, M., Williams, D., and Berguer, R. (2011). Determination of the elastic modulus of ascending thoracic aortic aneurysm at different ranges of pressure using uniaxial tensile testing. *Journal of Thoracic and Cardiovascular Surgery*, 142(3):682–686.

Khodabakhshi, G., Walker, D., Scutt, A., Way, L., Cowie, R., and Hose, D. (2013). Measuring threedimensional strain distribution in tendon. *Journal of microscopy*, 249(3):195–205.

Kielty, C. M. (2006). Elastic fibres in health and disease. *Expert Reviews in Molecular Medicine*, 8(19):1–23.

Kjaer, M. (2004). Role of extracellular matrix in adaptation of tendon and skeletal muscle to mechanical loading. *Physiological Reviews*, 84(2):649–698.

Kvist, M. (1994). Achilles tendon injuries in athletes. *Sports medicine*, 18(3):173–201.

Lanir, Y. (1978). Structure-function relations in mammalian tendon: the effect of geometrical nonuniformity. *Journal of Bioengineering*, 2(1):119–128.

Lavagnino, M., Arnoczky, S. P., and Gardner, K. (2011). In situ deflection of tendon cellcilia in response to tensile loading: an in vitro study. *Journal of Orthopaedic Research*, 29(6):925–930.

Lavagnino, M., Arnoczky, S. P., Kepich, E., Caballero, O., and Haut, R. C. (2008). A finite element model predicts the mechanotransduction response of tendon cells to cyclic tensile loading. *Biomechanics and Modeling in Mechanobiology*, 7(5):405–416.

Lee, A. A., Delhaas, T., McCulloch, A. D., and Villarreal, F. J. (1999). Differential responses of adult cardiac fibroblasts to in vitro biaxial strain patterns. *Journal of molecular and cellular cardiology*, 31(10):1833–1843.

Lee, T., Midura, R., Hascall, V., and Vesely, I. (2001). The effect of elastin damage on the mechanics of the aortic valve. *Journal of Biomechanics*, 34(2):203–210.

Leesa, M., Craig, M., Sharlene, A., William, D., and Ken, Y. (2004). The outcome and repair integrity of completely arthroscopically repaired large and massive rotator cuff tears. *The Journal of Bone and Joint Surgery*, 86(2):219–224.

Lillie, M. A., Chalmers, G. W. G., and Gosline, J. M. (1994). The effects of heating on the mechanical properties of arterial elastin. *Connective Tissue Research*, 31(1):23–35.

Lorber, M. (1989). Elastic fibers in the rat exorbital lacrimal gland duct system. *Investigative Ophthalmology and Visual Science*, 30(9):2002–2011.

Lorenzo, A. C. and Caffarena, E. R. (2005). Elastic properties, young's modulus determination and structural stability of the tropocollagen molecule: a computational study by steered molecular dynamics. *Journal of biomechanics*, 38(7):1527–1533.

Lowry, O. H., Gilligan, D. R., and Katersky, E. M. (1941). The determination of collagen and elastin in tissues, with results obtained in various normal tissues from different species. *Journal of Biological Chemistry*, 139(2):795–804.

Lujan, T. J., Underwood, C. J., Jacobs, N. T., and Weiss, J. A. (2009). Contribution of glycosaminoglycans to viscoelastic tensile behavior of human ligament. *Journal of Applied Physiology*, 106(2):423–431.

Maffulli, N. (1998). Overuse tendon conditions: time to change a confusing terminology. *Arthroscopy: The Journal of Arthroscopic and Related Surgery*, 14(8):840–843.

Magnusson, S. P. and Kjaer, M. (2003). Region-specific differences in achilles tendon cross-sectional area in runners and non-runners. *European journal of applied physiology*, 90(5):549–553.

Marieb, E. N. and Hoehn, K. (2007). *Human anatomy and physiology*. Pearson Education.

McGough, R., Debski, R., Taskiran, E., Fu, F., and Woo, S. L. (1996). Mechanical properties of the long head of the biceps tendon. *Knee Surgery, Sports Traumatology, Arthroscopy*, 3(4):226–229.

Millesi, H., Reihsner, R., Hamilton, G., Mallinger, R., and Menzel, E. J. (1995). Biomechanical properties of normal tendons, normal palmar aponeuroses, and tissues from patients with dupuytren's disease subjected to elastase and chondroitinase treatment. *Clinical Biomechanics*, 10(1):29–35.

Minns, R. J., Soden, P. D., and Jackson, D. S. (1973). The role of the fibrous components and ground substance in the mechanical properties of biological tissues: A preliminary investigation. *Journal of Biomechanics*, 6(2):153–165.

Mithieux, S. and Weiss, A. (2005). Elastin. *Advances in Protein Chemistry*, 70:437–461.

Monici, M. (2005). Cell and tissue autofluorescence research and diagnostic applications. *Biotechnology annual review*, 11:227–256.

Montes, G. S. (1996). Structural biology of the fibres of the collagenous and elastic systems. *Cell Biology International*, 20(1):15–27.

Mosler, E., Folkhard, W., and Knorzer, E. (1985). Stress-induced molecular rearrangement in tendon collagen. *Journal of Molecular Biology*, 182(4):589–596.

Myllyharju, J. and Kivirikko, K. I. (2004). Collagens, modifying enzymes and their mutations in humans, flies and worms. *TRENDS in Genetics*, 20(1):33–43.

Oakes, B. W. and Bialkower, B. (1977). Biomechanical and ultrastructural studies on the elastic wing tendon from the domestic fowl. *Journal of Anatomy*, 123(2):369–387.

O'Brien, F. J., Harley, B., Yannas, I. V., and Gibson, L. J. (2005). The effect of pore size on cell adhesion in collagen-gag scaffolds. *Biomaterials*, 26(4):433–441.

O'Brien, M. (1997). Structure and metabolism of tendons. *Scandinavian Journal of Medicine and Science in Sports*, 7(2):55–61.

Öhberg, L., Lorentzon, R., and Alfredson, H. (2001). Neovascularisation in achilles tendons with painful tendinosis but not in normal tendons: an ultrasonographic investigation. *Knee Surgery, Sports Traumatology, Arthroscopy*, 9(4):233–238.

Oxlund, H., Manschot, J., and Viidik, A. (1988). The role of elastin in the mechanical properties of skin. *Journal of Biomechanics*, 21(3):213–218.

Parry, D., Barnes, G., and Craig, A. (1978). A comparison of the size distribution of collagen fibrils in connective tissues as a function of age and a possible relation between fibril size distribution and mechanical properties. *Proceedings of the Royal Society of London. Series B. Biological Sciences*, 203(1152):305–321.

Petersen, W., Stein, V., and Tillmann, B. (1999). Blood supply of the tibialis anterior tendon. *Archives of orthopaedic and trauma surgery*, 119(7):371–375.

Pezzin, G., Scandola, M., and Gotte, L. (1976). The low temperature mechanical relaxation of elastin. i. the dry protein. *Biopolymers*, 15(2):283–292.

Pufe, T., Petersen, W., Mentlein, R., and Tillmann, B. (2005). The role of vasculature and angiogenesis for the pathogenesis of degenerative tendons disease. *Scandinavian journal of medicine and science in sports*, 15(4):211–222.

Raspanti, M., Manelli, A., Franchi, M., and Ruggeri, A. (2005). The 3d structure of crimps in the rat achilles tendon. *Matrix Biology*, 24(7):503–507.

Reddy, G. K. and Enwemeka, C. S. (1996). A simplified method for the analysis of hydroxyproline in biological tissues. *Clinical Biochemistry*, 29(3):225–229.

Reese, S. P., Maas, S. A., and Weiss, J. A. (2010). Micromechanical models of helical superstructures in ligament and tendon fibers predict large poisson's ratios. *Journal of Biomechanics*, 43(7):1394–1400.

Reihsner, R., Menzel, E. J., Mallinger, R., and Millesi, H. (1991). Biomechanical properties of elastase treated palmar aponeuroses. *Connective Tissue Research*, 26(1):77–86.

Rigby, B., Hirai, N., Spikes, J., and Eyring, H. (1959). The mechanical properties of rat tail tendon. *The Journal of General Physiology*, 43(2):265.

Riley, G. (2005). Chronic tendon pathology: Molecular basis and therapeutic implications. *Expert Reviews in Molecular Medicine*, 7(5):1–25.

Ritty, T., Ditsios, K., and Starcher, B. (2002). Distribution of the elastic fiber and associated proteins in flexor tendon reflects function. *The Anatomical Record*, 268(4):430–440.

Ritty, T. M., Roth, R., and Heuser, J. E. (2003). Tendon cell array isolation reveals a previously unknown fibrillin-2-containing macromolecular assembly. *Structure*, 11(9):1179–1188.

Sasaki, N. and Odajima, S. (1996). Elongation mechanism of collagen fibrils and force-strain relations of tendon at each level of structural hierarchy. *Journal of Biomechanics*, 29(9):1131–1136.

Schwartz, A. and Thomopoulos, S. (2013). *The Role of Mechanobiology in the Attachment of Tendon to Bone*. Springer.

Schwartz, M. A. (2010). Integrins and extracellular matrix in mechanotransduction. *Cold Spring Harbor perspectives in biology*, 2(12):5006.

Screen, H. R. C., Bader, D. L., Lee, D. A., and Shelton, J. C. (2004). Local strain measurement within tendon. *Strain*, 40(4):157–163.

Screen, H. R. C., Chhaya, V. H., Greenwald, S. E., Bader, D. L., Lee, D. A., and Shelton, J. C. (2006). The influence of swelling and matrix degradation on the microstructural integrity of tendon. *Acta Biomaterialia*, 2(5):505–513.

Screen, H. R. C. and Evans, S. L. (2009). Measuring strain distributions in the tendon using confocal microscopy and finite elements. *Journal of Strain Analysis for Engineering Design*, 44(5):327–335.

Screen, H. R. C., Lee, D. A., Bader, D. L., and Shelton, J. C. (2002). Development of a technique to determine strains in tendons using the cell nuclei. *Biorheology*, 40(1):361–368.

Selvanetti, A., Cipolla, M., and Puddu, G. (1997). Overuse tendon injuries: Basic science and classification. *Operative Techniques in Sports Medicine*, 5(3):110–117.

Shadwick, R. E. (1990). Elastic energy storage in tendons: Mechanical differences related to function and age. *Journal of Applied Physiology*, 68(3):1033–1040.

Sherratt, M., Baldock, C., Louise Haston, J., Holmes, D., Jones, C., Adrian Shuttleworth, C., Wess, T., and Kielty, C. (2003). Fibrillin microfibrils are stiff reinforcing fibres in compliant tissues. *Journal of Molecular Biology*, 332(1):183–193.

Shigley, J., Mischke, C., Budynas, R., Liu, X., and Gao, Z. (1989). *Mechanical engineering design*. McGraw–Hill.

Slomianka, L. (2014). Connective tissues: www.lab.anhb.uwa.edu.au/mb140/.

Smith, J. W. (1965). Blood supply of tendons. *The American Journal of Surgery*, 109(3):272–276.

Smith, K., Vaughan Thomas, A., Spiller, D., Innes, J., Clegg, P., and Comerford, E. (2011). The organisation of elastin and fibrillins 1 and 2 in the cruciate ligament complex. *Journal of Anatomy*, 218:600–607.

Smith, L. J., Byers, S., Costi, J. J., and Fazzalari, N. L. (2008). Elastic fibers enhance the mechanical integrity of the human lumbar anulus fibrosus in the radial direction. *Annals of Biomedical Engineering*, 36(2):214–223.

Smith, L. J. and Fazzalari, N. L. (2009). The elastic fibre network of the human lumbar anulus fibrosus: Architecture, mechanical function and potential role in the progression of intervertebral disc degeneration. *European Spine Journal*, 18(4):439–448.

Snedeker, J. G., Pelled, G., Zilberman, Y., Ben Arav, A., Huber, E., Muller, R., and Gazit, D. (2009). An analytical model for elucidating tendon tissue structure and biomechanical function from in vivo cellular confocal microscopy images. *Cells Tissues Organs*, 190(2):111–119.

Starkey, P. (1976). The effect of human neutrophil elastase and cathepsin g on the collagen of cartilage, tendon, and cornea. *Acta biologica et medica Germanica*, 36(11):1549–1554.

Stäubli, H. U., Schatzmann, L., Brunner, P., Rincón, L., and Nolte, L.-P. (1999). Mechanical tensile properties of the quadriceps tendon and patellar ligament in young adults. *The American Journal of Sports Medicine*, 27(1):27–34.

Svensson, R. B., Hassenkam, T., Grant, C. A., and Magnusson, S. P. (2010). Tensile properties of human collagen fibrils and fascicles are insensitive to environmental salts. *Biophysical Journal*, 99(12):4020–4027.

Tang, Y., Ballarini, R., Buehler, M. J., and Eppell, S. J. (2010). Deformation micromechanisms of collagen fibrils under uniaxial tension. *Journal of the Royal Society Interface*, 7(46):839–850.

Tempelhof, S., Rupp, S., and Seil, R. (1999). Age-related prevalence of rotator cuff tears in asymptomatic shoulders. *Journal of Shoulder and Elbow Surgery*, 8(4):296–299.

Theobald, P., Benjamin, M., Nokes, L., and Pugh, N. (2005). Review of the vascularisation of the human achilles tendon. *Injury*, 36(11):1267–1272.

Theodossiou, T. A., Thrasivoulou, C., Ekwobi, C., and Becker, D. L. (2006). Second harmonic generation confocal microscopy of collagen type i from rat tendon cryosections. *Biophysical Journal*, 91(12):4665–4677.

Tuite, D., Renström, P., and O'brien, M. (1997). The aging tendon. *Scandinavian journal of medicine and science in sports*, 7(2):72–77.

Urbán, Z. and Boyd, C. D. (2000). Elastic-fiber pathologies: primary defects in assembly—and secondary disorders in transport and delivery. *American journal of human genetics*, 67(1):4–7.

van der Rijt, J. A., van der Werf, K. O., Bennink, M. L., Dijkstra, P. J., and Feijen, J. (2006). Micromechanical testing of individual collagen fibrils. *Macromolecular bioscience*, 6(9):697–702.

Vehvilainen, P., Hyytiainen, M., and KeskiOja, J. (2009). Matrix association of latent tgfbeta binding protein2 (ltbp2) is dependent on fibrillin1. *Journal of cellular physiology*, 221(3):586–593.

Vesely, I. (1997). The role of elastin in aortic valve mechanics. *Journal of Biomechanics*, 31(2):115–123.

Viidik, A. (1968). A rheological model for uncalcified parallel-fibred collagenous tissue. *Journal of Biomechanics*, 1(1):3–11.

Viidik, A. (1972). Simultaneous mechanical and light microscopic studies of collagen fibers. *Zeitschrift für Anatomie und Entwicklungsgeschichte*, 136(2):204–212.

Wang, J. H. C. (2006). Mechanobiology of tendon. *Journal of Biomechanics*, 39(9):1563–1582.

Watanabe, T., Imamura, Y., Suzuki, D., Hosaka, Y., Ueda, H., Hiramatsu, K., and Takehana, K. (2012). Concerted and adaptive alignment of decorin dermatan sulfate filaments in the graded organization of collagen fibrils in the equine superficial digital flexor tendon. *Journal of Anatomy*, 220(2):156–163.

Weiss, J. and Gardiner, J. (2001). Computational modeling of ligament mechanics. *Critical reviews in biomedical engineering*, 29(3):303–374.

Williams, L. N., Elder, S. H., Horstemeyer, M. F., and Harbarger, D. (2008). Variation of diameter distribution, number density, and area fraction of fibrils within five areas of the rabbit patellar tendon. *Annals of Anatomy*, 190(5):442–451.

Wren, T. A., Yerby, S. A., Beaupré, G. S., and Carter, D. R. (2001). Mechanical properties of the human achilles tendon. *Clinical Biomechanics*, 16(3):245–251.

Yang, G., Crawford, R. C., and Wang, J. H. (2004). Proliferation and collagen production of human patellar tendon fibroblasts in response to cyclic uniaxial stretching in serum-free conditions. *Journal of biomechanics*, 37(10):1543–1550.

Yoon, J., Halper, J., et al. (2005). Tendon proteoglycans: biochemistry and function. *J Musculoskelet Neuronal Interact*, 5(1):22–34.

You, L., Cowin, S. C., Schaffler, M. B., and Weinbaum, S. (2001). A model for strain amplification in the actin cytoskeleton of osteocytes due to fluid drag on pericellular matrix. *Journal of Biomechanics*, 34(11):1375–1386.

Zoumi, A., Lu, X., Kassab, G. S., and Tromberg, B. J. (2004). Imaging coronary artery microstructure using second-harmonic and two-photon fluorescence microscopy. *Biophysical Journal*, 87(4):2778–2786.